Floquet theory of electronic stopping processes of projectiles in solids

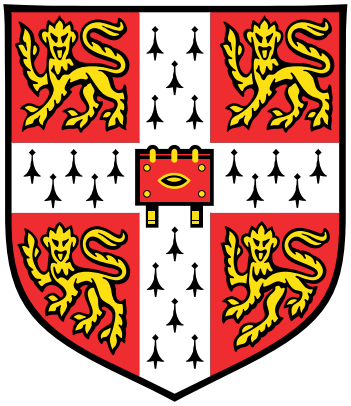

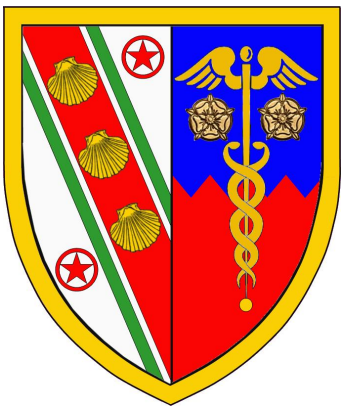

Nicolò Forcellini

Physics Department
University of Cambridge

This Thesis is submitted for the degree of
Doctor of Philosophy

Darwin College

July 2020

To my family.

Declaration

This Thesis is the result of my own work and includes nothing which is the outcome of work done in collaboration except as declared in the Preface and specified in the text. It is not substantially the same as any that I have submitted, or, is being concurrently submitted for a degree or diploma or other qualification at the University of Cambridge or any other University or similar institution except as declared in the Preface and specified in the text. I further state that no substantial part of my Thesis has already been submitted, or, is being concurrently submitted for any such degree, diploma or other qualification at the University of Cambridge or any other University or similar institution except as declared in the Preface and specified in the text. It does not exceed the prescribed word limit for the relevant Degree Committee.

The core part of the Thesis appearing in Chapters 3 and 4 is based on research appearing in

Floquet theory for the electronic stopping of projectiles in solids, N. Forcellini and E. Artacho, Phys. Rev. Research **2**, 033151 (2020).

Chapter 5 contains research that will appear in a forthcoming publication with E. Artacho and M. Famili.

Nicolò Forcellini
July 2020

Acknowledgements

Firstly, I would like to thank Emilio for the support and guidance through these years. He has always been available for advice and help, but he also gave me the freedom to pursue what I find interesting, and has contributed to shape the physicist that I am today. I would like to thank him also for allowing me to spend some time working in CIC nanoGUNE in San Sebastian, where some of the most fruitful discussions of my PhD time took place during the summer of 2019.

On this note, I would like to thank Daniel Sánchez Portal, Iñaki Juaristi, Andres Arnau, José María Pitarke and Achilleas Lazarides for useful discussions. Furthermore, I would like to thank Marjan Famili for our collaboration that led to most of the content in Chapter 5 of this Thesis.

A very big thank you to everyone in TCM who has made my PhD time very enjoyable. I would especially like to thank my officemates Chris, Max and Yuchen as well as Beñat, Eze and many other friends on the TCM floor. A special thanks to Dima Khmelnitskii and Volker Heine for their endeavour to educate TCM graduate students, and for introducing me to so many different aspects of condensed matter and mathematical physics.

I thank my incredible girlfriend Cynthia for reminding me that there is much more to life than physics. A special thanks to my friends in the Cambridge University Volleyball Club, especially Gianmarco, Max, Mateus, Marta, Antonella, Gia and Lukas, to my housemates Oli, Torben, Stef and Soda in 99 Norwich Street, as well as to Darmates, for making my time in Cambridge one of the best of my life. I would also like to thank my old fiends from Imperial College and back in Italy for our deep discussions about physics and life.

Finally, I am profoundly thankful to my parents. I can always rely on them for love and support.

Abstract

The Thesis proposes a new theoretical framework for the study of electronic stopping of particle projectiles in crystalline solids. It does not rely on perturbative or linear response approximations. Moreover, it goes beyond nonlinear models for the homogeneous electron gas, which assume ideal metal hosts. The theory exploits a discrete symmetry in the trajectory of the projectile following a direction of crystalline periodicity, which allows a treatment based on Floquet theory for time-periodic systems. Floquet theory allows to find the solutions of time-periodic Hamiltonians through the same techniques used in time-independent problems: this provides the new framework with an intrinsic advantage over the the real time first principles calculations that are currently employed for analysing electronic stopping, which rely on the explicit solution of the time-dependent Schrödinger equation, and are therefore very computationally expensive. The (stroboscopic) stationary solutions of the stopping problem are found using a Bloch-Floquet scattering treatment. The expressions for electronic stopping of previous perturbative and nonlinear models are readily recovered from the theory in the corresponding limits. The so-called "threshold velocity effect" for stopping is analysed and interpreted using quasienergy conservation, and it is suggested to display a much richer behaviour compared to both experimental observations (due to limited resolution), and previous phenomenological theoretical explanations. A method for numerical calculations is proposed: it is based on a tight-binding model, in which a time-evolving localised basis set is introduced to allow the treatment of the moving crystal in the projectile frame of reference and a Dyson equation can be solved for the Green's function in the local basis set. While the model is presented for the one-band tight-binding model for simplicity, it can be generalised to higher dimensions and to arbitrary number of basis states per unit cell. In addition, other fundamental questions on this paradigmatic nonequilibrium problem, such as the adiabatic limit for a slow projectile, are discussed.

Table of contents

Chapter 1

Introduction to electronic stopping

In this Chapter electronic stopping of ion projectiles is introduced, and the most widely used theoretical and computational models used for its description and for numerical calculations are outlined. Specifically, Lindhard linear response theory and the non-linear model for the homogeneous electron gas (jellium) developed by Echenique, Nieminen and Ritchie [1] –and its higher-order extensions using time-dependent density functional theory (TDDFT)– which are the most widely applicable theoretical paradigms, are described. Additionally, an effect that is referred to as the threshold velocity effect in stopping processes in semiconductors and insulators is introduced.

1.1 Overview and historical context

The effect of particle penetration in matter is one of the oldest and most widely studied problems in modern physics, whose experimental observations started even before the knowledge of the fundamental constituents of matter. Experiments conducted around 1850 in gas-discharge tubes were not completely understood until many decades later, when beams of electrons were identified by Thomson in 1897 and of ions by Goldstein in 1902, paving the foundations of atomic physics. Since then, it became clear that the observed surface modification effects such as wear caused by sputtering –the ejection of particles from a surface caused by energetic beams of particles– were of relevance, and that understanding the interactions between particles and matter was of paramount importance [2].

Furthermore, those experiments inspired the realisation of more complex investigations on the interaction of particles with matter. Moreover, the discovery of radioactivity, with alpha and beta rays penetrating matter much more deeply than what was possible with discharged-gas particles, allowed for better and more sophisticated quantitative measurements of the

ion-matter interactions. Indeed, one of the most important and clear effects observed when particles shoot through matter is that they slow down, losing energy. The oldest paper about energy loss of radiation in matter, which will be later defined as the *stopping power* of the target on the projectiles, is by Bragg and Kleeman in 1905 [3]. Stopping power is defined as $S = -dE/dx$, the projectile loss of energy E per unit path length x: it has the dimensions of a force and it is, in practice, the force exerted on the projectile by the constituents of the solid. A few years later, Rutherford [4] established the nature of the atomic nucleus by analysing the interaction of alpha radiation with matter, introducing important ideas such as the scattering cross-section, which is a fundamental concept in scattering theory to describe particle-particle interactions. A general result, which emerges from Rutherford's formula for the energy transfer from an incoming charge to stationary target particles, is that the stopping due to the electrons in the target material (electronic stopping S_e) dominates at high particle velocity ($v \gg v_F$, v_F denoting the Fermi velocity) compared to the nuclear stopping S_n. In this range, nuclear collisions represent just a small perturbation, since the scattering cross section is very small. For slow particles, both nuclear stopping and electronic stopping are relevant. Nuclear stopping refers to the collision processes between the projectile ion and the atomic nuclei of the target, mediated by electromagnetic interaction. Since the bare charge of the nuclei is screened by the bound electrons, nuclear stopping can be well approximated within the framework of classical scattering theory [5].

The type of particles, or projectiles, creating damage when propagating in a medium can be either coming from outside the medium (cosmic rays or products of radioactive decays such as alpha particles, etc.), or nuclei of the medium itself, whenever the nuclei themselves get accelerated via a knock-on collision with incoming projectiles. In this way, they are set into motion with an energy that is high enough to cause them to be ejected from their original sites. Projectile types in stopping processes can have a wide range in both energy and weight. For instance, projectiles can be high-energy neutrons ($\sim$ 10 MeV) created by radioactive decays or very high-energy cosmic rays, going up to the GeV scale. However, they can also be slow or intermediate-velocity heavy or light charged particles set in motion from collision cascades, whose energy can range from a few keV to hundreds of keV. Moreover, light, intermediate and heavy projectiles are normally classified according to their atomic number with $Z_1 \leq 2$, $3 \leq Z_1 \lesssim 18$ and $Z_1 \gtrsim 19$ respectively [6]. Even in the range where the energy is mainly lost to the electrons, experimental results show that damage along the projectile track can be explained by the energy transfer between the highly-excited electrons and the nuclear subsystem. The true mechanism of this ion track formation is debated [6], but the most studied models include *Coulomb explosion* [7], where the ejection of electrons from the region allows for a strong bare repulsion between the nuclei in the track; the *thermal*

spike model, instead, attributes the displacement track to local melting of the material due to the very high temperature reached by the electron system, and subsequent energy transfer to the ions through electron-electron and electron-phonon interaction [8]. The electron-phonon interaction properties are therefore very important in stopping processes, and considerable theoretical efforts have been dedicated to their modelling [6]. Regarding the inclusion of ion-ion many-body interactions responsible for nuclear stopping, this is usually achieved using molecular dynamics (MD) [9]. All of the above processes, which include thermal, ballistic, hydrodynamic, classical and semi-classical dynamics of the atoms, describe the stages of what is usually referred to as *collision cascade*, started by some initial event that causes an energetic projectile to shoot through a material [6]. However, the nonadiabatic response of the electronic system to the large perturbation of the projectile (especially at medium and low velocities) is generally ignored by the aforementioned models. Even when the effect of the electrons is taken into account, such as in MD, the electrons are usually treated using the Born-Oppenheimer approximation [9, 10], where the electrons instantaneously adjust their state to the dynamics of the ions. In fact, the electronic excitation process in response to the projectile perturbation is important in almost all classes of stopping media, projectiles' energy ranges and atomic numbers, and its accurate description is of fundamental relevance.

When analysing electronic stopping processes, there are various ways in which the energy loss of the projectile can be modelled. For instance, the electrons in the medium can be treated classically or quantum mechanically; electrons in metals can be treated as a free-electron gas, or one can consider the collective excitations induced by the field given by the charged projectile. From the theoretical side, the most important early contributions for the modelling of electronic stopping in matter were the models developed by Bohr, Bethe and Bloch [11–13], and later on by Fermi and Teller [14]. Bohr's model evaluates the energy transfer between a point charge and the classically-bound electrons in the material modelled as harmonic oscillators, whereas Bethe's formula uses a perturbative quantum scattering theory for free electrons (1^{st} Born approximation) to get an expression for stopping. Together with Bloch's correction, these models represent good approximations at high velocities of the particles compared to the Fermi velocity of the electron system ($v \gg v_F$), where electronic stopping has the strongest contribution and the projectile acts as a weak perturbation to the electron system. The model of Fermi and Teller, on the other hand, looks at the opposite limit of the free-electron model, namely the case where the projectile velocity is less than the Fermi velocity. In this case, the predicted electronic stopping has the form $S_e \propto v$, which is in agreement with the observed electronic stopping of most metals. In 1954, Lindhard introduced a linear-response theory for stopping in a free electron gas [15], which takes into account the force acting on the projectile due to the induced change in an electric

field. In fact, in [15] Lindhard characterises the expression for the dielectric function of the stopping medium through a density-density response function which is now widely known as *Lindhard function*. The derived expression for stopping can be regarded as the link between the Fermi-Teller and Bethe approximations.

However, since radiating particles in many cases can hardly ever be considered weak perturbations, theories are needed to treat the response of the electrons in materials beyond Lindhard's paradigm, especially at low velocities and at electron densities that in a real material can be too high to be modelled with linear response. A fundamental step in this direction was made by Ferrell and Ritchie in 1977 [16]. They proposed an approach based on considering electrons at the Fermi surface as being scattered by the screened potential of the ion, thus deriving a nonlinear expression for stopping at $v \gtrsim 0$. Interestingly, the same model is valid when considering an impurity in a metal, thereby calculating the contribution to the resistance due to electron scattering: this case was analysed much earlier in the 1$^{\text{st}}$ Born approximation by Mott and Jones [17]. Ferrell's and Ritchie's approach was pursued shortly afterwards by Echenique, Nieminen and Ritchie [1], who managed to perform calculations with this nonlinear theory using Density Functional Theory (DFT). In their work, through DFT calculations, the screened potential of the projectile could be calculated more accurately compared to the heuristic approximations used by Ferrell and Ritchie, providing very accurate material-specific results. This approach proved to be very accurate for metals and, even though strictly valid in the $v \to 0$ limit, proved to be reliable in predicting the stopping properties of a wide range of target materials for velocities up to v_F [18]. An example of many of the nonlinear effects that can be analysed from the model in [1] are, for instance, the oscillations in S_e as a function of the projectile ion nuclear charge Z_1, termed Z_1 oscillations.

However, there are materials classes whose nonlinear stopping properties cannot be modelled with Echenique's approach. This is because the method is fundamentally based on a description of the electrons in the material as a free, noninteracting electron gas (jellium), and it is derived in the limit $v \to 0$, which accurately predicts the properties of certain metals, e.g. $s-p$ bonded metals [19, 20], as well as the Z_1 oscillations. However, the behaviour of ion projectiles in noble metals, semiconductors and wide-gap insulators cannot be accurately described [21, 22]. Although the theory has been extended to finite velocities for the projectile [23–26], the main limitation is that treating the electrons in the jellium approximation cannot access nontrivial effects caused by the electronic structure of the stopping medium. An example is given by the appearance of a minimum velocity for the onset of electronic stopping in gapped materials, the threshold velocity effect [27–31] (this phenomenon is reviewed in more detail in Section 1.7): the jellium approximation predicts electronic stopping to be $S_e \propto v$ at low velocities, failing to capture this important effect.

Other methods for electronic stopping calculations, which allow for a treatment of the electrons beyond the jellium approximation, treat the electrons in the material, and their time-dependent evolution due to the projectile, explicitly. In this direction, the most successful and general methods for the treatment of electrons in stopping power calculations are time-dependent DFT (TDDFT) and time-dependent tight-binding (TDTB) methods. Aided by the improvement of computing power in the past decades, they are able to calculate the nonadiabatic response of the electron system [6]. TDDFT allows for explicit first-principles calculations of electronic excitations caused by time-dependent Hamiltonians by computing the real-time evolution of the Kohn-Sham wavefunctions [32]. While in a closed system the total energy is conserved, by forcing an ion to move at constant velocity in TDDFT simulations, electronic stopping can be calculated from the total energy increase [21]. Indeed, by removing the projectile position and velocity from the dynamical variables, the system becomes energy nonconservative, and the energy increase in this nonconservative system can then be related to stopping. In fact, the projectile can be safely assumed to travel at a constant velocity along a rectilinear trajectory within the relevant timescale of the electronic stopping problem, without sacrificing accuracy: a light projectile with kinetic energy of a few MeV will excite the electron system at a rate of a few eV/Å. While this constitutes a strong excitation for the electron system, the slowing down of the projectile is barely noticeable over a significant distance in the atomic scale. The constant velocity assumption is not only used in TDDFT calculations for stopping, but also in the nonlinear theory of Echenique, Nieminen and Ritchie and its generalisations, and in Lindhard's linear response. Therefore, based on the negligible effect of on the modelling of a projectile with non-constant velocity, in this Thesis the constant velocity approximation will be assumed throughout, unless stated otherwise.

TDDFT has been successfully applied not only for calculations of nonlinear electronic stopping effects in systems exposed to light projectiles (H/He ions), where the energy loss is in the order of 10 eV/Å [21, 22, 33–46], but also for stopping in the keV/Å range [47]. The response of the ions can be computed through Ehrenfest dynamics: the electronic structure provided by TDDFT simulations can be used to compute the forces acting on the ions, which are used to evolve their equations of motion, ensuring that the nonadiabatic electronic response is taken into account [9]. TDTB provides a more crude approximation for the electron system, which is less limited by the system size and is therefore able to simulate larger systems for longer times: band structure effects can be simulated and, despite not being an accurate representation of real materials, the main aspects of nonadiabatic evolution of the system can be analysed [6, 48, 49].

Albeit these notable successes in the application of TDDFT methods constitute a remarkable progress, there lacks a coherent, nonlinear theory for the electronic response, such as the one of Echenique, Nieminen and Ritchie, as well as its generalisations [1, 23–25], which can take band-structure effects of arbitrary crystalline solids into account. In order to lay the foundations to fill this gap in the theory, in this Thesis a new framework for electronic stopping calculations in arbitrary crystals based on Floquet theory for time-periodic systems is introduced. It generalises the approach of Echenique, Nieminen and Ritchie building on similar assumptions; in addition, it crucially treats the electron system beyond the free electron gas paradigm, and paves the way for more efficient first-principles calculations. Indeed, through Floquet theory, the time-dependent Schrödinger equation can be transformed into an equivalent, but *time-independent-like*, Schrödinger equation. Hence, instead of having to explicitly solve the full time-dependent problem through from the time-dependent Schrödinger equation, the simpler and more efficient techniques used to solve time-independent problems can be used. This, together with the fact that the Floquet theory can help in obtaining a better physical intuition on the stopping processes in crystals compared to brute-force first-principles calculations, represents the main advantage of the new framework.

The outline of the thesis is as follows: in Chapter 2, Floquet theory is introduced; in Chapter 3, results are derived on the threshold problem for gapped systems and adiabatic low-velocity limits; in Chapter 4, the new theoretical framework is explicitly and fully formalised; in Chapter 5, a practical framework for electronic stopping calculations is introduced, based on the formulation of the theory for the special case of a periodic localised basis set; in Chapter 6, the main results are summarised, and an outlook to future work is presented.

In the next section, the main applications for the research on ion radiation-matter interactions are summarised. Subsequently, some of the most important theories for electronic stopping calculations are summarised, including the linear response and the nonlinear jellium theory, in order to serve as an introduction for some of the theoretical basis of the Floquet formalism for stopping.

1.2 Applications

While the results of radiation damage in materials are accessible and visible experimentally, the mechanisms are very difficult to probe directly using current experimental methods. Since the timescale of such processes is of the order of a few picoseconds, the physical process needs to be modelled theoretically. Therefore, a sizeable amount of efforts, summarised in the previous section, have been devoted into the theoretical research.

One of the main industries and research fields that can benefit from better materials for radiation shielding is the space industry [2]. Cosmic rays such as protons or alpha particles, as well as electrons and neutrons, which in our Solar System are parts of the solar wind and flares, can cause severe short-term and long-term damage (both structural and electronic) to equipment and to the well-being of astronauts. Therefore, effective long-term protection from damaging cosmic rays are necessary and crucial for medium to long-term space missions.

Furthermore, radiation damage plays an important role in the nuclear energy industry as well. One of the major challenges for obtaining viable nuclear fusion power plants is the damage caused by the interaction of the plasma with the walls in the containing chamber. The hydrogen isotopes in plasma used in nuclear fusion research have energies in the order of tens of keV: long, damaging interactions with the metallic alloys usually employed in containment structures can compromise their integrity. Moreover, tungsten, a leading candidate as a plasma-facing structural material, is liable to become embrittled due to structural modifications induced by the alpha particles produced during the fusion reactions. Furthermore, energetic neutrons, which are the main products of fusion reactions and whose energy needs to be converted into electricity, cannot be contained through magnetic or inertial confinement, and thus also will impact the structural integrity of the reactor. Therefore, the fabrication of reliable materials ensuring leakage safety and structural integrity is crucial for the commercial usage of nuclear power.

Ion beam radiation has also historically been used for studying the scattering properties of materials. For instance, Rutherford backscattering (with H and He ions in the keV-MeV range) has been used for the analysis of defects and dopants in crystals. Furthermore, ion beams are also used to modify the structure of materials, as for the case of ion implantation applications: the implantation depth for an ion beam at a given energy depends on the stopping properties of the target. Creation of defects in superconductors can also be beneficial on raising the transition temperature [2]. In biomedical research, the knowledge of the stopping properties of soft tissues allows for precise energy deposition where, for example, a tumour is located. If the beam energy is in the right range, healthy tissue will have almost no damage. This happens because in the electronic stopping regime, only a small fraction of the beam energy is lost along the track, and only once an ion is slow enough, the energy deposition will have a peak (the Bragg peak), with the ions coming to rest.

In addition to electronic stopping, the problem of an impurity causing excitations in many-body quantum systems is of fundamental interest: it is a canonical problem in the study of nonequilibrium many-body systems, which is connected to issues regarding thermalisation, nonequilibrium dynamics and the existence of nonequilibrium steady-states. Some of these issues are investigated in this Thesis: they represent practical challenges for the

implementation of the new framework for electronic stopping calculations into first-principles calculations. Others will be merely touched upon and would require more investigation from a more fundamental perspective, and represent interesting research directions which still have many open questions.

1.3 Early analytical models

The well-known Rutherford formula for the energy transfer of an incoming charge at velocity v to stationary charges with particle density n is $T(b) = 2e_P^2 e^2/mv^2b^2$, where b indicates the impact parameter, and e_P and e are the charges of the incoming projectile and the targets, and m is the mass of the target particles. The recoil of the projectile is neglected in this approximation. By performing an integration over valid impact parameters $b \in (b_m, b_M)$, the stopping power takes the form [6]

$$S(v) = \frac{4\pi e_P^2 e^2 n}{mv^2} \ln \frac{b_M}{b_m}. \tag{1.1}$$

From this formula one can note that for large v, the dominant contribution would come from the recoil of the electrons with target mass m_e, while the contribution from much more massive nuclei will be negligible.

This fully classical treatment is in fact a good approximation for the scattering between heavy particles [2]. More sophisticated models for the electron stopping were needed, and the ones by Bohr, Bethe and Bloch [11–13], which are essentially based on the use of perturbation theory, have limited validity to the case of swift projectiles. Bohr's treatment [11] models the classical electrons as harmonically bound to the target atoms, with frequency ω_i for the i^{th} electron. The total energy transferred to one of the electrons by the collision with the ion can then be calculated from the classical equations of motion: summing over all of the electrons in the atoms, assuming a density n of the target atoms and free Coulomb scattering for close collisions, Bohr's formula is obtained [2, 6, 11]

$$S(v) = \frac{4\pi e^2 e_P^2 n}{mv^2} \sum_j f_j \ln\left(\frac{Cmv^3}{e_P^2 \omega_j}\right), \tag{1.2}$$

with the dimensionless constant $C \approx 1.123$ and the f_j are normalised factors quantifying the strength of the interaction. This expression correctly predicts a $1/v^2$ dependence of stopping at high energy, and gives a good estimate for the location of the Bragg peak, i.e. the maximum of stopping as a function of projectile velocity [6]. Bethe's formulation is inspired

by Bloch's when considering the validity of the dipole's approximation for distant interaction [2]. Bethe's approach is based on a perturbative (Born) approximation of quantum scattering theory. This approximation leads to a stopping of the form [6, 12]

$$S(v) = \frac{4\pi e^2 e_P^2 n}{mv^2} \sum_j f_j \ln\left(\frac{2m_e v^2}{\hbar\omega_j}\right), \tag{1.3}$$

where in this case the strength factors f_j are proportional to the matrix element coupling the initial and final states of the electrons. Theories correcting for the Bohr and Bethe approximations were subsequently developed, e.g. by Bloch [13], correcting the failure of Bethe's perturbation treatment for close collisions, treated instead as free Coulomb collisions as in Bohr's theory. Further corrections to Bohr's and Bethe's static-target approximation, termed *shell corrections* [2], take into account the motion of the target electrons. The perturbative approach is accurate for the case of fast and light projectiles (with energy in the MeV range), but fails for the case of slow light or heavy ion projectiles, where models that can capture higher-order effects are needed.

1.4 Lindhard's linear response theory for stopping

Lindhard's treatment of electronic stopping is formalised by considering the force on the projectile caused by the change in the electronic density distribution due to the projectile electric field [15]. It is formulated, within linear response, in terms of the dielectric function, which makes it applicable to a vast range of materials. Consider an electron system with charge density $n(\mathbf{r},t)$ deviating from the equilibrium value $n_0(\mathbf{r})$ by $\delta n(\mathbf{r},t)$ because of the interaction with a time-dependent external scalar potential $V_P(\mathbf{r},t)$ (the projectile). The resulting total potential seen by the projectile is given by the screened potential

$$V_{\text{sc}}(\mathbf{r},t) = V_P(\mathbf{r},t) + V_{\text{ind}}(\mathbf{r},t), \tag{1.4}$$

where the last term is the induced potential

$$V_{\text{ind}}(\mathbf{r},t) = \int d\mathbf{r}' \, \frac{e^2 \delta n(\mathbf{r},t)}{|\mathbf{r}-\mathbf{r}'|}. \tag{1.5}$$

Assuming that the coupling of the electron system with the projectile is weak, the relationship between the induced density $\delta n(\mathbf{r},t)$ and the external potential will be linear, and in terms of

the density-density linear response function $\chi_{nn}(\mathbf{r},\mathbf{r}',t)$ [50]

$$\delta n(\mathbf{r},t) = \int_0^\infty dt' \int d\mathbf{r}'\ \chi_{nn}(\mathbf{r},\mathbf{r}',t')V_P(\mathbf{r}',t-t'). \tag{1.6}$$

By combining Eq. 1.4, 1.5 and 1.6 and taking the Fourier transform with respect to t and $|\mathbf{r}-\mathbf{r}'|$, which is valid under the assumption of a homogeneous electron gas, the relation between the Fourier components of the screened and projectile potential is given by

$$V_{\mathrm{sc}}(\mathbf{q},\omega) = \frac{V_P(\mathbf{q}.\omega)}{\varepsilon(q,\omega)}, \tag{1.7}$$

where $\varepsilon(q,\omega)$ is the Fourier component of the dielectric function, which is related to the density-density response function by

$$\frac{1}{\varepsilon(q,\omega)} = 1 + v_q\chi_{nn}(q,\omega), \tag{1.8}$$

where v_q is the Fourier component of the Coulomb potential. Lindhard [15] considers the special case of a projectile with charge Ze travelling at velocity $\mathbf{v}$ in the electron medium $\rho = Ze\delta(\mathbf{r}-\mathbf{v}t)$. In Fourier space, the screened potential takes the form [51]

$$V_{\mathrm{sc}}(\mathbf{q},\omega) = \frac{8\pi^2 Ze}{\varepsilon(q,\omega)}\frac{\delta(\mathbf{q}\cdot\mathbf{v}+\omega)}{q^2}, \tag{1.9}$$

and the stopping power (force on the projectile) is given by

$$S_e(v) = -\frac{Ze}{v}\mathbf{v}\cdot\mathbf{E}_{\mathrm{sc}}(\mathbf{r}=\mathbf{v}t,t), \tag{1.10}$$

where $\mathbf{E}_{sc}$ is the screened electric field seen by the projectile. Expanding the electric field in Fourier components and using the expression of Eq. 1.9 one gets

$$S_e(v) = -\frac{(Ze)^2}{\pi^2 v}\Im\left\{\int_0^\infty \frac{dq}{q}\int_{-qv}^{qv} d\omega \frac{\omega}{\varepsilon(q,\omega)}\right\}, \tag{1.11}$$

Where $\Im\{z\}$ indicates the imaginary part of z.

Lindhard [15] calculates the dielectric function in the random phase approximation (RPA) for the interacting electron gas, in which the dielectric function can be expressed in terms of the noninteracting density-density response function $\chi_{nn}^{(0)}$ as [50]

$$\varepsilon(q,\omega) = 1 - v_q\chi_{nn}^{(0)}(q,\omega), \tag{1.12}$$

with the Lindhard's function

$$\chi_{nn}^{(0)}(q,\omega) = \sum_{\sigma} \int \frac{d\mathbf{k}}{(2\pi)^d} \frac{n_{\mathbf{k}\sigma} - n_{\mathbf{k}+\mathbf{q}\sigma}}{\hbar\omega + E_\sigma(\mathbf{k}) - E_\sigma(\mathbf{k}+\mathbf{q}) + i\hbar\eta\,\mathrm{sign}(\omega)}, \tag{1.13}$$

where a sum over the spin states σ has been included, $n_{\mathbf{k}\sigma}$ is the Fermi-Dirac occupation of the free-electron state $\psi_{\mathbf{k}}(\mathbf{r}) = \frac{1}{\sqrt{V}} e^{i\mathbf{k}\cdot\mathbf{r}}$ with spin σ, and $E_\sigma(\mathbf{k})$ is the free-electron energy.

Lindhard's formulation represented a very important advancement in the theory of stopping, given its simplicity and wide applicability, with the RPA already giving a good estimate of the dielectric constant: the integral in Eq. 1.13 can be evaluated analytically for the one, two and three-dimensional cases, and more accurate approximations for the dielectric constant can improve the accuracy of this model [50].

1.5 Nonlinear theory for metals

Lindhard's treatment assumes a linear-response of the electron gas, which is only valid for weak interactions between the projectile and the electron system. It corresponds to a first-order perturbation treatment for the scattering of the electrons with the projectile [52], and it is most accurate for high projectile velocities and low electron densities, similarly to the other perturbative treatments. However, stopping processes are, in many cases, highly nonlinear and nonperturbative. An improvement on the linear theory result has been achieved via the nonlinear theory proposed by Ferrel and Ritchie [16]. In their model, based on a scattering theory for a free electron gas with the screened potential of the projectile, the electronic stopping for a projectile having velocity v is given by

$$S_e = n\sigma_T(v_F)v_F v, \tag{1.14}$$

where n is the electron density and $\sigma_T(v_F)$ is the transport cross-section, calculated at the Fermi level, v_F is the Fermi velocity, $\sigma_T(v)$ defined in terms of the differential scattering cross-section $\sigma(v,\theta)$ as

$$\sigma_T(p) = \int d\Omega(1-\cos\theta)\sigma(v,\theta). \tag{1.15}$$

The expression 1.14 has been firstly proposed by Lindhard, and subsequently reported to have been used in the thesis of Finnemann [53] by Ferrel and Ritchie in their paper.

By considering a spherically symmetric screened potential, the transport cross-section can be expanded in terms of the phase shifts of the electrons calculated at the Fermi energy

$\delta_l(E_F)$ for a spherically symmetric potential, and it is given by

$$\sigma_T(v_F) = \frac{4\pi}{v_F}\sum_{l=0}^{\infty}(l+1)\sin\left[\delta_l(E_F)-\delta_{l+1}(E_F)\right] \tag{1.16}$$

so that the stopping can be expressed as

$$S_e = \frac{4\pi n v}{k_F}\sum_{l=0}^{\infty}(l+1)\sin\left[\delta_l(E_F)-\delta_{l+1}(E_F)\right], \tag{1.17}$$

where k_F is the Fermi wavevector. An equivalent formulation of this model was used by Mott and Jones [17] for the calculation of the resistivity by impurities in metals, but their formulation employed the first-order Born approximation for scattering. Since the potential is assumed to be completely screened by the electronic medium, the phase shifts obey the Friedel sum rule to a good accuracy, $Z = \frac{2}{\pi}\sum_l(2l+1)\delta_l(E_F)$. Therefore, if the screened potential of the projectile when shooting through the electron medium is known, the stopping can be calculated very accurately through Eq. 1.17. In their calculation, Ferrel and Ritchie [16] assume a Yukawa potential of the form $V(r) = Ze^{-\lambda r}/r$, which is only valid in a linear-response regime. Echenique, Nieminen and Ritchie use DFT to find the screened potential of the projectile in an electron gas, which is then used to find the corresponding phase shifts [1, 54]. The reason why the DFT result is more accurate in the nonlinear regime, when the electron density of metals is too high for a linear treatment, is that DFT is very efficient in calculating the ground state of the electronic system. Indeed, the stopping power calculated using the above DFT method correctly predicts the oscillating behaviour of stopping as a function of the ion charge Z_1 (the Z_1-*oscillations*), which originates from the formation of closed shells of electrons around the projectile [1]. However, in this formulation, the theory is limited to the $v \to 0$ regime. A generalisation was developed by Schönhammer [23] for spherically symmetric potentials and later generalised to self-consistent potentials by Zaremba, Arnau and Echenique [25], and is summarised in the next section, since it is related to the Floquet stopping theory for crystals developed in Chapters 3 and 4.

1.6 Nonlinear theory for finite velocity and related models

Consider an electron gas with Hamiltonian $H_0(\mathbf{r}')$, and a localised, scalar potential $V_P(\mathbf{r}',t) = V_P(\mathbf{r}'-\mathbf{v}t)$ describing a projectile at constant velocity $\mathbf{v}$ in the laboratory frame. As explained in section 1.1, the constant-velocity approximation applies most of the typical stopping regimes and the usual size of simulation boxes in first-principles calculations. Since the projectile degrees of freedom are removed from the equation of motion, there is no energy

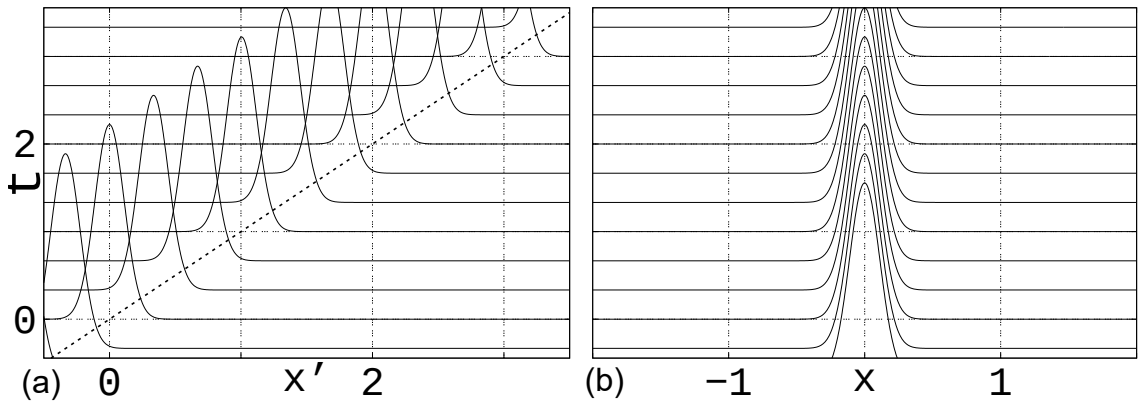

Fig. 1.1 Potential landscape for a Hamiltonian describing the projectile shooting through an homogeneous medium in the laboratory reference frame (a) and in the projectile (b). v is the projectile velocity (slope of dotted line). The curves (potential vs x) are shifted for different times. The problem becomes time-independent in the projectile reference frame, allowing for the treatment within the formalism of the free-particle scattering theory. Arbitrary units.

conservation, or, from an alternative point of view, the energy change in the electron system compensates the work needed to keep the projectile moving at constant velocity. This energy change can be quantified by defining an energy transfer rate (ETR) via the Hellman-Feynman theorem [23]

$$\frac{dE(t)}{dt} = \langle \Psi'(\mathbf{r}',t)| \frac{dV_P(\mathbf{r}',t)}{dt} |\Psi'(\mathbf{r}',t)\rangle \,, \tag{1.18}$$

where $|\Psi'(\mathbf{r}',t)\rangle$ are the solutions to the time dependent Schrödinger equation (TDSE) for $H'(\mathbf{r}',t) = H_0(\mathbf{r}') + V_P(\mathbf{r}' - \mathbf{v}t)$. By performing a Galilean transformation to put the projectile at rest at the origin, the problem becomes the time-independent one of an impurity in a homogeneous electron gas, with Hamiltonian $H(\mathbf{r}) = H_0(\mathbf{r}) + V_P(\mathbf{r})$ (primed/unprimed indices indicating lab/projectile frame, respectively). This holds for a homogeneous electron gas because the trajectory of the projectile is homogeneous in the space-time diagonal that it defines (see Fig. 1.1). Assuming that the projectile potential is introduced in the electron system at some time t_0, for the special case of noninteracting electrons letting $t_0 \to -\infty$ maps the problem to time-independent free-electron scattering for the single-particle states. The free-particle scattering solutions with outgoing boundary conditions are eigenstates of the Hamiltonian $H(\mathbf{r})$. They can be expressed through the Lippmann-Schwinger equation as

$$|\mathbf{k}^{(+)}\rangle = |\mathbf{k}\rangle + g^{(+)}[E(\mathbf{k})] V_P |\mathbf{k}^{(+)}\rangle \,, \tag{1.19}$$

with free-particle states $\psi_{\mathbf{k}}(\mathbf{r}) = \langle \mathbf{r}|\mathbf{k}\rangle$, $g^{(+)}(E) = [E - H_0 + i\eta]^{-1}$ ($\eta \to 0^+$) being the unperturbed retarded Green's function.

As a first example for ETR and stopping calculations in this scattering picture, consider the one-dimensional case because of its simplicity and intuitiveness, only requiring the very basics of quantum mechanics. In the projectile frame, moving at velocity v, the energy of free-particle waves is conserved, and the wavefunction for a free particle scattered by the scalar potential fixed at $x = 0$ has the asymptotic form

$$\psi_k^{(+)}(x) \sim C \begin{cases} e^{ikx} + r(k)e^{-ikx}, & \text{for } x \to -\infty \\ t(k)e^{ikx}, & \text{for } x \to \infty \end{cases} \tag{1.20}$$

for a particle coming from $x = -\infty$, and

$$\psi_k^{(+)}(x) \sim C \begin{cases} t(k)e^{-ikx}, & \text{for } x \to -\infty \\ e^{-ikx} + r(k)e^{ikx}, & \text{for } x \to \infty \end{cases} \tag{1.21}$$

if the particle comes from $x = +\infty$, where C is a normalisation constant which, for example, can be taken $C = 1/\sqrt{2\pi\hbar}$ using δ-function normalisation for the momentum eigenstates [55], which gives a current density $j = \hbar k/2\pi\hbar m = v_k/2\pi\hbar$ for an unperturbed free-particle state $|k\rangle$. The latter case is illustrated in Fig. 1.2, showing the momentum transfer to the reflected wave in the laboratory frame.

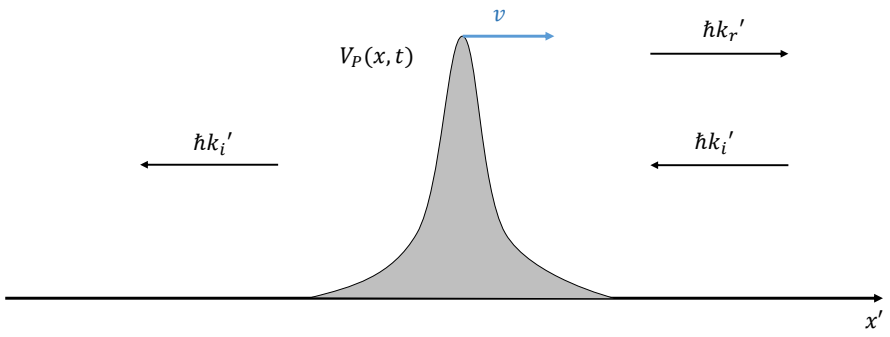

Fig. 1.2 One-dimensional scattering of a free particle in the laboratory frame for an arbitrary projectile potential moving at velocity v. The energy of the reflected wave with momentum $\hbar k_r'$ for an incoming left-moving particle increases due to the "kick" given by the projectile. The ETR can be found by considering the problem as energy conserving in the projectile frame.

The reflection and transmission coefficients satisfy $|r(k)|^2 + |t(k)|^2 = 1$. In the laboratory frame, there will be a net ETR to this single-particle current given by

$$\left(\frac{dE}{dt}\right)_{sp} = \Delta E |j_r|, \tag{1.22}$$

where ΔE is the energy transfer from a single collision of an electron with the projectile, and j_r is the reflected probability current density in the projectile frame (the absolute value is introduced since we are interested in absolute energy differences, and therefore we need to discard the direction of the reflected current). The momentum in the laboratory frame $p' = \hbar k'$ of an electron can be expressed as $p' = mv + p$, where $p = \hbar k$ is the center of mass momentum of the system moving with projectile defined by the stationary scattering problem. The energy transfer in the laboratory frame for this case is

$$\Delta E = \frac{1}{2m}\left[(\hbar k_r')^2 - (\hbar k_i')^2\right] = \hbar v(k_r - k_i), \tag{1.23}$$

where $\hbar k_{i/r}$ denotes incident and reflected momenta respectively. In our problem, we have simply $-k_r = k_i = k$, and $\Delta E = -2v\hbar k$. Substituting $j_r = \frac{v_k}{2\pi\hbar}|r(k)|^2$, the ETR can be expressed as

$$\left(\frac{dE}{dt}\right)_k = -\frac{v|v_k|k|r(k)|^2}{\pi}. \tag{1.24}$$

The same result can be obtained by noting that the ETR for single-particle states can be expressed in terms of a force matrix element [23]. Considering the more general three-dimensional case, the expression for the ETR becomes

$$\left(\frac{dE(t)}{dt}\right)_{\mathbf{k}} = \left\langle \mathbf{k}^{(+)} \middle| \mathbf{v} \cdot \frac{\partial V_P(\mathbf{r})}{\partial \mathbf{r}} \middle| \mathbf{k}^{(+)} \right\rangle, \tag{1.25}$$

This can be expressed in terms of a commutator with the momentum operator $\hat{\mathbf{p}}$ as [56]

$$\frac{i}{\hbar}\left\langle \mathbf{k}^{(+)} \middle| \mathbf{v} \cdot \frac{\partial V_P(\mathbf{r})}{\partial \mathbf{r}} \middle| \mathbf{k}^{(+)} \right\rangle \equiv \langle \mathbf{k}^{(+)} | [\mathbf{v} \cdot \hat{\mathbf{p}}, \hat{V_P}] | \mathbf{k}^{(+)} \rangle \tag{1.26}$$

which, after substituting the Lippmann-Schwinger solution 1.19 leads to

$$\left(\frac{dE(t)}{dt}\right)_{\mathbf{k}} = \frac{2\pi}{\hbar}\int \frac{d\mathbf{k}'}{(2\pi)^3} |\langle \mathbf{k}' | V_P | \mathbf{k}^{(+)} \rangle|^2 \mathbf{v} \cdot \hbar(\mathbf{k} - \mathbf{k}') \delta(E(\mathbf{k}) - E(\mathbf{k}')). \tag{1.27}$$

Integrating over occupied states and assuming a spherically symmetric potential representing the projectile, the total ETR $\dot{E}$ is obtained, which leads to the expression for stopping

[23, 25, 56]

$$S_e = 2\int \frac{d\mathbf{p}}{(2\pi\hbar)^3}\frac{p}{m}\mathbf{p}\cdot\hat{\mathbf{v}}f(E_{p+mv})\sigma_T(p), \tag{1.28}$$

since $S_e = \dot{E}/v$. $f(E_{p+mv})$ is the shifted Fermi distribution, which represents the momentum distribution of the homogeneous electron gas in the projectile frame. In the low-velocity limit, it reduces to the expression in Eq. 1.14, in which the transport cross-section is evaluated at the Fermi level. While Schönhammer and Bönig [23, 56] analysed the case of a hard sphere potential, Zaremba, Arnau and Echenique [25], as explained in section 1.5, calculated the scattering potential self-consistently using DFT to get the phase shifts required for the evaluation of 1.14. While an effective spherically symmetric potential is used for such calculations, allowing for the solution of the Schrödinger equation for outgoing scattering states of the usual form, the resulting electron density calculated with DFT is not in general spherically symmetric.

The expression for the ETR in Eq. 1.27, derived using the explicitly time-dependent Hamiltonian, gives good insight on the nature of the energy nonconserving process in the laboratory frame due to the constant-velocity approximation. The expression for stopping in a framework which makes use of conservation laws for elastic scattering was already known for some time, with one of the oldest references being the work of Trubnikov and Yavlinskii [57]. In a derivation attributed to Lindhard [2], instead of considering the change in energy to the electron system due to the time-dependent external potential, one can consider, in line with the one-dimensional example presented at the beginning of the section, the equivalent calculation of the averaged momentum transfer to the projectile due to electrons with velocity $\mathbf{v}_e$ and scattered by an angle θ. This is given by

$$\Delta\mathbf{p} = m\mathbf{w}_e(1-\cos\theta), \tag{1.29}$$

where $\mathbf{w}_e = \mathbf{v}_e - \mathbf{v}$, $\mathbf{v}$ being the projectile velocity, m is the electron mass and the interaction potential is assumed to be spherically symmetric, with the transverse components of the momentum transfer from the uniform current density averaging out. The force on the ion, $F_e = d\mathbf{p}/dt$, can be integrated over the velocity distribution $f(\mathbf{v}_e)$ in the laboratory frame, leading to the equivalent of Eq. 1.28

$$S_e = -nm\int d\mathbf{v}_e f(\mathbf{v}_e)\frac{|\mathbf{w}_e|}{v}\mathbf{v}\cdot\mathbf{w}_e\sigma_T(|\mathbf{w}_e|). \tag{1.30}$$

The low-velocity limit for the case of a degenerate electron gas (the nonlinear jellium model) by considering the low-velocity limit of Eq. 1.30, given by [58]

$$S_e \approx \frac{mv}{3} \int d\mathbf{v}_e f(\mathbf{v}_e) \frac{1}{v_e^2} \frac{d}{dv_e} \left(v_e^4 \sigma_T(v_e) \right), \tag{1.31}$$

and inserting the probability distribution for a degenerate Fermi gas

$$f(v_e) = \frac{3}{4\pi v_F^3} \Theta(v_F - v), \tag{1.32}$$

then Eq.1.30 reduces to Eq. 1.14.

More recently, another method was proposed [59], which is not based or connected to the momentum-transfer method leading to the transport cross section formulations above, but rather it is based on the calculation of the retarding force on the ion due to the induced charge density (always limited to the homogeneous electron gas), more in line with Lindhard's approach. This leads to an expression for stopping that is identical to Eq. 1.28, with an effective transport cross section which has the slightly different form

$$\sigma_T^{eff}(v) = \frac{2\pi Z_1}{v^3} \sum_{l=0}^{\infty} \sin\left(2[\delta_l(v) - \delta_{l+1}(v)]\right), \tag{1.33}$$

with the projectile atomic number Z_1. This expression, for high projectile velocities, converges well to the Bethe and Bloch formulas, and seems to provide a link between nonlinear stopping power calculations and high-velocity perturbative methods.

1.7 Threshold velocity effect

The threshold velocity v_{th} for the projectile is defined as the minimum velocity below which electronic stopping is absent. For ideal metals, a stopping $\propto v$ derived through the nonlinear theory for metals does not admit a threshold, i.e. $v_{th} = 0$. However, the model cannot accurately calculate electronic stopping in semiconductors and insulators, which have been shown to have a nontrivial low-velocity limit for stopping. An important example, which proved to be quite controversial in experiments [27, 29, 60], is the large band-gap insulator LiF. The most accurate experimental results up to date, shown in Fig. 1.3, provide a confirmation of the existence of a threshold velocity at $v \approx 0.1$ a.u., with the onset of stopping having the approximate functional form $S_e(v - v_{th}) \propto v$.

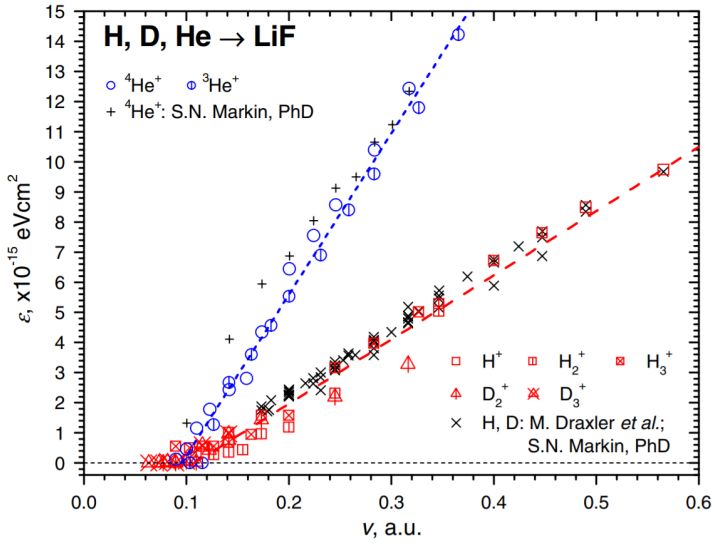

Fig. 1.3 Electronic stopping cross section $\varepsilon = (1/n)S_e$ (y axis) as a function of projectile velocity, showing the clearest experimental proof to date of the threshold velocity effect for the case of Hydrogen and Helium nuclei shooting through LiF, a large band-gap insulator (band gap energy $\sim$ 13 eV). Figure from [27], and reproduced with the editor's permission.

To illustrate the origin of the threshold, consider a simple parabolic insulator model –at the independent particle level– with parabolic energy bands around the gap and isotropic effective masses m_e and m_h for electrons and holes. We can consider the cases of direct and indirect band gap as displayed in Fig. 1.4. The band gap energy is E_g, and for the indirect case the bottom of the conduction band is displaced by $\mathbf{k}_0$ from the top of the valence band, and the projectile is assumed to have velocity $\mathbf{v} = v\hat{\mathbf{k}}_0$. From perturbation theory, it can be derived that the excitation induced by the projectile must have frequency [61]

$$\omega = \mathbf{v} \cdot \Delta\mathbf{k}, \tag{1.34}$$

where $\Delta\mathbf{k} = \mathbf{k}_f - \mathbf{k}_i$ is the difference in wave-vectors of the states $\psi_{\mathbf{k}} \propto e^{i\mathbf{k}\cdot\mathbf{r}}$ participating in the transitions. This can be derived by considering the projectile potential of the $V_P(\mathbf{r},t) = V_P(\mathbf{r}-\mathbf{v}t)$, which can be regarded as a superposition of harmonic perturbations of the form $e^{i\omega(\mathbf{r}-\mathbf{v}t)}$, giving the condition of Eq. 1.34 using time-dependent perturbation theory. The probability of excitations is modulated by the real-space Fourier transform $\tilde{V}_P(\Delta\mathbf{k})$, which decays for large $\Delta\mathbf{k}$ for any smooth $V_P(\mathbf{r})$. Eq. 1.34 corresponds to the expression relating energy and momentum change of a light particle of mass m when colliding with a much more massive particle ($M \to \infty$) with velocity $\mathbf{v}$, i.e. $\Delta E = \mathbf{v} \cdot \Delta\mathbf{k}$ [38]. For the case of a direct gap,

the threshold velocity for which excitations are allowed under the condition 1.34 is

$$v_{th} = \sqrt{\frac{E_g}{m_h + m_e}}, \tag{1.35}$$

where E_g is the band gap. The threshold velocity condition in this case is given by imposing v_{th} to be the value of the slope of the common tangent between the two parabolas in Fig. 1.4 (a), i.e. the slope of the red line. Below this value of v_{th}, no excitation is possible for this model.

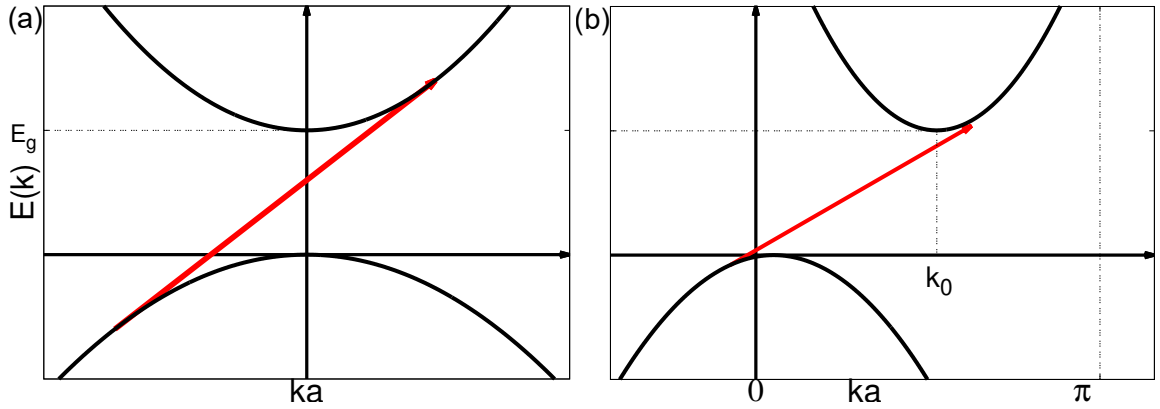

Fig. 1.4 Model of parabolic insulator with direct (a) and indirect (b) band gap. The projectile threshold velocity for electron-hole excitations is given by the slope of the red arrow in each of the two figures. In the indirect band gap analysis, we assume that the projectile velocity is aligned with the displacement vector $\mathbf{k}_0$ for the upper band.

For the indirect band gap case, where the bottom of the upper band is displaced from the top of the bottom one by $\mathbf{k}_0$, if the projectile velocity is collinear with $\mathbf{k}_0$ the threshold is given by the condition [38]

$$\frac{1}{2}(m_e + m_h)v_{th}^2 + k_0 v_{th} - E_g = 0. \tag{1.36}$$

This simple analysis for this model, which gives a strict threshold velocity for excitations induced by the projectile, was implemented as a phenomenological constraint (see e.g. Archubi and Arista [62]) for the nonlinear model for stopping, where the transport cross-section in Eq. 1.28 is modified to only allow transitions above E_g. When considering real materials, involving transitions between Bloch states, this simple picture seems to lose validity. Actually, already from perturbation theory [61] it was shown that the low-velocity limit, related to the threshold effect, can in principle show a highly nontrivial behaviour

with, in principle, no real strict threshold velocity, in disagreement to the above simplified model. A mechanism in which dynamical defect states introduced by the projectile act as "elevators" for transitions across the gap in some types of projectile-target systems has also been proposed [42, 63], showing no strict threshold. This in fact holds for general gapped materials, as it will be shown in Chapters 3 and 4 with the formalisation of the Floquet-Bloch scattering formalism.

1.8 Many-body effects

In the nonlinear theory presented in the previous section, many-body effects governed by dynamical correlations between the electrons in the stopping process are not taken into account beyond the mean-field approximation provided by the Kohn-Sham method. However, it was shown by Nazarov and collaborators [64, 65] that these effects, even in the low-velocity limit where it was expected that they did not play an important role, can be relevant. In their work, which is limited to low projectile velocities, the effect of the dynamical exchange and correlation interaction is included within the TDDFT formalism. Consider the friction coefficient Q –which is in fact simply the stopping power divided by the projectile velocity– in the $v \to 0$ limit

$$Q \equiv \lim_{v\to 0} -\frac{1}{v} S_e. \tag{1.37}$$

It can be shown, by taking into account the exchange-correlation kernel in the local density approximation (LDA), that it can be divided into the contribution of the noninteracting Kohn-Sham electrons Q_1, which corresponds to the nonlinear theory of Echenique et al. based on the theory of elastic scattering presented in the previous section, and the dynamical correlation given by the excitonic contribution Q_2, with [64]

$$\begin{aligned} Q_1 &= \frac{1}{(2\pi)^3} \int d\mathbf{q} d\mathbf{k} \tilde{v}_{\mathbf{q}} \tilde{v}_{\mathbf{k}} \frac{(\mathbf{q}\cdot\mathbf{v})}{v} \frac{(\mathbf{k}\cdot\mathbf{v})}{v} \frac{\partial \Im \chi^0_{\mathbf{q},\mathbf{k}}(\omega)}{\partial \omega}\bigg|_{\omega=0}; \\ Q_2 &= -\frac{1}{(2\pi)^3} \int d\mathbf{q} d\mathbf{k} n^0_{\mathbf{q}} n^0_{\mathbf{k}} \frac{(\mathbf{q}\cdot\mathbf{v})}{v} \frac{(\mathbf{k}\cdot\mathbf{v})}{v} \frac{\partial \Im f^{xc}_{\mathbf{q},\mathbf{k}}(\omega)}{\partial \omega}\bigg|_{\omega=0}; \end{aligned} \tag{1.38}$$

where $\tilde{v}_{\mathbf{q}}$ indicates the Fourier transform of the effective Kohn-Sham potential, $n^0_{\mathbf{q}}$ is the Fourier transform of the electron density, $\chi^0_{\mathbf{q},\mathbf{k}}(\omega)$ is the Fourier transform of the noninteracting Kohn-Sham electron density-density response function, and $f^{xc}_{\mathbf{q},\mathbf{k}}(\omega)$ accounts for the exchange-correlation kernel. The dynamical correlation factor Q_2 becomes comparable to Q_1 for intermediately charged ions, enhancing their stopping power and providing better

agreement with experimental results for projectiles of charge $Z_1 < 15$ in the LDA for the exchange-correlation kernel [64].

The above theory is limited to the low-velocity limit and to the specific choice of exchange-correlation functional within TDDFT, as well as being only valid for the treatment of the homogeneous electron gas. However, it already shows how taking into account dynamical many-body effects can in principle be important for corrections to stopping power calculations based on single-particle momentum-conserving scattering. In fact, there are other theoretical methods that include corrections due to electron-electron interactions in nonequilibrium systems, such as nonequilibrium Green's function methods based on the Keldysh formalism, which could be in principle incorporated when starting from a noninteracting single-particle picture, such as the one considered in the development of the Floquet formulation of electronic stopping in the present Thesis.

In addition, all of the above theories assume stationary stopping processes, with the projectile travelling at a constant velocity. Corrections to these assumptions, including a slowing down of the projectile and/or oscillatory behaviours due to the effects of the underlying crystal, can be in principle implemented into the above methods, but their effects on the projectile velocity are typically very small. Therefore, the assumption of a stationary motion of the projectile is quite generally applicable. Regarding the stationary behaviour of the electron system out of equilibrium, which is implicitly assumed in the above linear-response and nonlinear theories for jellium and is connected to the observed stationary energy increase in real-time TDDFT simulations after a short transient [21, 22, 36, 38, 47], it is likely that taking into account the effect of many-body interactions would lead to a modification of the properties of the excitations as described by single-particle mean-field theories, and it would be a very interesting direction for future investigations.

Chapter 2

Floquet theory for time-periodic Hamiltonians

In this Chapter, the Floquet formalism for Hamiltonians periodic in time is presented, and some of the general properties of Floquet systems are described. The Floquet formalism will be applied in the Chapters 3 and 4 for the construction and description of the Bloch-Floquet scattering theory, used to model electronic stopping in crystalline systems.

2.1 Floquet Formalism

The Floquet formalism for time-dependent Hamiltonians in quantum mechanics was developed by Shirley [66] in 1965, and the presentation in this section is inspired by the introductory notes by Hänggi [67] and Santoro [68]. Consider a Hamiltonian $H(t)$ periodic in time with period τ, i.e. $H(t) = H(t+\tau)$. Floquet theorem tells us that there exists a basis of solutions to the time-dependent Schrödinger equation (TDSE), the *Floquet states*, that are of the form

$$|\Psi_\alpha(t)\rangle = e^{-i\varepsilon_\alpha t/\hbar}|\Phi_\alpha(t)\rangle\,, \tag{2.1}$$

with the periodicity of the Hamiltonian reflected in the *Floquet modes* $|\Phi_\alpha(t)\rangle = |\Phi_\alpha(t+\tau)\rangle$, and where the real parameters ε_α are termed *quasienergies*. It is the equivalent of the Bloch theorem for particles in crystalline potentials, with the Floquet states corresponding to Bloch waves and the quasienergy being the equivalent of quasimomentum. The analogy with Bloch states can be made even more explicit: define a new Hermitian operator, the *Floquet Hamiltonian*, as

$$\mathscr{H}(t) = H(t) - i\hbar\partial_t\ ; \tag{2.2}$$

the TDSE can be written as

$$\mathscr{H}(x,t)\Psi(x,t) = 0\,. \tag{2.3}$$

It is then easily found from this that the Floquet modes are eigenstates of the Floquet Hamiltonian with corresponding eigenvalues given by the quasienergies from

$$\mathscr{H}(x,t)\Psi(x,t) = (H(x,t) - i\hbar\partial_t)e^{-i\varepsilon_\alpha t/\hbar}\Phi_\alpha(x,t) = e^{-i\varepsilon_\alpha t/\hbar}(H - i\hbar\partial_t - \varepsilon_\alpha)\Phi_\alpha(x,t) = 0, \tag{2.4}$$

which can be expressed as a time-independent-like Schrödinger equation, the *Floquet mode equation*

$$\mathscr{H}(x,t)\Phi_\alpha(x,t) = \varepsilon_\alpha\Phi_\alpha(x,t). \tag{2.5}$$

Using the fact that the Floquet modes are periodic, equivalent physical states are easily defined as

$$|\Psi_{p\alpha}(t)\rangle = e^{-i\varepsilon_{p\alpha}t/\hbar}\,|\Phi_{p\alpha}(t)\rangle\,, \tag{2.6}$$

where the modes are given by

$$|\Phi_{p\alpha}(t)\rangle = e^{ip\omega t}\,|\Phi_\alpha(t)\rangle\,, \tag{2.7}$$

with $\omega = 2\pi/\tau$, $p \in \mathscr{Z}$ is an integer and the shifted quasienergies are

$$\varepsilon_{p\alpha} = \varepsilon_\alpha + p\hbar\omega. \tag{2.8}$$

Given that the physical states are determined for the quasienergies being modulo $\hbar\omega$, one may restrict them, without loss of generality, to any interval in energy of this length, e.g. $-\hbar\omega/2 < \varepsilon_{0\alpha} \leq \hbar\omega/2$. This is equivalent to the choice for a 1st Brillouin Zone (BZ) for Bloch waves, where the quasimomenta are also defined within the finite interval determined by the length of reciprocal lattice vectors. Therefore, physically different states can be characterised by the reduced quasienergies within the chosen interval in energy space. Since the choice of an interval is arbitrary, some conventions may be more convenient than others in specific cases, and there is freedom in choosing the most convenient one: for instance, it may be appropriate to set the Floquet energy interval to correspond most closely to the one of the static system [69].

Consider the time-evolution operator $\mathscr{U}$ for the Floquet Hamiltonian. With its usual definition

$$|\Psi_\alpha(t)\rangle = \mathscr{U}(t,t_0)\,|\Psi_\alpha(t_0)\rangle\,, \tag{2.9}$$

for $t \in [t_0, t_0+\tau]$, it has the property

$$\mathscr{U}(t+n\tau,t_0) \equiv \mathscr{U}(t,t_0)\left[\mathscr{U}(t_0+\tau,t_0)\right]^n. \tag{2.10}$$

This illustrates the fact that, in order to describe the time-evolution of a state from some initial t_0 to some general $t+n\tau$, it is enough to know $\mathscr{U}(t,t_0)$ for t within $[t_0,t_0+\tau]$. The one-period unitary

$$\mathscr{U}_0(t_0+\tau,t_0) = \mathrm{T}\exp\left[-i/\hbar\int_{t_0}^{t_0+\tau} dtH(t)\right],\ \mathrm{T} \equiv \text{time ordering operator}, \tag{2.11}$$

has the Floquet modes as eigenvectors, obeying

$$\mathscr{U}_0(t_0+\tau,t_0)\left|\Phi_\alpha(t_0)\right\rangle = e^{-i\varepsilon_\alpha\tau/\hbar}\left|\Phi_\alpha(t_0)\right\rangle, \tag{2.12}$$

which leads to the definition of an effective Hamiltonian operator H^0_{eff} through

$$\mathscr{U}_0(t_0+\tau,t_0) \equiv \exp\left[-\frac{i}{\hbar}H^0_{eff}\tau\right]. \tag{2.13}$$

The effective Hamiltonian, which depends on the specific choice of t_0 for the unitary, is therefore associated with the quasienergy eigenvalues ε_α and eigenmodes $|\Phi_\alpha(t_0)\rangle$. Hence, H^0_{eff} is linked to $\mathscr{H}(t)$ defined in Eq. 2.2. In addition, the nonuniqueness of the choice for the quasienergy $\varepsilon_\alpha = \varepsilon_\alpha + p\hbar\omega$ is clear in Eq. 2.12 from the fact that it leaves the physics invariant. This indefiniteness can be interpreted as the freedom in choosing the operator logarithm in Eq. 2.13 to obtain H^0_{eff}. In practice, starting from some initial state, expressed as a superposition of Floquet modes at $t=0$

$$|\psi(0)\rangle = \sum_\alpha c_\alpha\left|\Phi_\alpha(0)\right\rangle,\ c_\alpha = \langle\Phi_\alpha(0)|\psi(0)\rangle \tag{2.14}$$

its time evolution is given by

$$|\psi(t)\rangle = \sum_\alpha c_\alpha e^{-i\varepsilon_\alpha t/\hbar}\left|\Phi_\alpha(t)\right\rangle. \tag{2.15}$$

Hence, the evolution operator becomes

$$\mathscr{U}(t',t) = \sum_\alpha e^{-i\varepsilon_\alpha(t'-t)/\hbar}\left|\Phi_\alpha(t')\right\rangle\left\langle\Phi_\alpha(t)\right|, \tag{2.16}$$

generalising the evolution of time-independent systems to time-periodic Hamiltonians, where the role of the stationary eigenstates is replaced by the Floquet modes. The above picture becomes somewhat clearer if one then introduces an *extended* Hilbert space, making use of the periodicity of the Floquet modes: in this space the fact that Eq. 2.5 resembles a time independent Schrödinger equation (TISE), where time seems to play the same role as spatial coordinates, finds a natural explanation. Following Sambe (1971) [70], the Hilbert space $\mathscr{T}$ of all the possible functions $f(t)$ of time t with period τ is introduced, with inner product

$$(a,b) = \frac{1}{\tau}\int_{t_0}^{t_0+\tau} dt\; a^*(t)b(t). \tag{2.17}$$

The functions $\langle t|n\rangle = e^{im\omega t}$, with $m \in \mathbb{Z}$, form a complete orthonormal set in $\mathscr{T}$. Define by $\mathscr{R}\otimes\mathscr{T}$ the composite linear Hilbert space given by the product of $\mathscr{R}$, the Hilbert space of square-integrable functions in configuration space, with $\mathscr{T}$. $\mathscr{R}$ is the usual Hilbert space in which wavefunctions in quantum mechanics "live". $\mathscr{R}\otimes\mathscr{T}$ is the space in which the Floquet Hamiltonian acts, and in which its eigenstates (the Floquet modes) obey orthonormality conditions, which can be formulated using a generalised inner product in this space

$$\begin{aligned}\langle\langle f(t),g(t)\rangle\rangle &= \frac{1}{\tau}\int^{\tau} dt\,\langle f(t),g(t)\rangle \\ &= \frac{1}{\tau}\int^{\tau} dt\int d\mathbf{r} f(\mathbf{r},t)g(\mathbf{r},t),\end{aligned} \tag{2.18}$$

where the range of integration in $\mathbf{r}$ is the entire configuration space, and the notation $\frac{1}{\tau}\int^{\tau}$ has been introduced for average integral in $\mathscr{T}$ defined by Eq. 2.17. Therefore, the orthonormality condition can be written as

$$\begin{aligned}\langle\langle\Phi_{p\alpha}|\Phi_{q\beta}\rangle\rangle &= \frac{1}{\tau}\int^{\tau} dt\int_{-\infty}^{+\infty} dx\;\Phi^*_{p\alpha}(x,t)\Phi_{q\beta}(x,t) \\ &= \frac{1}{\tau}\int^{\tau} dt\,\langle\Phi^*_{p\alpha}(t)|\Phi_{q\beta}(t)\rangle = \delta_{\alpha,\beta}\delta_{p,q}.\end{aligned} \tag{2.19}$$

Moreover, the Floquet modes form a complete set in $\mathscr{R}\otimes\mathscr{T}$

$$\sum_{\alpha,p}\Phi^*_{p\alpha}(\mathbf{r},t)\Phi_{p\alpha}(\mathbf{r}',t') = \delta(\mathbf{r}-\mathbf{r}')\delta(t-t') \tag{2.20}$$

and, at equal times ($t = t'$), the Floquet modes in the 1st BZ $\Phi_{0\alpha}(\mathbf{r},t) \equiv \Phi_\alpha(\mathbf{r},t)$ form a complete set in $\mathscr{R}$

$$\sum_{\alpha}\Phi^*_{\alpha}(\mathbf{r},t)\Phi_{\alpha}(\mathbf{r}',t) = \delta(\mathbf{r}-\mathbf{r}'). \tag{2.21}$$

Using these properties of the Floquet modes, we may rewrite Eq. 2.5 in matrix form. To do this, consider the Fourier expansion of the Floquet modes

$$|\Phi_\alpha(t)\rangle = \sum_{m=-\infty}^{\infty} e^{im\omega t} |\phi_{\alpha,m}\rangle , \tag{2.22}$$

where $|\phi_{\alpha,m}\rangle$ is defined as the m^{th} Fourier component of the Floquet mode, and observe that the time-derivative term, when applied to one of the $|\phi_{\alpha,m}\rangle$, gives

$$-i\hbar\frac{\partial}{\partial t}\left(e^{im\omega t}|\phi_{\alpha,m}\rangle\right) = m\hbar\omega\left(e^{im\omega t}|\phi_{\alpha,m}\rangle\right). \tag{2.23}$$

Moreover, one can also expand the Hamiltonian in Fourier components as

$$H_{m-n} = \frac{1}{\tau}\int^{\tau} dt\; H(t)e^{-i(m-n)\omega t}, \tag{2.24}$$

which means that the Floquet mode Eq. 2.5 can be written as the eigenvalue equation

$$\sum_{n=-\infty}^{\infty} H_{m-n}|\phi_{\alpha,n}\rangle - (m\hbar\omega)|\phi_{\alpha,m}\rangle = \varepsilon_\alpha|\phi_{\alpha,m}\rangle , \tag{2.25}$$

The usual case when studying Floquet systems is the one of an Hamiltonian periodic in time of the form $H(t) = H_0 + V_{ext}(t)$, i.e. the sum of a static Hamiltonian H_0, of which we know the eigenvectors $\{|\varphi_j\rangle\}$, and an external potential $V_{ext}(t) = V_{ext}(t+\tau)$. Expanding the Fourier component of equation Eq. 2.22 in terms of the eigenvectors of H_0

$$|\phi_{\alpha,m}\rangle = \sum_j C^j_{\alpha,m}|\varphi_j\rangle , \tag{2.26}$$

and defining the new Fourier basis as $\langle t|\varphi_j,m\rangle \equiv e^{im\omega t}|\varphi_j\rangle$, Eq. 2.25 can be expressed as

$$\sum_{n=-\infty}^{\infty}\sum_{l=-\infty}^{\infty}\langle\langle\varphi_j,m|\mathscr{H}|\varphi_l,n\rangle\rangle C^l_{\alpha,n} = \varepsilon_\alpha C^j_{\alpha,m}, \tag{2.27}$$

where the matrix elements of the Floquet Hamiltonian are given by

$$\langle\langle\varphi_j,m|\mathscr{H}|\varphi_l,n\rangle\rangle = \langle\varphi_j|H_{m-n}|\varphi_l\rangle + n\hbar\omega\delta_{j,l}\delta_{m,n}. \tag{2.28}$$

Note that no restriction has been imposed in the strength of the external potential $V_{ext}(t)$. Indeed, the fact that calculations can be easily extended beyond perturbation theory is one of the main advantages of Floquet theory.

The eigenvalue equation 2.25 can be expressed visually in matrix form by explicitly constructing the Floquet Hamiltonian in the extended Fourier space. Firstly, define a vector of the Fourier coefficients $\{|\phi_{\alpha,m}\rangle\}$ denoted by $\mathbf{x}_\alpha$

$$\mathscr{H}\mathbf{x}_\alpha = \varepsilon_\alpha \mathbf{x}_\alpha \ , \tag{2.29}$$

where the Floquet matrix and the vector of Fourier coefficients have the form

$$\mathscr{H} = \begin{bmatrix} \ddots & \vdots & \vdots & \vdots & \\ \dots & H_0-(n-1)\omega & H_{-1} & H_{-2} & \dots \\ \dots & H_1 & H_0-n\omega & H_{-1} & \dots \\ \dots & H_2 & H_1 & H_0-(n+1)\omega & \dots \\ & \vdots & \vdots & \vdots & \ddots \end{bmatrix}, \ \mathbf{x}_\alpha = \begin{bmatrix} \vdots \\ |\phi_{\alpha,m-1}\rangle \\ |\phi_{\alpha,m}\rangle \\ |\phi_{\alpha,m+1}\rangle \\ \vdots \end{bmatrix} \tag{2.30}$$

and where the Hamiltonian Fourier components are defined as in Eq. 2.24. The above matrix has in fact a block structure: when considering a Hilbert space of size d for the time-dependent Hamiltonian $H(t)$, each of the elements in the above definition of $\mathscr{H}$ is itself a matrix of size $d \times d$, with the matrix extending infinitely due to the infinite sum in the Fourier series.

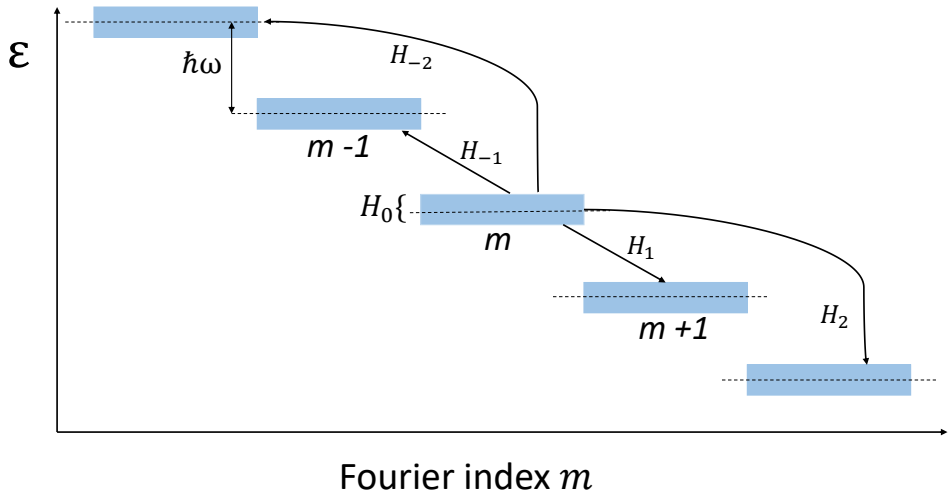

Fig. 2.1 Schematic illustration of the structure of the Floquet Hamiltonian defined in Eq. 2.30 in the extended Fourier space. H_0 is the time-averaged Hamiltonian (see definition 2.24) with the higher-order terms of the Fourier expansion that can be interpreted as hopping terms between different "unit cells" in Fourier space.

Due to the particular structure of the extended Floquet matrix, it can be shown that a truncation in the Fourier indices, approximating the infinite matrix with a finite one, can give accurate numerical solutions to Eq. 2.29. A physical intuition can be gained by mapping the form of the Floquet Hamiltonian in the representation 2.30 to a Wannier-Stark ladder. An illustration of such a mapping is showed in Fig. 2.1. Consider a simple periodic perturbation, so that the only nonzero matrix element will be $H_{\pm 1}$ (harmonic drive). This gives the matrix a tridiagonal structure. Then, the structure of the Hamiltonian can be considered as analogous to the one of a tight-binding lattice with nearest-neighbour hopping, with a uniform potential along the lattice –for more details, see e.g. [71]. Assuming H_0 to be finite-dimensional, the presence of the $n\hbar\omega$ terms, which create the Fourier ladder, have the effect of effectively localising the eigenstates in Fourier space: depending on the frequency and the spectral properties of the Hamiltonian, higher-order modes become effectively inaccessible with the Fourier-space mode decaying exponentially fast –see the Appendix in [72] for more details. Practically, the difference between the numerical approximation of the Floquet modes coming from the truncation of the Hamiltonian and the true eigenmodes can be made arbitrarily small by increasing the range of the Fourier coefficients taken into account. However, as shown in [71], the truncation in Fourier space might not be a good approximation in the limiting case of small ω, and further resonance effects appear in this case (see section 3.6 for a more detailed discussion on this limit).

To conclude this section, it is appropriate to summarise how the dynamics of a time-dependent system can be obtained numerically through Floquet theory:

- Calculation of the one-period unitary evolution operator as defined in Eq. 2.11, through brute-force integration of the TDSE. Since the Floquet modes are eigenstates of this operator, they can be obtained through diagonalisation, together with the corresponding eigenvalues. Furthermore, having access to the one-period unitary evolution operator allows, in principle, to obtain the exact dynamics of the problem from any initial state.

- The time periodicity of the Floquet modes themselves can be exploited to transform the time-integration procedure for the unitary operator into a problem of a diagonalisation of a unique Hamiltonian, which is defined in the extended space $\mathscr{H} \otimes \mathscr{T}$. This amounts to solving the Floquet mode equation 2.5 in the Shirley matrix representation 2.30. This methodology is usually preferred for numerical calculations since, while the size of the Hamiltonian in the extended Hilbert space is in principle infinite (due to the Fourier expansion), in fact its structure means that the numerical result converge very effectively when truncating it over a finite range of indices in Fourier space.

2.2 The t-t' formalism and Floquet Green's function

As highlighted in the previous section, the Floquet Hamiltonian $\mathscr{H}(t') = H(t') - i\hbar\partial_{t'}$ operates in the extended Hilbert space $\mathscr{R} \otimes \mathscr{T}$, and the stationary states $|\Phi_\alpha(t')\rangle$ obey a time-independent-like Schrödinger equation given by Eq. 2.5. In fact, the parameter t' corresponds to the real time t only if it is made to be equal to the evolution time parameter t of the TDSE, in a framework referred to as the t-t' formalism. This formalism can actually be applied to compute the evolution of Hamiltonian that is not periodic in time: this is possible when, in considering the normalisation length τ for the space $\mathscr{T}$, one makes it very large, and the single-period unitary operator can actually approximate the true system evolution very well.

In this formalism, one considers a two-time state which satisfies a $t-independent$ Schrödinger equation associated with $\mathscr{H}(t')$

$$i\hbar\frac{\partial}{\partial t}|\chi(t',t)\rangle = \mathscr{H}(t')\,|\chi(t',t)\rangle\,. \tag{2.31}$$

By separation of variables the state can be written as

$$|\chi(t',t)\rangle = e^{-i\varepsilon_\alpha t/\hbar}\,|\Phi_\alpha(t')\rangle\,, \tag{2.32}$$

which, combined with 2.31 gives the mode equation 2.5. From this, the Floquet state $|\psi(t)\rangle = |\chi(t'=t,t)\rangle$ can be obtained, thus solving the TDSE with Hamiltonian $H(t)$ [67].

In fact, this formalism provides a different perspective on the fact that the time-independent-like Schrödinger equation in the extended space provides all the required information for the full time evolution of any initial state. Consider an initial state $\vec{\psi}(t=0) \equiv \vec{x}_\alpha$, an eigenstate of the Floquet Hamiltonian as defined in the matrix representation of the previous section in the extended space. Evolving the state in the auxiliary time variable t as in equation 2.32, which is conjugate to the quasienergy parameter ε_α, leads to

$$\vec{\psi}(t) = e^{-i\varepsilon_\alpha t/\hbar}\vec{x}_\alpha. \tag{2.33}$$

The components of $\mathbf{x}_\alpha$ are the components of the Fourier expansion of the time-periodic Floquet modes 2.22, so they can be mapped back from the extended space to $\mathscr{H}$, with the equation above becoming

$$|\psi(t)\rangle = e^{-i\varepsilon_\alpha t/\hbar}\sum_m e^{im\omega t'}\,|\phi_{\alpha,m}\rangle\,, \tag{2.34}$$

which, setting $t = t'$ as the physical time, becomes the physical state at time t.

From now on, when considering the Floquet mode equation, the t-t' formalism will be assumed. This means that the above process of setting the auxiliary time to be equal to the physical time at the end of the calculation (for the solution of the TDSE) will be implicitly assumed. As a consequence, the usual techniques of the time-independent formalism can be used to find the stationary solutions, without the need of the time-ordering procedures implied by the unitary evolution operator in Eq. 2.11. The Green's function corresponding to the Floquet Hamiltonian for the extended Hilbert space can be defined as [73]

$$[\varepsilon - \mathscr{H}(t)]\mathscr{G}(\varepsilon|t,t') = \delta_\tau(t-t'), \tag{2.35}$$

with δ_τ being the τ-periodic delta function. Using completeness of the Floquet modes in $\mathscr{R}\otimes\mathscr{T}$, the Green's function can be expressed as

$$\mathscr{G}(\varepsilon|t,t') = \sum_p \int d\varepsilon_\alpha \frac{|\Phi_{p\alpha}(t)\rangle \langle\Phi_{p\alpha}(t')|}{\varepsilon - \varepsilon_{p\alpha}}, \tag{2.36}$$

where the integral notation stands for a sum over α, taking into account the case of a continuum of eigenstates $|\Phi_\alpha(t)\rangle$, running over the 1$^{\text{st}}$ BZ in quasienergy, and $|\Phi_{p\alpha}(t)\rangle$ and $\varepsilon_{p\alpha}$ are defined as in 2.7 and 2.8. The summation in the index p makes sure that the whole quasienergy spectrum is covered. Note that the Green's function depends on the quasienergy parameter ε, while still depending on the time variables. This appears unusual, since the energy (or frequency) is usually the conjugate of the time parameter, and the spectral form of the Green's operator should therefore be independent of time. This is, in fact, another demonstration of the key aspect of the t-t' formalism for Floquet theory; the quasienergy ε is the conjugate of the auxiliary time t of Eq. 2.31, while t and t'[1], in the above expression, represent actual time variables, on the same footing as spatial variables in the generalised Hilbert space. The t-t' Green's function for time-periodic Hamiltonians allows for the formulation of the electronic stopping problem, which is formalised in Chapter 4.

Noting that this Green's function is periodic in both t and t', and that the periodicity comes from the complete set of Floquet modes $\{\Phi_{p\alpha}(t)\}$, the Fourier representation of the Green's function in $\mathscr{R}\otimes\mathscr{T}$ can be found. By expanding the modes in Fourier series as in Eq.

[1] In [73], in fact, t and t' are labelled as t' and t'', to avoid confusion with the auxiliary time t. However, here the above notation will be kept to simplify the expressions in the next latter chapters, while keeping in mind the fact that all of the related expressions are considered in the extended space $\mathscr{R}\otimes\mathscr{T}$

2.22, the Fourier components are obtained

$$\mathscr{G}_{m,n}(\varepsilon) = \sum_p \int d\varepsilon_\alpha \frac{|\phi_{p\alpha,m}\rangle \langle \phi_{p\alpha,n}|}{\varepsilon - \varepsilon_{p\alpha}}. \tag{2.37}$$

This representation allows, upon the introduction of the projectile, for the implementation of familiar techniques used for the solution of impurity problems using Green's functions: this is possible because the Fourier index n of the expansion, within the context of the generalised Hilbert space $\mathscr{R} \otimes \mathscr{T}$ introduces an effective additional dimension in the problem, which can be regarded as introducing a tight-binding coupling in energy space [74]. Hence, methods for the tight-binding Green's function formalism can be adapted to suit the problem [75]. This will be exploited in Chapter 5, where a tight-binding Floquet model for stopping calculations in crystalline solids will be introduced.

Green's function methods are generally very useful since they provide information about the whole spectrum of excitations in a system. In addition, the Floquet Green's function formalism is well suited to generalise the theory from the noninteracting single particle picture to interacting many-body systems out of equilibrium. This can be achieved, for instance, through a nonequilibrium dynamical mean field formalism, including self-energy corrections and dissipation to external heat baths [76].

2.3 Some properties of Floquet systems

In recent years, Floquet theory has been widely used in the description of periodically driven systems: since the physics of systems out of equilibrium in quantum mechanics is in general difficult to describe beyond the linear response regime, Floquet theory can naturally take into account higher-order effects; the Floquet matrix of Eq. 2.25, which encodes the solutions to the nonequilibrium problem, can be computed quite efficiently as explained in section 2.1.

One of the most important features of Floquet systems, which is clear from the time-independent-like formalism just introduced, is that the quasienergy is conserved (or, equivalently, the energy is conserved up to an integer number of $\hbar\omega$) in the same way as quasimomentum is conserved in Bloch theory. In the case of an external drive such as a monochromatic electric field, this can be interpreted with the exchange of photons of energy $\hbar\omega$ [67]. Therefore, depending on how many Fourier indices are retained in the Floquet matrix, the theory can in principle include processes involving an arbitrary number of photon exchanges. This picture corresponds, in systems where photon exchange processes are not involved, to highly nonlinear energy exchange processes, which is the reason why Floquet theory can be

very useful for nonperturbative calculations. The off-diagonal elements in the Floquet matrix correspond to the probability amplitude of transition from a Floquet mode to another, i.e. the probability of a state transitioning to another mode from the influence of the driving field, while the diagonal elements correspond to the case in which the state remains in the same mode.

While the total energy is not conserved due to the broken time-translation symmetry, the averaged energy can still be expressed over a τ-cycle for a Floquet state $\Psi_\alpha(t)$ as [67]

$$\begin{aligned}\langle E_\alpha(t)\rangle_t &= \frac{1}{\tau}\int^{\tau} dt\,\langle\Psi_\alpha(t)|H|\Psi_\alpha(t)\rangle \\ &= \sum_m (\varepsilon_\alpha + m\hbar\omega)\,\langle\phi_{\alpha,m}|\phi_{\alpha,m}\rangle\,.\end{aligned} \tag{2.38}$$

Therefore, energy is accumulated in each of the harmonic components of the Floquet state. This is connected to the fact that, in general, isolated Floquet systems approach an infinite-temperature state, caused by an "unbounded heating" due to the periodic drive. This effect is caused by the fact that, in analogy with static ergodic systems, in Floquet systems the entropy tends to be maximised. However, in the absence of other local conserved quantities, the entropy grows without bound and eventually yields the infinite-temperature state [77–79], regardless of the starting conditions. Hence, all the expectation values of local observables synchronise with the period of the drive [80]. This result can be derived from the expectation value of some local observable $O(t) = \langle\Psi(t)|\hat{O}(t)|\Psi(t)\rangle$, where the wavefunction can be expanded in Floquet basis as in Eq. 2.14 yielding

$$O(t) = \sum_\alpha |c_\alpha|^2 O_{\alpha,\alpha}(t) + \int f_O(\omega) e^{-i\omega t} d\omega, \tag{2.39}$$

where $O_{\alpha\beta} = \langle\Phi_\alpha(t)|\hat{O}(t)|\Phi_\beta(t)\rangle$ and $f_O(\omega) \equiv \sum_{\alpha\neq\beta} O_{\alpha\beta}(t) c_\alpha^* c_\beta \delta(\hbar\omega - (\varepsilon_\beta - \varepsilon_\alpha))$. The second term, describing fluctuations of the off-diagonal elements, vanishes by the Riemann-Lebesgue lemma in the thermodynamic limit when the Floquet quasienergy spectrum approaches a continuum [80]. This observation can be applied to both interacting and non-interacting systems. Hence, there have been many efforts, both from the theoretical and experimental sides, to understand whether this unbounded increase in entropy can be avoided for many-body interacting systems and whether ordered, stable phases of matter can be achieved in Floquet systems; if this is the case, how can they be formed and stabilised? In addition to these fundamental questions regarding the long-time behaviour and stability of the Floquet modes, one of the most important features of driven systems is that they allow *Floquet engineering*.

The Floquet engineering concept is, in a way, to reverse the logic of the Floquet formalism introduced earlier in the Chapter, which is to start from a time-periodic Hamiltonian of interest, calculate the one-period evolution $\mathscr{U}_0(t_0+\tau,t_0)$, and access the Floquet Hamiltonian that gives the *stroboscopic* evolution of the system (the evolution at times separated by a multiple of the period). Instead, a time-periodic Hamiltonian could be constructed purposefully in order to achieve an effective Floquet Hamiltonian with the desired properties. These may include the formation and modification of nontrivial topological phases of matter, the enhancement and suppression of tunneling, the creation of artificial gauge fields in optical lattices, just to give some examples [67, 81–85].

One important effect in Floquet systems is dissipation. For instance, in Floquet engineering experiments involving optical lattices and cold atoms, it is possible to control and minimise coupling with the external environment. While such systems allow for a good level of control on the effective Hamiltonian, most application require engineered properties to be stable against dissipation and interactions with external environments.

An important class of systems that shows ordered phases, related to Floquet systems for their realisation, is the one of *time crystals*, which were first proposed by Frank Wilczek in 2012 [86, 87]. The original proposal was that, in the same way in which the continuous space symmetry is broken by crystals in space, the continuous time-translation symmetry might be spontaneously broken in closed quantum systems, leading to physical observables showing persistent periodic oscillations in the ground state. Wilczek's proposal was swiftly disproved for the ground state of systems in equilibrium [88, 89]. The current definition of a time crystal is the one of a state with a periodic two-time correlation functions between different spatial points, such as $\mathscr{C}_{ij} = \langle \sigma_i^z(t)\sigma_j^z(0)\rangle$, or $\langle m(x,t)m(x',0)\rangle$ with order parameter m oscillating periodically in time. The reason why the correlation needs to be considered between different spatial points is that one wants to ensure that the periodic correlation is nontrivial, by which it is meant, for example, the oscillation performed by a two-level system, or a set of independent two-level systems. With the above definitions, it is ensured that the observed correlation happens in both space and time [90].

However, even though time crystals as spontaneously appearing as ground states of equilibrium systems were ruled out, the no-go theorem in [88, 89] does not preclude nonequilibrium systems from achieving a time-crystalline phase. This prompted research from both theorists and experimentalists, leading to the discovery of the novel nonequilibrium phase named π-spin glass, or discrete time crystal (DTC) [91–96]. The avoidance of unbounded energy increase, which is fundamental for the stabilisation of the DTCs, can be achieved by disorder-induced localisation or coupling with an external environment.

In the nondissipative cases, where disorder-induced localisation is used to ensure that the infinite temperature state is avoided, Floquet eigenstates have, in addition, a discrete-symmetry broken spatial glassy order and are separated by π/τ in quasienergy, showing oscillations with a period that is a multiple of the period of the Hamiltonian, leading to a lower symmetry [93]. However, coupling such a system with some external dissipative (Markovian) environment in general destroys the time crystalline phase [97]. Nonetheless, it has been shown [98] that dissipation can actually stabilise the ordered phases, such as DTC, in Floquet systems.

From the next Chapter, the description of electronic excitations in stopping processes caused by a projectile shooting through a crystalline material will be approached through Floquet theory. The stroboscopically stationary Floquet solutions can be connected to the steady total energy increase observed in first-principles calculations using TDDFT, from which electronic stopping is calculated [99]. On the other hand, while the Floquet solutions will be shown to constitute a good basis for the modelling of stopping processes, they are not the only solutions that, in principle, the many-body electron system can admit. In fact, instabilities with the respect to the nonequilibrium steady states (Floquet modes) can be foreseen, such as periodic modulations or correlations. These, if they exist, could be interpreted as a time-crystal according to the definition that was given in the previous paragraph. Indeed, a similar behaviour has been observed in TDDFT simulation for the stopping processes in self-irradiated nickel [47]: the projectile core electrons, for a certain range of projectile velocities, exhibit a nontrivial *flapping* instability response, whose frequency is independent of the projectile velocity. While this does not necessarily imply that the phenomenon can be classified as a DTC as it is currently interpreted and investigated in the literature, it is definitely a many-body effect that shows a nontrivial time periodicity –assuming that it is not an artifact of the TDDFT simulation. While the investigation of Floquet DTCs is not the focus of in the present thesis, it is a very important field of research, with many unanswered questions. Some of the most interesting phenomena regarding DTC, and nonequilibrium steady states in Floquet systems are intrinsically many-body in nature. As mentioned in section 1.8, dynamical many-body effects seem to also play an important role in the theory of electronic stopping. Hopefully, getting a better description and insight on highly nonequilibrium processes such as electronic stopping power will also help answer some of the fundamental questions regarding these interesting and exotic nonequilibrium quantum systems.

Chapter 3

Floquet theory of a projectile in a crystal

In this Chapter, the problem of a projectile shooting through a crystal is mapped, via a Galilean transformation to the projectile frame, to a time-periodic problem which can be analysed using Floquet theory. A parabolic band model, approximating the effective band structure of insulators and semiconductors, is presented and analysed based on quasienergy conservation. From this simple model a novel interpretation of the threshold velocity effect emerges: it is shown that, while transitions across the gap are in theory allowed for any finite velocity of the projectile, the appearance of an effective threshold behaviour can be linked to the suppression of the scattering rate of transitions to higher-order Floquet modes. While this type of behaviour is quite hard to resolve experimentally, the model provides an alternative interpretation to the established semi-classical and linear-response based approaches.

3.1 Moving to the projectile reference frame

The theory for jellium [1, 16, 23, 24], which was introduced in Chapter 2, is implicitly built on the fact that the problem of a projectile of constant velocity $\mathbf{v} = v\hat{\mathbf{v}}$ moving in a homogeneous electron liquid, although a time-dependent, nonconservative problem, retains a continuous symmetry and related conservation, which neither stems from time nor space homogeneity, but rather from invariance along a space-time diagonal. The change to the projectile reference frame aligns this trajectory with the time axis and the problem becomes energy conservative, while still dissipative in the laboratory frame. This was illustrated in Fig. 1.1, where the frame transformation clearly maps the problem into the one of a static impurity in a homogeneous system. Consider the same projectile in a crystalline periodic solid, with a spatial periodicity a along its trajectory. The translational invariance becomes discrete along the same line of space-time: the system is invariant under combined space-time translations $\mathscr{T}^* : \mathbf{r} \to \mathbf{r} + na\hat{\mathbf{v}},\ t \to t + n\tau$ with $n \in \mathscr{Z}$, and $\tau = a/|\mathbf{v}|$. Moving to the

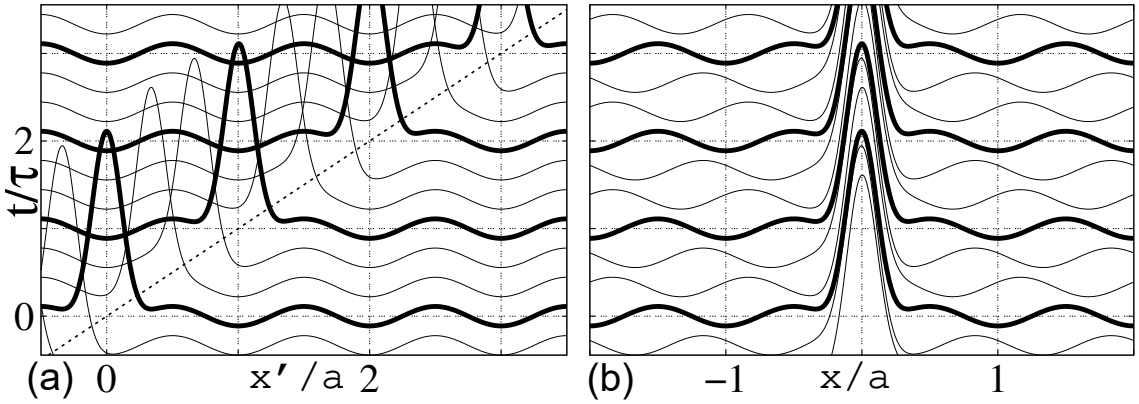

Fig. 3.1 Evolution of crystalline plus projectile potential in one dimension, in (a) the laboratory reference frame and in (b) the projectile. a is the lattice parameter, $\tau = a/v$, and v is the projectile velocity (slope of dotted line). The curves (potential vs x) are shifted for different times. Thicker lines indicate times separated by τ. Compare this with figure 1.1 of Chapter 1, which highlights the difference between the continuous translational invariance of the projectile trajectory in a homogeneous system and the discrete translational invariance of the trajectory in a periodic system.

projectile reference frame, the problem becomes purely time-periodic with period τ and the previous $\mathscr{T}^*$ symmetry becomes $\mathscr{T} : t \to t + \tau$ (Fig. 3.1). In this frame, both the electrons in the target and the crystalline potential move past the projectile with velocity $-\mathbf{v}$. The $\mathscr{T}$ symmetry is the main point exploited in this Thesis as it allows the use of Floquet theory for time-periodic Hamiltonians [66, 67].

Consider a general potential landscape in the laboratory frame, including the crystal and projectile,

$$V_{\text{lab}}(\mathbf{r}',t) = V_0(\mathbf{r}') + V_P(\mathbf{r}',t), \tag{3.1}$$

where $V_0(\mathbf{r}')$ is the crystal potential and $V_P(\mathbf{r}',t) = V_P(\mathbf{r}' - \mathbf{v}t)$ describes a projectile with velocity $\mathbf{v}$. This gives the $\mathscr{T}^*$ symmetry introduced earlier for the associated Hamiltonian $H_{\text{lab}}(\mathbf{r}',t)$. In the reference frame moving with the projectile, $\mathbf{r} = \mathbf{r}' - \mathbf{v}t$, the potential becomes

$$V(\mathbf{r},t) = V_0(\mathbf{r} + \mathbf{v}t) + V_P(\mathbf{r}), \tag{3.2}$$

which is associated with an Hamiltonian $H(\mathbf{r},t)$ that is time-periodic with period $\tau = a/|\mathbf{v}|$. Primed and unprimed indices indicate lab and projectile reference frame respectively, in a notation that will be kept throughout the Thesis. The fact that the projectile potential $V_P(\mathbf{r})$ is assumed to be localised around the origin [$V_P(\mathbf{r}) \to 0$ as $|\mathbf{r}|$ gets large] allows for a treatment that generalises the scattering theory for jellium, which will be fully formalised in Chapter 4.

3.2 Galilean Transformations in quantum mechanics

A Galilean transformation to the projectile reference frame allows very intuitively to understand how the problem can be in principle treated using Floquet theory for time-periodic Hamiltonians. However, let us step back for now and consider the system without the projectile: a Galilean transformation of the crystal alone. The problem is still manifestly Floquet from the argument of the previous section. In addition, it is not only the potential that is transformed, but also the electron states in the crystal. In practice, the eigenstates of the static crystals, transformed in a new reference frame moving at velocity $\mathbf{v}$ in a periodic direction, must be eigenstates of the Floquet Hamiltonian in the new frame. Therefore, the solutions of the Floquet problem are readily available from a simple Galilean transformation of the crystal wavefunctions.

Hence, consider how a quantum mechanical wavefunction transforms when moving to a reference frame moving at velocity $\mathbf{v}$. The velocity regime in the stopping problem is assumed to be nonrelativistic throughout the rest of the Thesis, making Galilean transformations applicable. Indeed, the lightest ions that are usually considered in TDDFT simulations are hydrogen nuclei, and in the typical velocity regimes of TDDFT simulations relativistic effects can be considered negligible [2]. In addition, when studying the threshold velocity effect, the energies are in the order of a few tens of keV. However, it is clear that this assumption will not hold for kinetic energies in the GeV range, as for the case of cosmic rays. The energy loss of ions in such energy ranges are usually investigated trough Monte Carlo methods (see e.g. the `Geant4` platform [100, 101]). Nonetheless, an extension of the Floquet formalism presented in this Thesis to include relativistic Lorentz transformations could be in principle formulated, and would represent a very interesting research direction.

The problem of applying a Galilean transformation to quantum mechanical wavefunctions is very well known, and the form of the transformed wavefunctions can be derived very simply (Landau [55]). The transformation of a general wavefunction $\psi'(\mathbf{r}',t)$ in the lab frame to $\psi(\mathbf{r},t)$ in a moving frame can be found by considering the transformation of a free particle (plane wave). Since plane waves can be used as a basis set for any arbitrary wavefunction, the transformation that is found for the plane wave corresponds to the general one. The two plane waves

$$\begin{aligned} \psi'(\mathbf{r}',t) &= C \times e^{\frac{i}{\hbar}(\mathbf{p}'\cdot\mathbf{r}'-E't)}, \\ \psi(\mathbf{r},t) &= C \times e^{\frac{i}{\hbar}(\mathbf{p}\cdot\mathbf{r}-Et)}, \end{aligned} \tag{3.3}$$

where C is a normalisation constant, m is the mass of the particle and $\mathbf{r} = \mathbf{r}' - \mathbf{v}t$, can be connected using the expressions $\mathbf{p} = \mathbf{p}' - m\mathbf{v}$ and $E = E' - \mathbf{v}\cdot\mathbf{p}' + \frac{1}{2}mv^2$ relating the particle momenta and energies between the two frames. Upon substitution, the wavefunction transformation takes the form

$$\psi(\mathbf{r},t) = \psi'(\mathbf{r}+\mathbf{v}t,t)e^{\frac{i}{\hbar}(m\mathbf{v}\cdot\mathbf{r}+\frac{1}{2}mv^2t)}, \tag{3.4}$$

which is the one that is valid for any arbitrary wavefunction.

In fact, the same result can be derived considering the unitary operator U_G enforcing the Galilean boost

$$U_G = e^{\frac{i}{\hbar}\mathbf{v}\cdot(\hat{\mathbf{p}}t - m\hat{\mathbf{r}})}, \tag{3.5}$$

which can be checked to give the correct transformations for the variable operators

$$\begin{aligned} U_G^\dagger \hat{\mathbf{r}} U_G &= \hat{\mathbf{r}} - \mathbf{v}t; \\ U_G^\dagger \hat{\mathbf{p}} U_G &= \hat{\mathbf{p}} - m\mathbf{v}; \end{aligned} \tag{3.6}$$

the transformed wavefunction is then found through

$$|\psi\rangle = U_G\,|\psi'\rangle\,. \tag{3.7}$$

Furthermore, the Galilean boost operator allows for a convenient derivation of the transformed Hamiltonian: given that the TDSE needs to be satisfied in both reference frames, the transformed Hamiltonian must take the form

$$H = U_G H' U_G^\dagger + i\hbar(\partial_t U_G)U_G^\dagger. \tag{3.8}$$

By expressing the unitary operator in the form [1]

$$U_G = e^{\frac{i}{\hbar}(\frac{1}{2}mv^2t)}e^{\frac{i}{\hbar}\hat{\mathbf{p}}\cdot\mathbf{v}t}e^{-\frac{i}{\hbar}m\mathbf{v}\cdot\hat{\mathbf{r}}}, \tag{3.9}$$

the transformed Hamiltonian in Eq. 3.8 can be rewritten as

$$H = U_G H' U_G^\dagger - \mathbf{v}\cdot\hat{\mathbf{p}} - \frac{1}{2}mv^2. \tag{3.10}$$

To check explicitly with a simple example that this is indeed the correct form of the transformed Hamiltonian in the moving frame, consider again a free particle, which is an eigen-

[1] The expression is derived by making use of the identity $e^{s\hat{X}}e^{s\hat{Y}} = e^{s(\hat{X}+\hat{Y})+s^2[\hat{X},\hat{Y}]/2}$ for the case in which $[\hat{X},\hat{Y}]$ commutes with both $\hat{X}$ and $\hat{Y}$.

state of the momentum operator $\hat{\mathbf{p}}\,|\psi'_{\mathbf{p}'}\rangle = \mathbf{p}'\,|\psi'_{\mathbf{p}'}\rangle$, whose energy in the transformed frame is calculated, using the identities 3.7 and 3.6 as

$$\begin{aligned}\langle\psi_{\mathbf{p}}|H|\psi_{\mathbf{q}}\rangle &= \langle\psi_{\mathbf{p}}|U_G H' U_G^{\dagger}|\psi_{\mathbf{q}}\rangle - \mathbf{v}\cdot\langle\psi_{\mathbf{p}}|U_G \mathbf{p} U_G^{\dagger}|\psi_{\mathbf{q}}\rangle - \frac{1}{2}mv^2\delta(\mathbf{p}-\mathbf{q}) \\ &= \left(E'_{\mathbf{p}} - \mathbf{v}\cdot\mathbf{p}' + \frac{1}{2}mv^2\right)\delta(\mathbf{p}-\mathbf{q}),\end{aligned} \tag{3.11}$$

which is indeed the correct transformation for the energy in the moving frame.

3.3 Transformation of Bloch states

It is time to consider the more interesting case of Bloch electrons, which provides the solutions to the Floquet problem without the projectile. In the laboratory frame, the Bloch states can be expressed, in the usual notation, as

$$\psi'_{n\mathbf{k}}(\mathbf{r}') = e^{i\mathbf{k}\cdot\mathbf{r}'}u_{n\mathbf{k}}(\mathbf{r}'), \tag{3.12}$$

with energy $E_n(\mathbf{k})$, band index n, and $u_{n\mathbf{k}}(\mathbf{r}')$ is a periodic modulation. The Galilean transformation of Eq. 3.4 brings the Bloch states into the form

$$\psi_{n\mathbf{k}}(\mathbf{r},t) = e^{-i\varepsilon_n(\mathbf{k})t/\hbar}e^{i(\mathbf{k}-m\mathbf{v}/\hbar)\cdot\mathbf{r}}u_{n\mathbf{k}}(\mathbf{r}+\mathbf{v}t), \tag{3.13}$$

where m is the electron mass. The quasienergy

$$\varepsilon_n(\mathbf{k}) = E_n(\mathbf{k}) - \hbar\mathbf{k}\cdot\mathbf{v} + mv^2/2 \tag{3.14}$$

and the Floquet modes, which shall be named *Bloch-Floquet modes* henceforth,

$$\phi_{n\mathbf{k}}(\mathbf{r},t) = u_{n\mathbf{k}}(\mathbf{r}+\mathbf{v}t)e^{i(\mathbf{k}-m\mathbf{v}/\hbar)\cdot\mathbf{r}} \tag{3.15}$$

are immediately identified by comparison with Eq. 2.1. Fig. 3.2 illustrates an example of a two-band system Floquet quasienergy spectrum. The Floquet BZ for quasienergy can be chosen to coincide with the BZ for the Bloch vectors: shifting $\mathbf{k}$ by $p\mathbf{G}_0$ [for $p \in \mathscr{Z}$ and $\mathbf{G}_0 = (2\pi/a)\hat{\mathbf{v}}$] shifts the quasienergy by $p\hbar\omega$, $\varepsilon_{pn}(\mathbf{k}) \equiv \varepsilon_n(\mathbf{k}+p\mathbf{G}_0)$ for the shifted Bloch-Floquet modes $\phi_{pn\mathbf{k}}(\mathbf{r},t)$. The 1st BZ defined in this way encodes all of the available states in the system. In principle, crystals have an infinite number of bands, which would make the equivalent picture of Fig. 3.2 much messier and unintelligible. In practice, one

is usually interested in transitions inside a limited range in energy: transitions involving higher-energy exchanges, which correspond in the Floquet picture to an higher number of exchanged photons, are not usually dominant. However, this assumption may lose validity when highly non-perturbative electron-projectile interactions must be considered.

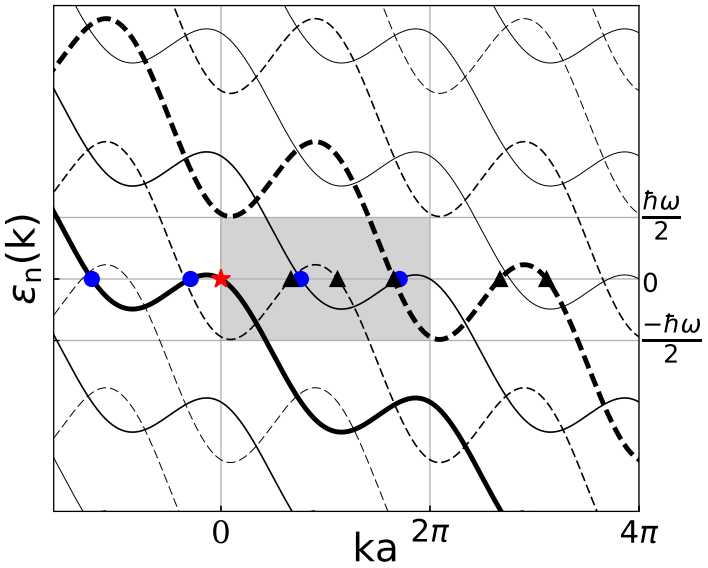

Fig. 3.2 Bloch-Floquet-mode quasienergies $\varepsilon_n(\mathbf{k}) = E_n(\mathbf{k}) - \hbar\mathbf{k}\cdot\mathbf{v} + \frac{1}{2}mv^2$ of a two-band model along the projectile-periodic direction in reciprocal space, extended zone scheme and Floquet replicas $\varepsilon_{pn}(\mathbf{k})$ included (thin lines), $v > 0$. The 1st BZ is highlighted in grey. Quasienergy conserving states are indicated for an incoming mode at $k = 0$ (red star). Blue circles and black triangles label allowed scattering modes in the lower and upper bands, respectively, both in the extended zone scheme (on thick curves) and folded back into the 1st BZ.

3.4 Asymptotic states in electronic stopping

In the theoretical modelling and most computational calculations of electronic stopping in projectiles, one of the key assumptions is that the ETR approaches a steady increase after a transient that can be neglected [99]. In fact, this steady-state assumption is either a direct consequence of the approximations made for the model, as for the case of nonlinear jellium [1, 16, 23, 25, 56] and linear-response [15], or it is observed numerically in first-principles (TDDFT) calculations. The existence of a regime that leads to a steady increase in energy (a constant or periodically oscillating ETR around a constant value for first-principles

calculations) follows directly from the fact that the projectile is forced to move at constant velocity. The projectile, swiftly moving along its path in the solid, continuously excites electrons that are in equilibrium.

Indeed, Floquet theory provides a solid theoretical grounding on why one should expect the existence of a steady-state regime. Since the introduction of the projectile does not change the periodicity of the Hamiltonian in the moving frame, the quasienergy of the Bloch-Floquet states remains a good quantum number. Stroboscopically steady states can be identified as eigenstates of the full Floquet Hamiltonian, since the system can be analysed using scattering theory in the Floquet modes obeying Eq. 2.5 in the extended Hilbert space $\mathscr{R} \otimes \mathscr{T}$. Hence, single-particle states obey

$$\mathscr{H}(\mathbf{r},t)\Phi_\alpha(\mathbf{r},t) = \varepsilon_\alpha \Phi_\alpha(\mathbf{r},t),$$

with

$$\mathscr{H}(\mathbf{r},t) = \mathscr{H}_0(\mathbf{r},t) + V_P(\mathbf{r}), \tag{3.16}$$

where $\mathscr{H}_0(\mathbf{r},t)$ is the Floquet Hamiltonian of the crystal without the projectile, whose eigenstates are given by the Bloch-Floquet states of Eq. 3.13. The eigenstates $\Phi_\alpha(\mathbf{r},t)$ of the full Floquet Hamiltonian $\mathscr{H}(\mathbf{r},t)$ can be described asymptotically as crystal Bloch-Floquet states of Eq. 3.13 that have the same quasienergy. For example, consider a one-dimensional (1D) system and the scattering process of a single mode. It is quite straight-forward to write down an expression for the asymptotic form of the solution; starting from an incoming Bloch-Floquet state $\phi_{nk_i}(x,t)$ coming from $x \to \infty$, using quasienergy conservation the allowed asymptotic Bloch-Floquet states can be found. This is shown schematically in Fig. 3.3. Practically, the asymptotic components can be found by solving

$$\varepsilon_m(k_f) = \varepsilon_n(k_i), \tag{3.17}$$

where k_f indicates the wavevector of the allowed asymptotic states and m indicates other quantum numbers, e.g. band index as before. In Fig. 3.2, for the case $\varepsilon_n(k) = 0$, the Bloch-Floquet asymptotic states that satisfy quasienergy conservation are highlighted.

In addition, scattering states must satisfy the appropriate (outgoing) boundary conditions: since the projectile is set to be fixed at $x = 0$, outgoing boundary conditions impose that the group velocity $v_g^m(k_f) = \hbar^{-1}\partial_k(E_m(k)) - v|_{k=k_f}$ should point away from the projectile for the asymptotic states (see Chapter 4 for more details). Therefore, the full Bloch-Floquet

scattering state, in the asymptotic regions $x \to \pm\infty$ takes the form

$$\Phi^{(+)}_{nk_i}(x,t) \sim \phi_{nk_i}(x,t) + \sum_{m,k_f} A_{k_i,k_f}\phi_{mk_f}(x,t), \tag{3.18}$$

subject to the above boundary conditions. The scattering amplitudes A_{k_i,k_f}, connecting the incoming with the outgoing Bloch-Floquet state, will be derived and defined in the next Chapter, together with the corresponding ones for the 3D formalism.

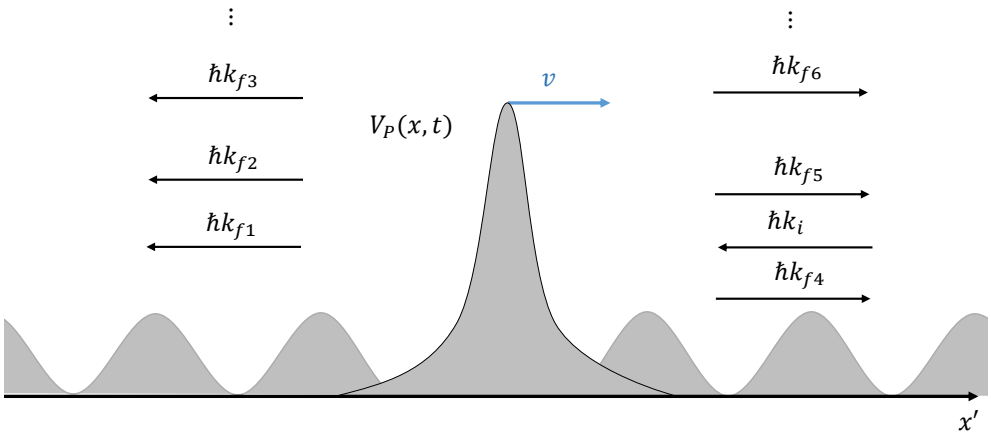

Fig. 3.3 Schematic representation of the scattering process of a 1D Bloch wave with quasi-momentum $\hbar k_i$ in the laboratory frame. While for free particles there are only two scattering channels (c.f. Fig. 1.2), quasienegy conservation for Bloch electrons allows for multiple scattering channels in general –see Eq. 3.19. The single-particle scattering states with wavevector k_f need to satisfy outgoing boundary conditions, as shown by the direction of the arrows.

Switching to 3D notation, quasienergy conservation implies, using the definition of Eq. 3.14, that

$$E_m(\mathbf{k}_f) - E_n(\mathbf{k}_i) = \hbar(\mathbf{k}_f - \mathbf{k}_i)\cdot\mathbf{v}\,. \tag{3.19}$$

This expression coincides to the one obtained from energy and momentum conservation in a binary collision of an electron with a projectile of mass $M_P \to \infty$ [38], and in perturbation theory [61], with the distinction that $\mathbf{k}$ values must be considered in the Bloch-Floquet extended zone/repeated band scheme (see Fig. 3.2). Despite the simplicity of this expression, its validity beyond the free-particle and perturbation theory had not be clearly shown. For allowed transitions between states with wavevectors $\mathbf{k}_i$ in the 1$^{\text{st}}$ BZ and $\mathbf{k}_f$ in the extended zone scheme at the p^{th} BZ, the energy of the electron-hole transition can be expressed as $\Delta E = \hbar(\mathbf{k}_f - \mathbf{k}_i)|_{1^{\text{st}}\text{BZ}} + p\hbar\omega$. This corresponds to the fact that the scattering process

involves transitions between different Brillouin zones, corresponding in the Floquet picture to transitions to higher or lower-order Floquet modes.

On a final note, the steady ETR regime that appears naturally from the above scattering arguments can be connected with the discussion in Section 2.3, where the problem of thermalisation in Floquet systems was introduced. This energy increase could be connected to the unbounded increase in energy leading to the infinite temperature state in strongly driven systems. At the same time, the stopping process is very different from the periodic driving of extended systems: the projectile, being a localised perturbation, will in general not be able to excite the electron system as extensively as, for instance, external induced fields such as a monochromatic lasers. In addition, the projectile swiftly moves in different parts of the solid, continuously exciting electrons that are in equilibrium. Therefore, when simulating stopping processes using finite-size boxes in first-principles calculations, the steady increase in energy may be interpreted as the manifestation of a stable prethermalisation regime. In Floquet systems, prethermalisation regimes are usually considered *metastable phases* before the infinite temperature state is achieved: it is in the prethermal time window is such systems that electron states with the desired properties can be engineered [102]. Therefore, in the "infinite box limit" in simulations, which corresponds to the idealised scattering picture that leads to the Bloch-Floquet steady states, the infinite temperature states can in fact never be reached due to the size of the crystal, and the fact that the interaction of the electron system with the projectile is quite localised. In addition, the possibility of reaching the infinite temperature state in the present model can be also thought as an artifact of forcing the motion of the projectile for the stopping calculations: in reality, the projectile slows down, and the projectile plus target energy is in fact conserved.

3.5 Phenomenology of the threshold effect using Floquet quasienergy conservation

The form of the solution of Eq. 3.18, together with the quasienergy conservation condition, can already provide a good phenomenological model of the stopping threshold effect observed in semiconductors and insulators introduced in Chapter 1.

Consider a model insulator with indirect gap as introduced in section 1.7. This simple model does not include plasmonic contributions to stopping, or quantitative predictions for the electron-hole contributions, which demand including electron-electron interactions. At this stage, however, the simple model already offers good insights into what to expect for the electron-hole excitation contribution in the nonlinear gapped case.

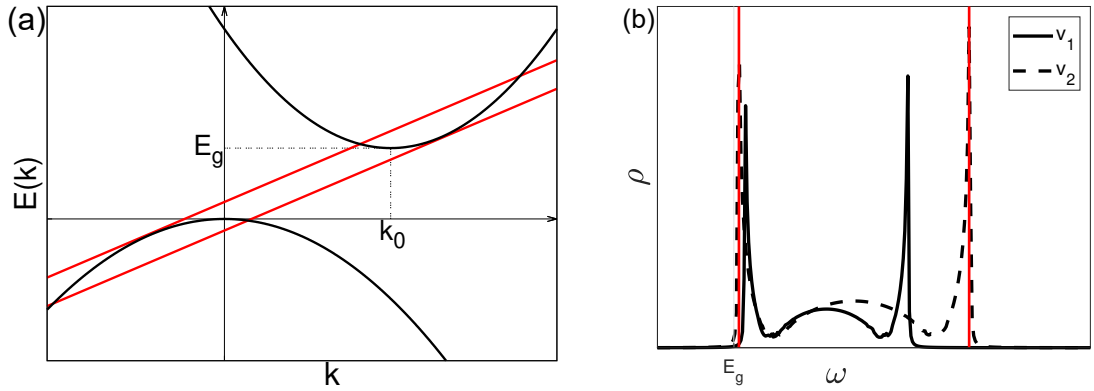

Fig. 3.4 (a) Model parabolic bands with indirect band gap, in 1D for illustration. Red lines delimit possible electron-hole pair transitions compatible with Eq. 3.17, with arbitrary projectile velocity $v > v_{th}$ defining their slope. (b) JDOS $\rho(\omega, v)$ vs excitation energy ω, for velocities $v_2 > v_1 > v_{th}$ for the same model. Red vertical lines highlight van Hove singularities.

A joint density of states (JDOS) can be defined in analogy with optical transitions [103]

$$\rho(\omega, v) = \sum_{nm} \int \frac{d\mathbf{k}_i}{(2\pi)^3} \int \frac{d\mathbf{k}_f}{(2\pi)^3} \delta(\Delta E_{mn,fi} - \mathbf{v} \cdot \Delta\mathbf{k}_{fi}) \delta(\Delta E_{mn,fi} - \hbar\omega), \tag{3.20}$$

where $\Delta E_{mn,fi} = E_m(\mathbf{k}_f) - E_n(\mathbf{k}_i)$ and $\Delta\mathbf{k}_{fi} = \mathbf{k}_f - \mathbf{k}_i$, offering interesting insights –see Fig. 3.4 for one dimension (1D), illustrative of the behavior in any dimensions. A two dimensional (2D) plot of the JDOS $\rho(\omega, v)$ is included in Appendix A. For the parabolic model in the figure, no stopping is allowed below a threshold velocity v_{th}, as described in section 1.7. When considering electron-hole excitations near the threshold velocity ($v \gtrsim v_{th}$) the scattering amplitude for transitions from states near the valence band maximum to states at the bottom of the conduction band can be assumed to be approximately constant: this gives an approximately constant scattering rate γ for the velocity range just defined. While more accurate estimations for the scattering rate in simulations for real materials might be needed, this approximation allows the derivation of some important results, and it is similar to approximations used to analyse direct electron-hole optical transitions [103]. Indeed, the JDOS near v_{th} can be integrated, assuming some constant scattering rate γ near the threshold, to get the approximate stopping power for the parabolic insulator

$$S_e(v) \propto \frac{1}{v} \int d\omega \rho(\omega, v) \hbar\omega = f(v)\Theta(v - v_{th}), \tag{3.21}$$

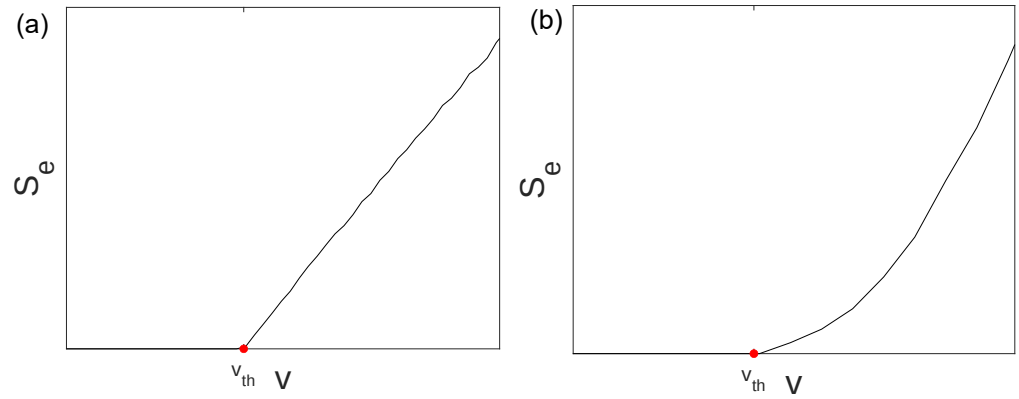

Fig. 3.5 Integrated JDOS illustrating the approximate behaviour of Eq. 3.21 for (a) the 1D parabolic insulator, showing a linear relationship between velocity and stopping power starting from v_{th}. (b) 3D case, in this case displaying a quadratic onset. Arbitrary units.

where $\Theta(x)$ is the Heaviside step function. When $v \gtrsim v_{th}$, $f(v) \propto v^m$, where m depends on dimension: from numerical calculations, using $\rho(\omega, v)$ as defined in Eq. 3.20 for the parabolic insulator model, $m = 1$ in 1D and $m = 2$ in three dimensions (3D). Figure 3.5 shows the numerical integration of Eq. 3.21, illustrating the functional form of $f(v)$ for the two cases in this simple model.

For an actual insulator, however, the threshold behavior is less clean. In fact, the adiabatic limit $v \to 0$ is quite nontrivial, as illustrated in Fig. 3.6: by quasienergy conservation (Eq. 3.19) transitions are allowed for arbitrarily small v even for gapped solids. This is shown in the figure using the repeated zone scheme, where the lines of allowed transitions decrease in slope with decreasing v.

The $S_e(v)$ curve is then characterized by a *series* of onset velocities, or partial thresholds, $v_{th}^{(p)}$, for $p \in \mathscr{Z}_{\geq 0}$ (slopes of red lines and red dots in the upper and lower panels of Fig. 3.6, respectively), defined by

$$E_g = \frac{1}{2}(m_e + m_h)(v_{th}^{(p)})^2 + \hbar(k_0 + \frac{2\pi}{a}p)v_{th}^{(p)} \ . \tag{3.22}$$

In the low-v limit (large p)

$$v_{th}^{(p)} \sim \frac{E_g}{2\pi/a}\frac{1}{p}. \tag{3.23}$$

In this limit, assume a decaying scattering rate γ_l for transitions to the l^{th} replica in the extended zone scheme. This assumption can be regarded as an adiabatic limit for the stopping power, since a $v \to 0$ limit should bring us back to the case of a static impurity (see section 3.6). For a projectile velocity $v \gtrsim v_{th}^{(l)}$, the electronic stopping power $S_e(v)$ can in principle be accurately approximated by a semi-infinite sum over the higher-order

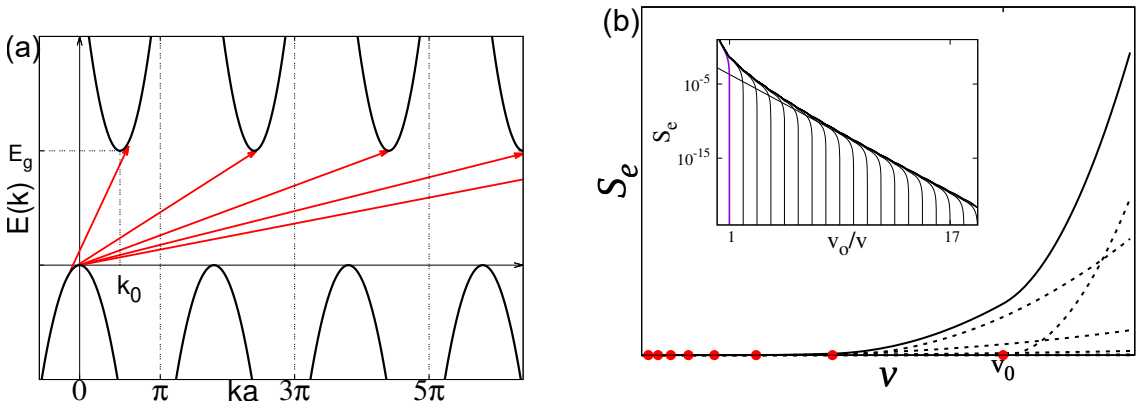

Fig. 3.6 (a) Partial threshold velocities (slopes of red lines, $v_{th}^{(p)}$) for replicas of parabolic bands in the extended zone scheme, corresponding to shifted Floquet modes, cf. Fig. 3.2. (b) Effective threshold behavior for S_e versus v in the small v limit, for a 3D indirect gap model with $\gamma_l \propto e^{-\alpha l}$. Red dots: $v_{th}^{(p)}$, v_0 is the threshold velocity for transitions within the 1$^{\text{st}}$ BZ. The solid line is the sum over all the contributions from the replicas (dashed lines). The inset: S_e (logarithmic scale) vs $1/v$, highlights the quick decay of stopping as $v \to 0$.

replica contributions. Each term of these contributions will have the form calculated for the single-parabola case, with a decaying coefficient given by the scattering rate γ_l; the expression for electronic stopping becomes

$$S_e(v_{th}^{(p)}) \approx \sum_{l=p}^{\infty} \gamma_l \, f(v_{th}^{(p)} - v_{th}^{(l)}). \tag{3.24}$$

Consider some examples for the behaviour of the scattering rates γ_l, whose behaviour depends on the strength of the projectile coupling through the scattering matrix elements for the transitions between occupied and unoccupied states, see section 4.4.3. As a prototype of slow decay, the algebraic form $\gamma_l \sim l^{-\mu}$ for some μ can be assumed. A much quicker decay may be given by the exponential form $\gamma_l \sim e^{-\alpha l^{\lambda}}$. In the former case, the electronic stopping can be expressed with the semi-infinite sum

$$S_e(v_{th}^{(p)}) \approx S_0 \sum_{l=p}^{\infty} \left(\frac{1}{p} - \frac{1}{l}\right)^m \frac{1}{l^{\mu}}, \tag{3.25}$$

where the expression 3.23 was used in Eq. 3.24. This sum can be approximated as an integral, leading to (details of the derivation in Appendix A)

$$S_e(v) \sim v^{m+\mu-1}. \tag{3.26}$$

Taking as an example the 3D case (m=2), it leads to $S_e \sim v^{\mu+1}$: from a very slow algebraic decay $\mu = 1$, one would expect a quadratic dependence $S_e \sim v^2$, with an increasing power in v as the scattering rate is made to decay more quickly. A exponential form for the decay implies

$$S_e(v) \sim e^{-(v^*/v)^\lambda}, \tag{3.27}$$

where v^* is a scaling constant. This form of the stopping decays much more quickly compared to the algebraic decay approximation, which would lead to an observed "hard" threshold.

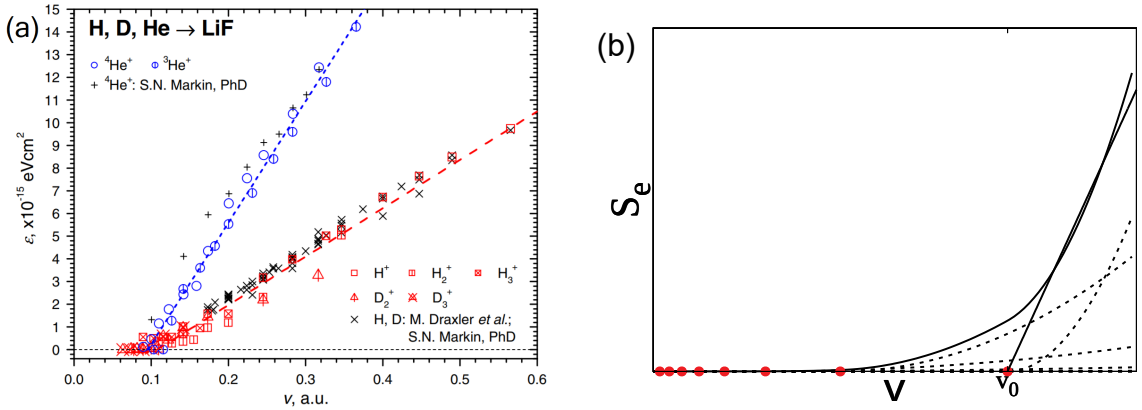

Fig. 3.7 (a) Experimental data (same as Fig. 1.3) showing the threshold behaviour of electronic stopping for the wide band-gap insulator LiF. Note that, at $v_{th} = 0.1$ a.u., the data points and their reported errors overlap with each other, and the behaviour close to the onset is not very clear, with the error bars becoming quite relevant. (b) Effective threshold behavior modelled from Eq. 3.24, where a line was fit to simulate an apparent linear onset for stopping starting at v_0, with transitions to higher-order replicas decaying coefficients.

Compare the right plot of Fig. 3.6 with the experimental results regarding threshold velocities in LiF [27]. In particular, Fig. 3.7 shows the experimental plot of Fig. 1.3, together with the exponential threshold decay of Fig. 3.6 in which a straight line has been fitted to simulate an apparent linear onset starting from the primary threshold velocity $v_{th}^{(0)}$. Indeed, while the stopping onset from the experimental data looks linear, the behaviour close to the onset, for projectile velocity $v = 0.1$ a.u., is not very clear, due to the reported uncertainty in the values. Indeed, the reported error bar of the experimental data is $\pm 0.2 \times 10^{-15}$ eVcm^2: compared to the scale of the right graph of Fig. 3.7, it would represent half of the y-axis. Therefore, while the relationship between S_e and v away from the onset is strongly dependent on the electronic properties of the specific target, the above results on the presence of an effective threshold, based on Bloch-Floquet scattering and quasi-energy conservation, could in theory capture a behaviour that has not, so far, been resolved by experiments. It would

be interesting to investigate, through further enhancements of the experimental techniques, or investigating other gapped materials which could show it more easily, whether such an effective threshold behaviour, showing a decaying tail for electronic stopping at velocities lower than the primary threshold, exists.

This result on the apparent threshold behaviour can be related to the work presented in [63] by Horsfield et al., which provides a theoretical modelling to the "electron elevator" mechanism through a dynamical state introduced in the band gap by a projectile ion, proposed on the basis of TDDFT simulations in [42] by Lim et al., and referred to in section 1.7. In [63], it is also found that transitions are allowed below the fundamental threshold, with transitions allowed at multiples of $\hbar\omega$ from unoccupied to occupied states, and hence no strict threshold. However, there are some fundamental differences between the model presented in this Thesis and the work in [63]. Firstly, in [63] the authors make use of the lowest-order perturbation theory, while the expression for stopping derived in section 4.4 is exact and independent of perturbation theory. Secondly, the Floquet Stopping model can in principle take into account the full electronic structure of the target, which was made possible by applying quasienergy conservation to the unperturbed Bloch states of the target material. In contrast, in [63] the target material was modelled as an ideal two-level insulator: the model for stopping is in fact closely related to the perturbative one of [61], which considers an ideal "flat band" insulator, with the difference that in [63] the single-particle states (orbitals) adiabatically adjust to the position of the projectile, thus modulating periodically. Nonetheless, the electron elevator model and the presented Floquet approach need not be incompatible with each other. Indeed, perturbation theory can be readily recovered from the exact, single-particle expression obtained through Floquet theory (see section 4.4.3). In this perspective, the model in [63] represents a special case of the full Floquet theory. Moreover, the presence of any projectile defect state appearing in the gap, which provides the proposed elevator mechanism, may in principle be probed through the Dyson equation formalism presented in Chapter 5 by considering, for instance, the local density of states in the proximity of the projectile.

3.6 The adiabatic limit

Looking back at the discussion over the stopping threshold, it is worth analysing in more depth the general problem of the adiabatic limit in Floquet systems, i.e. the limit for $\omega \to 0$. In the Bloch-Floquet scattering problem the scattering rates are assumed to decay when considering transitions to the higher-order replicas because, in the static limit, the problem becomes the one of a static impurity in a solid whose electronic system is in equilibrium, with no stopping. Moreover, in the limit $v \to 0$, it can no longer be safely assumed that the

timescale for the relaxation of the electronic excitations is much longer than the period τ determined by the projectile moving in a periodic lattice direction. In the nonlinear theory for jellium, the $v \to 0$ behaviour is better defined, since the spectrum of the homogeneous electron liquid is much simpler than the Bloch-Floquet picture which takes into account electronic band structures: indeed, $S_e \propto v$ leads to a well-defined adiabatic limit.

In order to get an intuition on the low-velocity limit in the Bloch-Floquet scattering picture, consider the simple two-band model, such as two-band picture of Fig. 3.2. In order to gain a better intuition, the bands can be represented in the Bloch repeated zone scheme –see Fig. 3.8– without losing generality, given the one-to-one correspondence between the repeated zone scheme in k and Floquet quasienergy space.

As the velocity v of the projectile is decreased, and therefore the periodicity of the Bloch-Floquet Hamiltonian that determines the scattering process is increased, the available asymptotic scattering states, given by the quasienergy conservation formula, become more distant in quasimomentum space: in the Floquet picture, only transition to higher-order modes are available. Indeed, when considering only two bands as in Fig. 3.8, while at higher velocities only a limited number of solutions for the asymptotic scattering states is available, when $v \to 0$ the number of possible solutions to the Floquet quasienergy conservation equation diverges. In fact, the limit $v \to 0^+$ can be regarded as a singular limit with respect to the solutions of the quasienergy conservation equation.

In fact, the adiabatic limit $\omega \to 0$ in Floquet theory is the subject of extensive discussions and theoretical work. A very interesting study of this limit is carried out by Russomanno and Santoro [71], who focus on the adiabatic limit of a periodically-driven spin-1/2 system in a magnetic field. The problem is mapped to a nearest-neighbour tight-binding form on a one-dimensional Floquet lattice, since the corresponding matrix form of the Floquet Hamiltonian is tridiagonal, given the harmonic form of the time-dependence in the Hamiltonian. Indeed, for harmonic Hamiltonians the Floquet matrix of Eq. 2.30, where H_0 describes a two-level system, takes the form

$$\mathscr{H} = \begin{bmatrix} \ddots & \vdots & \vdots & \vdots & \\ \dots & H_0-(n-1)\omega & H_1 & 0 & \dots \\ \dots & H_{-1} & H_0-n\omega & H_1 & \dots \\ \dots & 0 & H_{-1} & H_0-(n+1)\omega & \dots \\ \vdots & \vdots & \vdots & \vdots & \ddots \end{bmatrix}. \tag{3.28}$$

It can be regarded, in the Shirley-Floquet picture, as a tight-binding model in the extended Hilbert space $\mathscr{R} \otimes \mathscr{T}$, with the Fourier label n giving rise to the extra dimension as $\omega \neq 0$,

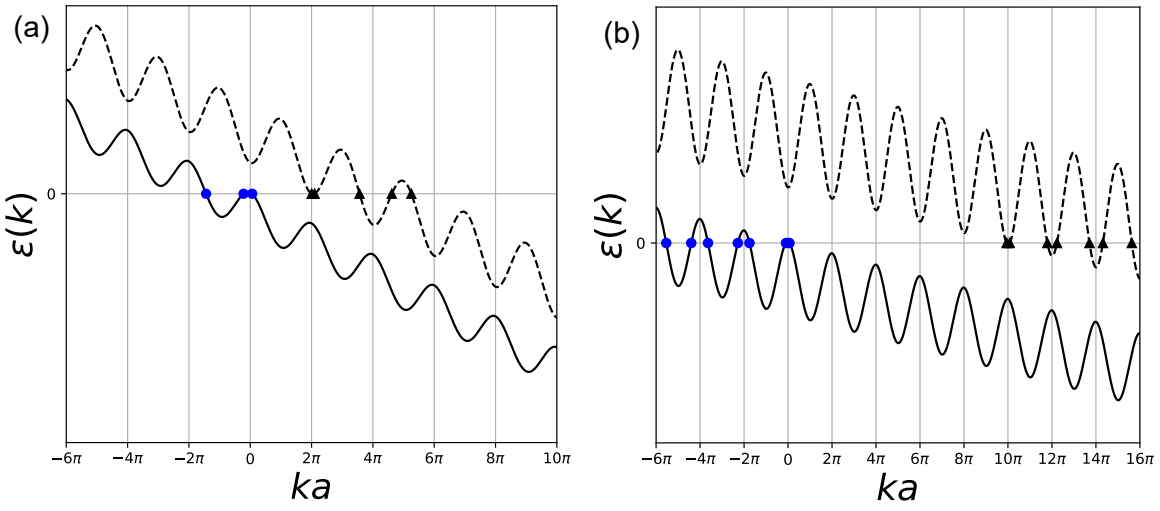

Fig. 3.8 Bloch-Floquet quasienergy spectrum in the repeated zone scheme for different projectile velocities, where v_1 [used in (a)] is greater than v_2 [used in (b)], arbitrary units. As with Fig. 3.2, blue circles and black triangles label allowed the solutions of the quasienergy conservation equation in the lower and upper bands, respectively, with quasienergy $\varepsilon = 0$. Note how the number of allowed modes increases as the projectile velocity is lowered, leading to a singular limit as $v \to 0$.

and creating a Floquet-Wannier-Stark ladder of spin doublets, with upper and lower spin components occupation undergoing Rabi oscillations that are caused by resonances. The resonances appear when the quasienergy of the Floquet mode related to the upper spin component is equal to an integer multiple of $\hbar\omega$ of the lower spin component quasienergy. In the limit $\omega \to 0$, there is a singular accumulation of resonances.

While this model is very different from the Bloch-Floquet scattering problem related to stopping, they do share some important similarities for the adiabatic limit. Indeed, the two-band Bloch-Floquet problem analysed in the previous section could be simplified by approximating the insulator as a collection of two-level atoms, as done in [61]. Even in the full two-band picture, the singular accumulation of allowed transitions at $v \to 0$, as illustrated in Fig. 3.8, can be connected to the singular accumulation of resonances in the limit $\omega \to 0$. However, as explained in Chapter 2, in general the matrix elements related to the scattering rates to such states decay quickly with the order of the Bloch-Floquet transition. Additionally, in [71] the effect of dissipation is analysed, and it is found that dissipation effects increase in the presence of resonances. In the low-velocity limit of the stopping problem, given the much slower timescale, it is very likely that the effect of dissipation would play an important role.

In fact, without the Floquet analysis of the threshold effect, it might appear that a threshold behaviour should not exist, not even as an effective threshold. Indeed, it might be tempting to treat the adiabatic limit in the following way: consider approximating the crystal as a collection of oscillators with given excitation energy ΔE as in [61]; when the velocity of the projectile is very small, it would only be able to induce localised excitations. In the true $v \to 0$ limit, a very large amount of time passes between the excitation at one of the oscillators and the next one, allowing for the the previous one to relax in the relevant dissipation channels. Assuming that the average excitation induced by the projectile has value ΔE, the stopping power is simply given by $S_e \sim \frac{1}{v}\Delta E/\tau = \Delta E/a$, i.e. it approaches a *constant* value, in clear contradiction with the threshold behaviour shown by experimental results and TDDFT calculations. However, it might be argued that, in fact, this constant value for stopping in the adiabatic limit would be too small for it to be accurately measured by experiments.

While the results presented in section 3.5 do not intend to represent the final word on the threshold velocity problem, I think that they provide an interesting perspective and starting point for discussion, apart from the stopping problem, even for the problem of adiabatic limit in Floquet systems. Indeed, so far, works in this direction have been mainly focused on the weak-perturbation regime [71, 104], and is clear that an effective description and understanding of this limit requite further investigations.

Chapter 4

Bloch-Floquet electronic stopping

In this Chapter, the Bloch-Floquet scattering theory introduced in Chapter 3, based solely on quasienergy conservation, is formalised. Firstly, a brief summary of the theory of free-particle scattering is provided, introducing the notation and the formalism which is then generalised to the Floquet problem. Then, the expressions for the single particle Bloch-Floquet scattering states and for electronic stopping power are derived for the 1D and 3D cases. It is shown that, in the appropriate limits, the expressions for stopping derived using perturbation theory and the non-linear model for jellium are recovered. The formalism will be presented for noninteracting particles, and the projectile will be represented by a local scalar potential. However, the model can be generalised to more realistic situations using time-dependent mean-field methods (such as Kohn-Sham) to include realistic crystals, projectiles, and electron-electron interactions. At the end of the Chapter, some of the limitations of the theory are discussed.

4.1 Summary of free-particle scattering

This section serves as a revision of free-particle scattering theory and its formalism, which will be useful to introduce the basic concepts that are generalised for the Bloch-Floquet scattering theory in the next sections. This section is inspired by the presentation in [105].

In elementary collision theory for free particles, the Hamiltonian is assumed to be of the form

$$H = H_0 + V, \tag{4.1}$$

where H_0 is the kinetic energy operator and the scattering potential V is assumed to be time-independent. As mentioned in Chapter 1, the eigenstates of the Hamiltonian are the scattering states defined by the Lippmann Schwinger equation 1.19, which is appropriate to

report here

$$|\mathbf{k}^{(\pm)}\rangle = |\mathbf{k}\rangle + g^{(\pm)}[E(\mathbf{k})]V\,|\mathbf{k}^{(\pm)}\rangle\,, \tag{4.2}$$

where the $\pm$ notation, labelling outgoing/incoming boundary conditions has been introduced. These states have the same eigenvalue $E(\mathbf{k})$ as eigenstates of H as $|\mathbf{k}\rangle$ for H_0. This can be interpreted by the fact that one can consider the energy-momentum free-particle eigenstate $|\mathbf{k}\rangle$ as being an incoming wave from the infinite past $t \to -\infty$, and that by energy conservation all the scattered components of the wave must have the same energy, with $|\mathbf{k}^{(\pm)}\rangle$ representing the plane wave evolved from $t \to -\infty$ by the scattering process with the potential. In fact, it is appropriate to remind that the states in Eq. 4.2 are *improper vectors*, which are not normalisable in the Hilbert space $\mathscr{R}$ of H, and therefore cannot represent physical states. Conveniently, though, for the purposes of scattering theory one can assume that they behave *as if* the eigenstates of H and H_0 are physical states. To see why this is the case more formally, the physically well defined wavepackets can be constructed by "smearing" the improper states in momentum space according to

$$\begin{aligned} |\phi^{(+)}\rangle &= \int d\mathbf{k}\phi(\mathbf{k})\,|\mathbf{k}^{(+)}\rangle\,, \\ |\phi\rangle &= \int d\mathbf{k}\phi(\mathbf{k})\,|\mathbf{k}\rangle\,, \end{aligned} \tag{4.3}$$

where the functions $\phi(\mathbf{p})$ are defined here to be amplitudes for the specific wavevector component, which make the wavefunction well-defined and normalisable, e.g. by making the state having the form of a Gaussian wave-packet. [1]

They satisfy the asymptotic conditions

$$\mathscr{U}(t)\,|\phi^{(\pm)}\rangle \underset{t\to\mp\infty}{\longrightarrow} \mathscr{U}_0(t)\,|\phi\rangle\,, \tag{4.4}$$

and the appearance of the unitary evolution operators related to the free-particle Hamiltonian H_0 and the full one H comes from the fact that they are in fact solutions of the TDSE. The physical significance of $|\phi^{(+)}\rangle$ is the following: if the *in-asymptote*, i.e. the incoming wavepacket from $t \to -\infty$, is $|\phi\rangle$, the actual state at $t = 0$ is $|\phi^{(+)}\rangle$. For $|\phi^{(-)}\rangle$, instead, the state at $t = 0$ is connected to the *out-asymptote*, which, practically, can be interpreted as

[1] A quick way to see how smeared plane waves are normalised is to invoke the Riemann-Lebesgue Lemma, which states that, for well-behaved functions $\phi(p)$, the integral

$$\lim_{x\to\infty}\int dp\phi(p)e^{ipx} \to 0,$$

which makes the wave-packet to be a well-defined state in $\mathscr{H}$, while the plane wave state $\psi(x) \sim e^{ikx}$ is not.

a computation "backwards in time". The use of the former expression for the scattering state will be preferred since its physical interpretation as a superposition of an "unperturbed" incoming wave and the disturbance caused by the scattering potential is more intuitive. The connection between the two is formally given by the *Möller wave operators*, defined as

$$\Omega_{\pm} = \lim_{t \to \mp\infty} \mathscr{U}(t)^{\dagger} \mathscr{U}^{o}(t), \tag{4.5}$$

which relate the initial states to the asymptotes as

$$|\phi^{(\pm)}\rangle \equiv \Omega_{\pm} |\phi\rangle . \tag{4.6}$$

Using the relations 4.3, the improper vectors $|\mathbf{k}^{(\pm)}\rangle$ can be connected to the plane wave states in the same way

$$|\mathbf{k}^{(\pm)}\rangle \equiv \Omega_{\pm} |\mathbf{k}\rangle . \tag{4.7}$$

The Möller operators can be interpreted as mapping the set of $\{|\mathbf{k}\rangle\}$ states in $\mathscr{R}$ onto the subspace $\mathscr{S}$ of scattering states, in which they form a complete orthonormal set. Together with the eigenvectors $|n\rangle$ of the subspace of the bound states $\mathscr{B}$ (the states that do not have in or out asymptotes, but can be regarded as staying localised around the impurity), they form an orthonormal basis in $\mathscr{R}$. Therefore, while the improper states $|\mathbf{k}^{(\pm)}\rangle$ and $|\mathbf{k}\rangle$ do not satisfy the asymptotic conditions 4.4, since they are eigenstates of H and H_0 [explicitly, $\mathscr{U}(t)|\mathbf{k}^{(\pm)}\rangle = e^{-iE(\mathbf{k})t}|\mathbf{k}^{(\pm)}\rangle$ and $\mathscr{U}_0(t)|\mathbf{k}\rangle = e^{-iE(\mathbf{k})t}|\mathbf{k}\rangle$] as they are stationary states with respect to the evolution operators, they do satisfy them when considered as components as a wavepacket, as one can quickly verify by considering Eq. 4.4 in terms of the expansion 4.3. Formally, this is the reason why, for example, the state $|\mathbf{k}^{(\pm)}\rangle$ can be considered to be the state into which the initial free-particle state $|\mathbf{k}\rangle$ evolves into due to the scattering process. Physically, when considering the scattering process of a particle beam that is incident on a scattering potential, the difference between a physical wave packet and stationary states becomes negligible if the particle beam is turned on for a long enough time, so that the system can be assumed to reach a steady state.

Introducing the real-space representation, the Lippmann-Schwinger equation assumes the explicit form –with the definition $\langle \mathbf{r}|\mathbf{k}\rangle \equiv \psi_{\mathbf{k}}(\mathbf{r})$–

$$\psi_{\mathbf{k}}^{(\pm)}(\mathbf{r}) = \psi_{\mathbf{k}}(\mathbf{r}) + \int d\mathbf{r}' g^{(\pm)}(E(\mathbf{k})|\mathbf{r},\mathbf{r}')V(\mathbf{r}')\psi_{\mathbf{k}}^{(\pm)}(\mathbf{r}'). \tag{4.8}$$

This equation can be used to establish the asymptotic behaviour of the scattering state at large $r = |\mathbf{r}|$, which is a standard exercise in quantum mechanics. The Green's operator is

defined as

$$g^{(\pm)}(E) \equiv (E - H_0 \pm i\eta)^{-1}, \tag{4.9}$$

where a limiting procedure $\eta \to 0$ is implied. Its explicit form in real space can be obtained using complex contour integration as

$$g^{(\pm)}[E(\mathbf{k})|\mathbf{r},\mathbf{r}'] = -\frac{m}{\hbar^2}\frac{e^{\pm ik|\mathbf{r}-\mathbf{r}'|}}{2\pi|\mathbf{r}-\mathbf{r}'|}, \tag{4.10}$$

and taking the large r limit the asymptotic form of the scattering state can be expressed as

$$\psi_{\mathbf{k}}^{(\pm)}(\mathbf{r}) \sim \frac{1}{(2\pi\hbar)^{3/2}}\left[e^{i\mathbf{k}\cdot\mathbf{r}} + f(\mathbf{k} \to k\hat{\mathbf{r}})\frac{e^{ikr}}{r}\right]. \tag{4.11}$$

In this expression, the scattering amplitude connecting the incoming plane wave defined by the wave-vector $\mathbf{k}$ and an outgoing component $\mathbf{k}'$ is defined as

$$f(\mathbf{k} \to \mathbf{k}') = -m(2\pi)^2\hbar\,\langle \mathbf{k}'|V|\mathbf{k}^{(\pm)}\rangle\,. \tag{4.12}$$

As shown in Chapter 1 for the case of the free-electron gas, the scattering formalism can provide a good modelling tool for electronic stopping processes in solids: for free particles, the stopping power can be conveniently written as a function of the scattering cross section, which can be expressed in terms of the scattering amplitude above.

The theory of free-particle scattering provides a simple framework in which one can build understanding and physical intuition on scattering processes. The formalism for the scattering of Bloch-Floquet waves presented in the next section, which will allow for a generalisation of the nonlinear theory for stopping in jellium, is simply a generalisation of free-particle scattering theory in the extended Hilbert space of Floquet modes.

4.2 Stopping power with Bloch-Floquet scattering theory

The theory presented in this chapter will provide a firm theoretical ground to the expressions and the results presented in Chapter 3, where an ansatz for the solution of the scattering problem in the projectile frame for Bloch states in the crystals was presented based simply on quasienergy conservation.

The theory is based on the mapping of the time-periodic problem in $\mathscr{H}$, which requires the solution of the TDSE, to the time-independent-like form given by the Floquet-mode equation 2.5. Making use of $t - t'$ formalism developed in section 2.2, a generalised Lippmann-

Schwinger solution to the problem is presented, which provides an exact integral expression for the scattering states.

The analogy with the formalism of free-particle scattering comes from the fact that, in place of the eigenstates $\psi_{\mathbf{k}}(\mathbf{r})$ of the free-particle Hamiltonian, the Bloch-Floquet modes $\phi_{n\mathbf{k}}(\mathbf{r},t)$ of Eq. 3.15 are considered. These states are eigenstates of the crystal Floquet Hamiltonian $\mathscr{H}_0(\mathbf{r},t) = H_0(\mathbf{r}+\mathbf{v}t) - i\hbar\frac{\partial}{\partial t}$ with quasienergy $\varepsilon_n(\mathbf{k})$, where $H_0(\mathbf{r}+\mathbf{v}t)$ is the crystal Hamiltonian in a moving frame as defined in Chapter 3. Since the Floquet eigenmode equation 2.5 has the form of a time-independent-like Schrödinger equation, the same techniques used to solve the stationary scattering problem for free particles presented in the previous section can be applied. Thus, consider a Bloch state $\psi_{n\mathbf{k}_i}(\mathbf{r},t)$ in the moving frame, which is defined according to Eq. 3.13. With the addition of the projectile, the Floquet Hamiltonian is now $\mathscr{H}(\mathbf{r},t) = \mathscr{H}_0(\mathbf{r},t) + V_P(\mathbf{r})$. Since this does not change the discrete time-translational symmetry (the Hamiltonian is still periodic with period τ), according to the Floquet theorem the full solution will be a Floquet state, which can be written as $\Psi^{(\pm)}_{n\mathbf{k}_i}(\mathbf{r},t) = e^{-i\varepsilon_n(\mathbf{k}_i)t/\hbar}\Phi^{(\pm)}_{n\mathbf{k}_i}(\mathbf{r},t)$. Here, $\Phi^{(\pm)}_{n\mathbf{k}_i}(\mathbf{r},t)$ labels the Floquet mode of the *full* solution, c.f. with $\phi_{n\mathbf{k}_i}(\mathbf{r},t)$, which denotes the Floquet mode of the unperturbed Bloch-Floquet initial state $\psi_{n\mathbf{k}_i}(\mathbf{r},t)$. Therefore, the Floquet state has the same quasienergy $\varepsilon_n(\mathbf{k}_i)$ of the incoming mode which can be expressed as an integral equation in the Lippmann-Schwinger spirit, with $\xi = (\mathbf{r},t)$,

$$\Phi^{(\pm)}_{n\mathbf{k}_i}(\xi) = \phi_{n\mathbf{k}_i}(\xi) + \int d\xi' \mathscr{G}^{(\pm)}_0(\varepsilon_n(\mathbf{k}_i)|\xi,\xi')V_P(\mathbf{r}')\Phi^{(\pm)}_{n\mathbf{k}_i}(\xi'), \tag{4.13}$$

where the $\pm$ sign shares its meaning with the free-particle scattering formalism. The integral measure for the generalised variable ξ is defined as

$$\int d\xi \equiv \frac{1}{\tau}\int^{\tau} dt \int d\mathbf{r},$$

i.e. an averaging over one time period is assumed. The Green's function is expressed in terms of the complete set of eigenstates given by the Floquet modes and is defined according to Eq. 2.36 as

$$\mathscr{G}^{(\pm)}_0(\varepsilon|\xi,\xi') = \sum_n \sum_{p=-\infty}^{\infty} \int_{1BZ} \frac{d\mathbf{k}}{(2\pi)^3} \frac{\phi_{pn\mathbf{k}}(\xi)\phi^*_{pn\mathbf{k}}(\xi')}{\varepsilon - \varepsilon_{pn}(\mathbf{k}) \pm i\eta}, \tag{4.14}$$

where $\phi_{pn\mathbf{k}}(\mathbf{r},t) \equiv e^{ip\omega t}\phi_{n\mathbf{k}}(\mathbf{r},t)$ are the shifted Floquet modes, since by definition of completeness of the Floquet modes the integral in energy of the Green's function should cover the whole quasienergy spectrum. An equivalent definition makes use of the correspondence

between shifted Floquet modes and Bloch-states in the repeated zone scheme, as explained in section 3.3, which leads to

$$\mathscr{G}_0^{(\pm)}(\varepsilon|\xi,\xi') = \sum_n \int \frac{d\mathbf{k}}{(2\pi)^3} \frac{\phi_{n\mathbf{k}}(\xi)\phi_{n\mathbf{k}}^*(\xi')}{\varepsilon - \varepsilon_n(\mathbf{k}) \pm i\eta}, \tag{4.14'}$$

where the integral in $\mathbf{k}$ has to go over all reciprocal space. Using these definitions, the asymptotic expression for the full Bloch-Floquet modes can be obtained. In the next section, it will be derived for the 1D and more general 3D case.

4.3 Bloch-Floquet scattering states derivation

4.3.1 One-dimensional case

In this section, the asymptotic form for the stationary states for the stopping problem are presented for the 1D case. As well as providing a simpler model, the 1D formalism can be understood more easily, and a 1D model will also be used for the formalisation of a method for stopping calculations in Chapter 5. With the Bloch-Floquet modes of the crystal Hamiltonian given by $\phi_{nk}(x,t) = u_{nk}(x+vt)e^{i(k-mv/\hbar)x}$, Eq. 4.14' becomes

$$\mathscr{G}_0^{(\pm)}(\varepsilon|x,x',t,t') = \sum_n \int \frac{dk}{2\pi} \frac{e^{i(k-mv/\hbar)(x-x')} u_{nk}(x,t)u_{nk}^*(x',t')}{\varepsilon - \varepsilon_n(k) \pm i\eta}, \tag{4.15}$$

To obtain the asymptotic form of the Green's function, the limit of interest is given by $\Delta x = |x-x'| \to \infty$ in the Lippmann-Schwinger expression. This can be derived by calculating the large-x asymptotic form of the Green's function above. Moreover, from now on only the scattering state with outgoing boundary conditions [i.e. only the (+)-expressions], which are the ones of physical interest, will be considered .

The main difficulty is given by the fact that an exact analytical expression for $\mathscr{G}_0^{(\pm)}$, in contrast to the free-particle case, is not generally available. This is due to the fact that the poles of the Green's function are defined by the zeros of the function $\varepsilon - \varepsilon_n(k)$ for some constant ε. However, it can be assumed that such zeros, if they exist, can be obtained, at least numerically, as done in Chapter 3 for the two-band model. Moreover, a difference between this problem and the case of scattering of Bloch waves from a static defect or impurity [106] is that the change of reference frame breaks the time-reversal symmetry of the static crystal, and therefore extra care needs to be taken when performing the complex integrations. This procedure allows to find an asymptotically exact expression for the Green's function, which in turn determines the one for the scattering state.

It is convenient to recast the integral in Eq. 4.15 in the form

$$\int \frac{dk}{2\pi} \frac{e^{i(k-mv/\hbar)x} f_n(k,x,x',t',t'')}{\varepsilon - \varepsilon_n(k) + i\eta} \tag{4.16}$$

where $f_n(k,x,x',t,t') = e^{-i(k-mv/\hbar)x'} u_{nk}(x,t) u^*_{nk}(x',t')$. As a preliminary analysis, it can be seen that the asymptotic limit $x \to \pm\infty$ is well defined since f_n is effectively bounded in this limit, given the periodicity of the Bloch states. It is assumed that the function $\mathscr{F}_n(k) = \varepsilon - \varepsilon_n(k)$ has zeros defined by the quantum number(s) m and k_f, which define the simple poles of the integrand. In the asymptotic limit, this integral is equivalent to

$$\sum_{m,k_f} \frac{f_m(k_f,x,x',t,t')}{-\hbar v_g^m(k_f)} \int \frac{dk}{2\pi} \frac{e^{i(k-mv/\hbar)x}}{k - k_f + i\eta/(-\hbar v_g^m(k_f))}, \tag{4.17}$$

where the group velocity is defined as $v_g^m(k_f) = \hbar^{-1}\partial_k(E_m(k)) - v|_{k=k_f}$. In fact, this expression for the group velocity is fairly intuitive: the group velocity of the Bloch-Floquet states is the one of the corresponding Bloch state in the lab frame shifted by the velocity of the moving reference frame. In order to see that this expression is indeed the correct limit consider the following decomposition of the integrand in Eq. 4.16 [106]

$$\begin{aligned} \frac{f_n(k)}{\varepsilon - \varepsilon_n(k) + i\eta} = \frac{f_n(k) - f_m(k_f)}{\varepsilon - \varepsilon_n(k) + i\eta} + f_m(k_f) \left[\frac{k - k_f + i\eta/(-\hbar v_g^m(k_f))}{\varepsilon - \varepsilon_n(k) + i\eta} - \frac{1}{-\hbar v_g(k_f)} \right] \\ \times \frac{1}{k - k_f + i\eta/(-\hbar v_g^m(k_f))} + \frac{f_m(k_f)}{(-\hbar v_g^m(k_f))} \frac{1}{k - k_f + i\eta/(-\hbar v_g^m(k_f))}, \end{aligned} \tag{4.18}$$

where the shorthand $f_n(k)$ is used in place of $f_n(k,x,x',t,t')$. In the limit $\eta \to 0$, which is implicit in Eq. 4.16 upon substitution of the above expression in the integral, it can be verified that the first two terms are regular everywhere along the integration axis, and they vanish by the Riemann-Lebesgue lemma as $|x| \to \infty$. Therefore, the only term contributing to the integral is the last one, which leads directly to expression 4.17. At this stage, the complex integral can be performed without problems by summing over the residues of the poles. The two limits $x \to \pm\infty$ are taken separately by closing into the upper and lower half plane for $x > 0$ and $x < 0$ respectively. The poles associated with positive $v_g^m(k_f)$ will be associated with the solutions at $x > 0$, and the ones with $v_g^m(k_f) < 0$ with $x < 0$, which is sensible given the fact that we are evaluating the retarded propagator for the Bloch-Floquet modes, which should give forward-time propagation. Thus, by evaluating the integral the asymptotic expansion of $\mathscr{G}_0^{(+)}$ is readily obtained; inserting it into the one-dimensional version of the

Lippmann-Schwinger solution 4.13 the asymptotic expression can be written as

$$\Phi^{(+)}_{nk_i}(x,t) \sim \phi_{nk_i}(x,t) + \sum_{m,k_f} A_{nk_i,mk_f}\phi_{mk_f}(x,t) \tag{4.19}$$

with the outgoing boundary conditions above, with the expression being valid at $x > (<)0$ if the group velocity of the outgoing scattering mode $v_g(k_f) > (<)0$: the boundary conditions are fulfilled with the group velocities pointing away from the projectile located around $x = 0$. The scattering amplitudes are

$$A_{nk_i,mk_f} = -\frac{i}{\hbar v_g^m(k_f)} \langle\langle \phi_{mk_f}(t)|V_P|\Phi^{(+)}_{nk_i}(t)\rangle\rangle\,, \tag{4.20}$$

and the explicit expression for the matrix element defined by the generalised Floquet scalar product 2.18 as

$$\langle\langle \phi_{mk_f}(t)|V_P|\Phi^{(+)}_{nk_i}(t)\rangle\rangle = \frac{1}{\tau}\int^{\tau} dt' \int dx' e^{-ik_f x'} u^*_{mk_f}(x',t')V_P(x')\Phi^{(+)}_{nk_i}(x',t'). \tag{4.21}$$

This proves the ansatz 3.18.

Therefore, the behaviour is already very complex, even in 1D, compared to free-particle scattering, where the only available states are the reflected and transmitted plane waves, since conservation of energy imposes $|k_f| = |k_i|$. As only quasienergy needs to be conserved, the number of possible solutions can be in principle infinite, as explained in Chapter 3, even for ideal one or two-band systems. In theory, these modes could be in principle observed experimentally in controlled conditions. For instance, in systems where a 1D Hamiltonian can be engineered to enforce a moving impurity at constant velocity in a lattice, it is possible that they could be directly observed by measuring the density profile of the excited states, which at set distances from the impurity could in theory be described by the asymptotic form of the wavefunction above.

4.3.2 Three-dimensional case

The 3D case can be thought simply as a generalisation of the 1D one, in a similar way in which 3D free-particle scattering can be related to 1D. However, while the derivation of the form of the asymptotic scattering states is quite similar, it is still worth going through some of the details; on the one hand because there are some differences, and on the other hand because it appears that it is the first time that such a scattering problem has been analysed, in particular with regards to the broken time-reversal symmetry which distorts the band

structure into the Bloch-Floquet spectrum, and from the fact that the theory is applicable to arbitrary crystals, whose electrons can be described by Bloch waves.

The expression for the Bloch-Floquet Green's function in 3D is given by

$$\mathscr{G}_0^{(+)}(\varepsilon|\mathbf{r},\mathbf{r}',t,t') = \sum_n \int \frac{d^3k}{(2\pi)^3} \frac{e^{i(\mathbf{k}-m\mathbf{v}/\hbar)\cdot(\mathbf{r}-\mathbf{r}')} u_{n\mathbf{k}}(\mathbf{r},t) u^*_{n\mathbf{k}}(\mathbf{r}',t')}{\varepsilon - \varepsilon_n(\mathbf{k}) + i\eta}. \tag{4.22}$$

Firstly, this integral needs to be split into two parts. Consider the expression (see [55], §125 "The unitary condition for scattering" for a similar example)

$$\int_0^\infty \frac{dk}{(2\pi)^3} k^2 \int d\Omega F(\mathbf{k}) e^{ikr\hat{\mathbf{k}}\cdot\hat{\mathbf{r}}}, \tag{4.23}$$

in which the integral over the 3D k-space is separated into angular and scalar components. For large $r = |\mathbf{r}|$, which is the limit of interest, by a stationary phase argument the integral is determined mainly in regions near the extrema, given by $\hat{\mathbf{k}}\cdot\hat{\mathbf{r}} = \cos\theta = \pm 1$. Therefore, for the angular part $f(\pm k\hat{\mathbf{r}})$ can be pulled out of the integral giving

$$\int d\Omega F(\mathbf{k}) e^{ikr\hat{\mathbf{k}}\cdot\hat{\mathbf{r}}} = 2\pi i F(-k\hat{\mathbf{r}}) \frac{e^{-ikr}}{kr} - 2\pi i F(k\hat{\mathbf{r}}) \frac{e^{ikr}}{kr}. \tag{4.24}$$

By identifying, in this case, $F(\mathbf{k}) = e^{-i(\mathbf{k}-m\mathbf{v}/\hbar)\cdot\mathbf{r}'} u_{n\mathbf{k}}(\mathbf{r},t) u^*_{n\mathbf{k}}(\mathbf{r}',t')/(\varepsilon - \varepsilon_n(\mathbf{k}) + i\eta)$, the remaining integration in k can be performed similarly to the previous sections. One of the two integrals that needs to be calculated when substituting 4.24 into 4.23 is

$$\frac{(2\pi i)}{r(2\pi)^3} \int_0^\infty dk\, k \frac{e^{-ikr} f_n(-k\hat{\mathbf{r}})}{\varepsilon - \varepsilon_n(-k\hat{\mathbf{r}}) + i\eta}, \tag{4.25}$$

and the second one is

$$\frac{(2\pi i)}{r(2\pi)^3} \int_0^\infty dk\, k \frac{e^{ikr} f_n(k\hat{\mathbf{r}})}{\varepsilon - \varepsilon_n(k\hat{\mathbf{r}}) + i\eta}, \tag{4.26}$$

with $f_n(\mathbf{k}) = e^{-i(\mathbf{k}-m\mathbf{v}/\hbar)\cdot\mathbf{r}'} u_{n\mathbf{k}}(\mathbf{r},t) u^*_{n\mathbf{k}}(\mathbf{r}',t')$. Since time-reversal symmetry is broken in the present case, in general $\varepsilon_n(-\mathbf{k}) \neq \varepsilon_n(\mathbf{k})$ and it is not possible to merge them into a single integral $\int_{-\infty}^{\infty} dk$ as usually done in similar problems where the time-reversal symmetry applies. In fact, it is easy to see that the two integrals, together, cover all the possible solutions of the quasienergy conservation equation $\varepsilon - \varepsilon(k\hat{\mathbf{r}}) = 0$, with the solutions $k_f < 0$ being taken into account by the poles of the first integral. This holds trivially because, given a zero $k_f < 0$ of $\varepsilon - \varepsilon(k\hat{\mathbf{r}})$, then $-k_f > 0$ is a zero of $\varepsilon - \varepsilon(-k\hat{\mathbf{r}})$. Consider first the integral in Eq. 4.25. Similarly to the integral for the 1D expression, it can be approximated, in the asymptotic

limit, as

$$\sum_{m,k_f>0} \frac{k_f f_m(k_f\hat{\mathbf{r}})}{-\hbar v_g^m(k_f\hat{\mathbf{r}})} \int dk \frac{e^{ikr}}{k-k_f-i\eta/\hbar v_g^m(k_f\hat{\mathbf{r}})}, \tag{4.27}$$

with the group velocity in the 3D case generalising the previous definition as $v_m^g(k_f\hat{\mathbf{r}}) = \frac{1}{\hbar}\frac{\partial}{\partial k}(\varepsilon_m(k\hat{\mathbf{r}}))|_{k=k_f}$. With the condition $v_g^m(k_f\hat{\mathbf{r}}) > 0$, closing the contour of the integral in the upper-half plane leads to the evaluation of the expression in 4.25 as

$$\sum_{k_f>0} \frac{k_f f_m(k_f)}{2\pi\hbar v_g^m(k_f\hat{\mathbf{r}})} \frac{e^{ik_f r}}{r}. \tag{4.28}$$

Now, consider the other integral in 4.26, and denote the zeros of the real part of the denominator as $k'_f = -k_f$, as just discussed. The corresponding asymptotic expression is

$$\sum_{m,k'_f>0} \frac{k'_f f_m(-k'_f\hat{\mathbf{r}})}{-\hbar v_g^m(-k'_f\hat{\mathbf{r}})} \int dk \frac{e^{-ikr}}{k-k'_f-i\eta/\hbar v_g^m(-k'_f\hat{\mathbf{r}})}. \tag{4.29}$$

The integral is then calculated by closing the contour in the lower-half plane with the condition $v_g^m(-k'_f\hat{\mathbf{r}}) < 0$, which is equivalent to $v_g^m(k_f\hat{\mathbf{r}}) > 0$, as expected. This means that the integral gives the same result 4.28 for the negative roots k_f of the quasienergy conservation equation. This leads, after substitution of the asymptotic form of the Green's function into the Lippmann-Schwinger equation, to the following asymptotic form of the Bloch-Floquet scattering state in 3D

$$\Phi^{(+)}_{n\mathbf{k}_i}(\mathbf{r},t) \sim \phi_{n\mathbf{k}_i}(\mathbf{r},t) + \sum_{m,k_f} A_{n\mathbf{k}_i,mk_f\hat{\mathbf{r}}} \frac{e^{i(k_f\hat{\mathbf{r}}-m\mathbf{v}/\hbar)\cdot\mathbf{r}}}{r} u_{mk_f\hat{\mathbf{r}}}(\mathbf{r},t), \tag{4.30}$$

where the scattering amplitudes are defined as

$$A_{n\mathbf{k}_\mathbf{i},mk_f\hat{\mathbf{r}}} = -\frac{k_f}{2\pi\hbar v_g^m(k_f\hat{\mathbf{r}})} \langle\langle \phi_{mk_f\hat{\mathbf{r}}}(t)|V_P|\Phi^{(+)}_{n\mathbf{k}_\mathbf{i}}(t)\rangle\rangle\,. \tag{4.31}$$

The full solution of the Schrödinger equation is then obtained by inserting the quasienergy phase factor $\Psi^{(+)}_{n\mathbf{k}_i}(\mathbf{r},t) = e^{i\varepsilon_n(\mathbf{k})t/\hbar}\Phi^{(+)}_{n\mathbf{k}_i}(\mathbf{r},t)$. The outgoing boundary conditions are clearly satisfied from the conditions on the group velocity for the outgoing states.

Looking at the derived expressions for the scattering states one gets a much richer behaviour compared to both the free-particle case and the scattering of Bloch waves from an impurity. Indeed, even when considering impurity scattering of Bloch waves in a crystal [106], depending on the band structure, the number of possible outgoing states is limited

to the ones satisfying energy conservation. Looking at the form of Eq. 4.30, it resembles the form of a plane wave scattering states in the form of Eq. 4.11, which consists of a superposition of a plane wave and outgoing spherical waves. The difference with the Bloch-Floquet scattering state 4.30 is in the summation of all (possibly infinite) number of allowed scattering states defined by $k_f\hat{\mathbf{r}}$.

4.4 Derivation of the electronic stopping power

As derived in Chapter 1, the ETR $\dot{E}$ and stopping power for a projectile of velocity v are related by the simple relation $S_e = \dot{E}/v$. However, in order to derive the expression for stopping power from the Bloch-Floquet scattering states, it is not possible to use the same methods used in [56] for Eq. 1.26 to compute the force matrix element: this stems from the fact that the Floquet Hamiltonian does not commute with the momentum operator, which holds instead for the case of a free-particle Hamiltonian. However, it is still possible to derive it using probability flux conservation, as in 1.22. It differs from that example in that the full spectrum of possible scattering states given by quasienergy conservation needs to be taken into account.

4.4.1 1D Bloch-Floquet energy transfer rate

Let us analyse the 1D case first for simplicity, and observe that the quasienergy conserving scattering process is particle-conserving. This means that the incoming probability current from some initial incoming state from $x \to \pm\infty$, is equal to the sum of the currents of the outgoing states. For the 1D Bloch-Floquet scattering process, where the outgoing states consist of a discrete spectrum with outgoing boundary conditions, probability flux conservation implies

$$\sum_{mk_f} |A_{nk_i,mk_f}|^2 |v_g^m(k_f)| = |v_g^n(k_i)|, \tag{4.32}$$

where the notation is derived from the expressions in Eq. 4.19, and only the group velocities of the modes satisfying the correct boundary conditions are considered.

The ETR can then be derived in the stationary regime by noting that each of the Floquet-Bloch asymptotic modes corresponds to a Bloch state with energy $E_n(k)$. The energy flux of the outgoing modes can therefore be expressed via the scattering amplitudes, since probability flux conservation holds in both the projectile and the laboratory frame. Therefore,

the single-particle ETR takes the form

$$\dot{E}_{ni} = \rho_i \sum_{mk_f} \left[|A_{nk_i,mk_f}|^2 |v_g^m(k_f)| E_m(k_f) - |v_g^n(k_i)| E_n(k_i) \right], \tag{4.33}$$

where ρ_i is the density of the incoming state. Using the identity 4.32, it can be expressed as

$$\dot{E}_{ni} = \rho_i \sum_{mk_f} |A_{nk_i,mk_f}|^2 |v_g^m(k_f)| (E_m(k_f) - E_n(k_i)). \tag{4.34}$$

This expression has the simple interpretation of a generalisation of the one-dimensional free-particle expression in Eq. 1.23. Furthermore, it can be recast in a form that generalises the expressions derived in [23, 56]: consider the following identity for the Dirac-delta

$$\delta[f(x)] = \sum_i \frac{\delta(x - x_i)}{|f'(x_i)|}, \tag{4.35}$$

where the x_i are zeros of $f(x)$, and $f'(x_i) = \frac{df}{dx}\big|_{x=x_i} \neq 0$, which leads to

$$\dot{E}_{ni} = \rho_i \frac{2\pi}{\hbar} \int \frac{dk}{2\pi} \Delta E_{mn,fi} |\langle\langle \phi_{mk_f}(t) | V_P | \Phi_{nk_i}^{(+)}(t) \rangle\rangle|^2 \delta(\Delta E_{mn,fi} - v\hbar \Delta k_{fi}), \tag{4.36}$$

with $\Delta E_{mn,fi} = E_m(k_f) - E_n(k_i)$ and $\Delta k_{fi} = k_f - k_i$. In the form above, the ETR expression can be linked to the Fermi golden rule, differing by the presence of the full scattering state $|\Phi_{nk_i}^{(+)}(t)\rangle$in the matrix element instead of the unperturbed Bloch-Floquet mode $|\phi_{nk_i}(t)\rangle$.

4.4.2 3D Bloch-Floquet energy transfer rate

In 3D a similar argument related to flux conservation holds: for single-particle scattering, as in the previous paragraph, one can still consider the ETR as the difference in energy flux between the incoming Floquet-Bloch state and the allowed outgoing scattering states. The ETR can be expressed in terms of the differential scattering cross-section $(d\sigma/d\Omega)(n\mathbf{k}_i \to m\mathbf{k}_f)$ from a Bloch-Floquet mode $|\phi_{n\mathbf{k}_i}\rangle$ to $|\phi_{n\mathbf{k}_f}\rangle$. It can be defined as the ratio between the scattered flux to the incident flux, which can be expressed in terms of the Bloch-Floquet matrix elements as

$$\frac{d\sigma}{d\Omega}(n\mathbf{k}_i \to m\mathbf{k}_f) = \frac{k_f^2 |\langle\langle \phi_{m\mathbf{k}_f} | V_P | \Phi_{n\mathbf{k}_i}^{(+)} \rangle\rangle|^2}{(2\pi\hbar)^2 v_g^m(\mathbf{k}_f) v_g^n(\mathbf{k}_i)}, \tag{4.37}$$

whose difference with the free-particle scattering case can be noted, especially in the appearance of the group velocities of the two states. This expression for the differential scattering

cross section is more similar to the form for inelastic scattering than to stationary scattering processes based on energy conservation [105], with the reason simply being that the group velocities of the allowed Floquet-Bloch states are, in general, different. The ETR can then be obtained by integrating the differential energy transfer rate

$$\frac{dE}{d\Omega}(n\mathbf{k}_i \to m\mathbf{k}_f) = j_{n\mathbf{k}_i}\frac{d\sigma}{d\Omega}(E_m(\mathbf{k}_f) - E_n(\mathbf{k}_i)), \tag{4.38}$$

where $j_{n\mathbf{k}_i} = \rho_i v_g^n(\mathbf{k}_i)$ is the probability current of the incoming state, over the solid angle obtaining

$$\dot{E}_{ni} = \int d\Omega \sum_{k_f} \rho_i \frac{k_f^2 |\langle\langle \phi_{m\mathbf{k}_f} | V_P | \Phi^{(+)}_{n\mathbf{k}_i} \rangle\rangle|^2}{(2\pi\hbar)^2 v_g^m(\mathbf{k}_f)}(E_m(\mathbf{k}_f) - E_n(\mathbf{k}_i)), \tag{4.39}$$

which can be recast via 4.35 in the form

$$\dot{E}_{ni} = \rho_i \frac{2\pi}{\hbar}\int \frac{d\mathbf{k}_f}{(2\pi)^3}\Delta E_{mn,fi} |\langle\langle \phi_{m\mathbf{k}_f}(t) | V_P | \Phi^{(+)}_{n\mathbf{k}_i}(t) \rangle\rangle|^2 \delta(\Delta E_{mn,fi} - \mathbf{v}\cdot\hbar\Delta\mathbf{k}_{fi}), \tag{4.40}$$

where $\Delta E_{mn,fi} = E_m(\mathbf{k}_f) - E_n(\mathbf{k}_i)$ and $\Delta\mathbf{k}_{fi} = \mathbf{k}_f - \mathbf{k}_i$ which is a simple generalization in 3D of the 1D form 4.36, with the Dirac-δ imposing quasienergy conservation.

4.4.3 Bloch-Floquet stopping power: expression and analysis

In order to obtain the electronic stopping power, the *total* ETR is needed. At temperature $T = 0$, assuming occupied bands n and unoccupied bands m, it can be expressed by integrating separately over initial and final Bloch-Floquet modes as

$$S_e(\mathbf{v}) = \frac{1}{v}\sum_{nm}\frac{2\pi}{\hbar}\int\frac{d\mathbf{k}_i}{(2\pi)^3}\int\frac{d\mathbf{k}_f}{(2\pi)^3}\Delta E_{mn,fi} |\langle\langle \phi_{m\mathbf{k_f}} | V_P | \Phi^{(+)}_{n\mathbf{k_i}} \rangle\rangle|^2 \delta(\Delta E_{mn,fi} - \mathbf{v}\cdot\hbar\Delta\mathbf{k}_{fi}). \tag{4.41}$$

The expression for the 1D case is simply the 1D version of the above expression. Eq. 4.41 can be regarded as the result of the generalisation of the nonlinear jellium theory for finite velocities [23, 56]. In fact, by simply substituting the Bloch-Floquet modes $\phi_{n\mathbf{k}}(\mathbf{r},t) = u_{nk}(\mathbf{r}+\mathbf{v}t)e^{i(\mathbf{k}-m\mathbf{v}/\hbar)\cdot\mathbf{r}}$ with plane waves with corresponding wavevector, the expression for the nonlinear stopping in jellium is readily recovered. Eq. 4.41 can be connected to the approximate one presented in section 3.5, Eq. 3.21, by rewriting it as

$$S_e(\mathbf{v}) = \frac{1}{v}\sum_{nm}\int d(\hbar\omega)\,\hbar\omega\gamma_{mn}(\omega,v)\rho(\omega,v), \tag{4.42}$$

where $\rho(\omega, v)$ is the JDOS as defined in Eq. 3.20 and the energy-dependent scattering rate $\gamma_{mn}(v,\omega)$ will depend nontrivially on the matrix elements $A_{n\mathbf{k}_i,m\mathbf{k}_f}$ connecting valence and conduction band modes that satisfy quasienergy conservation. In section 3.5, when analysing the threshold velocity effect, the assumption was that the matrix elements in the region of interest in energy space do not change much with the value of the wavevectors $\mathbf{k}_i, \mathbf{k}_f$, in analogy with the analysis of direct optical transitions in gapped solids [103]. While Eq. 4.41 is more general compared to Eq. 3.21, for actual numerical calculations either 4.41 or 4.42 may be more suitable, depending on which approximations can be made, and choosing the most efficient one. While for 1D systems the from of 4.41 appears to be more suitable (given the discreteness of the quasienergy conserving solutions), for numerical schemes in higher dimensions the version of 4.42 may prove to be better.

To extend this to $T \neq 0$ and partially filled bands the relevant occupation numbers can be introduced which, in a first approximation, can be done as follows:

$$\begin{aligned} S_e(\mathbf{v}) = \frac{1}{v}\sum_{nm}\frac{2\pi}{\hbar}\int\frac{d\mathbf{k}_i}{(2\pi)^3}\int\frac{d\mathbf{k}_f}{(2\pi)^3}\Delta E_{mn,fi} \\ \times f(E_n(\mathbf{k}_i))[1-f(E_m(\mathbf{k}_f))]|\left\langle\langle\phi_{m\mathbf{k_f}}|V_P|\Phi^{(+)}_{n\mathbf{k_i}}\rangle\right\rangle|^2\delta(\Delta E_{mn,fi}-\mathbf{v}\cdot\hbar\Delta\mathbf{k}_{fi}), \end{aligned} \tag{4.43}$$

where here $f(E)$ is the Fermi distribution function. For higher-order correction of the theory, which take into account many-body effects beyond single particle mean-field approximations, the above expression(s) for stopping would likely have to be corrected. However, the above expression constitutes the starting point for a more general nonlinear stopping theory for arbitrary crystalline system including higher-order many-body corrections, in the same way as the theory in [64, 65] generalised the nonlinear theory for jellium.

The constant-velocity assumption for the projectile was motivated in Chapter 1. However, small deviations from the constant velocity regime are usually expected. In fact, the expression 4.41 is still valid for a periodically varying velocity (and therefore periodically oscillating potential in the moving frame), as long as the average v is constant. This would allow the application of the theory in cases where oscillations are induced in the projectile motion. Such oscillations could be expected as a reflection of the flapping observed in the core electrons energy levels in first-principle calculations [47]. Oscillations in the projectile motion are also expected when the ion is "bouncing" while channelling through the solid (a channel being a constrained path in 3D for the ion in the crystal which does not cross crystalline atoms that act as effective "walls" for the ion). However, this effect should lead to a very long period of oscillation, and in such case the expression for constant velocity should constitute a good approximation.

Moreover, let us consider, briefly, how the model could change for the case in which the projectile is not travelling in a direction in the crystal lattice defined by one of the primitive lattice vectors (which this is clearly not possible in 1D, since by definition the projectile would move in the primitive lattice vector direction). If the deviation from the periodic direction is minimal, it can be assumed that the theory retains validity to a good approximation. The system can still be analysed as a Floquet model if the projectile velocity points along some arbitrary lattice vector $\mathbf{R}$, which is by definition constructed through all the possible combinations of primitive lattice vectors, multiplied by integers; however, the bigger the real-space unit cell determined by the periodicity, the more complicated the picture in reciprocal Bloch-Floquet space, with the band structure having a much more complex structure compared to the quite intuitive one in Fig. 3.2. Indeed, by considering a periodicity determined by a lattice vector $\mathbf{R}$, for a projectile velocity $\mathbf{v} = v\hat{\mathbf{R}}$, the period is given by $\tau = R/v$ ($R = |\mathbf{R}|$) which, for $R \gg a$, makes the frequency ω much smaller than the case in which $\tau = a/v$, $\mathbf{a}$ being a primitive lattice vector. The small-ω limit has been discussed with relation to the adiabatic limit analysis in Chapter 3. However, the $\omega \to 0$ limit in this case is radically different: instead of letting the projectile velocity $v \to 0$, it is the lattice vector $R \to \infty$. To reach the actual limit, the direction of $\mathbf{R}$ can be set so that the ratio between the primitive unit cell indices is *irrational*, obtaining a trajectory that retains the crystal ordered structure, but with no periodicity, similarly to how one-dimensional quasicrystals such as Fibonacci chains are obtained by projection of higher-dimensional crystalline structures onto a line [107]. In fact, rectilinear trajectories for the projectile that are incommensurate with the crystal lattice vectors have been proposed for accurate first-principles calculations of electronic stopping [39]. However, another recent proposal suggests that other geometric criteria of projectile trajectory sampling lead to more efficient and accurate first-principles calculations [108].

In fact, the Galilean transformation for the Bloch states is also valid in this "quasicrystalline" case, with the difference that $\varepsilon_n(\mathbf{k})$ and $\phi_{n\mathbf{k}}(\mathbf{r},t)$ cannot be regarded anymore as quasienergies and Floquet modes in the projectile frame, but could be interpreted simply as the transformed energy and a quasiperiodic modulation. The above expressions still make sense and should be valid in the $\tau \to \infty$ limit, by increasing the unit cell in time in the extended Hilbert space. However, while it would be plausible that a quasiperiodic regime is reached in such cases, described by scattering states of the form 4.30, with quasiperiodic modes and energy, the problem becomes basically intractable with the current formalism. In order to see why it is the case, consider again what the $\omega \to 0$ limit means in this circumstance: by folding the states into the 1$^{\text{st}}$ BZ in Floquet quasienergy space, and with the reciprocal lattice vectors becoming smaller and smaller, the unit cell in Bloch-Floquet states of 3.2 would become

infinitesimal, losing much of the information and insight that, for example, one could draw for the velocity threshold in insulator. However, by keeping the extended-zone picture, it is in principle still possible perform a meaningful analysis by truncating the spectrum for large $\mathbf{k}$. In addition, such nonperiodic trajectories for real stopping events could still in principle be approximated by a suitable periodic trajectory that is not too far to the nonperiodic one, since the actual numerical results should not be very different. In fact, the analysis of the adiabatic limit $\omega \to 0$ stemming from the $v \to 0$ limit for the projectile, and the shrinking 1$^{\text{st}}$ BZ in quasienergy, is also nontrivial, and will need to be addressed in practical calculations.

One of the main advantages of the Bloch-Floquet scattering theory is that in principle, having access to the exact stationary states of the stopping process, it allows for more accurate results for stopping power. However, the exact stationary states needed to compute the matrix elements in Eq. 4.41 are highly nontrivial to obtain, since they are defined in terms of the Lippmann-Schwinger equation 4.13, which is an integral equation. This difficulty is usually circumvented when considering an interaction potential that couples only perturbatively with the electron system: a weak potential would make a 1$^{\text{st}}$ Born approximation applicable, and a Bloch-Floquet perturbation theory is obtained: substituting $|\Phi^{(+)}_{n\mathbf{k}_i}\rangle$ by $|\phi_{n\mathbf{k}_i}\rangle$ and assuming a smooth projectile $V_P(\mathbf{r})$, the matrix element (Eq. 4.20) becomes (see Appendix B)

$$\langle\langle \phi_{m\mathbf{k}_f} | V_P | \phi_{n\mathbf{k}_i} \rangle\rangle \propto \tilde{V}_P(\Delta\mathbf{k}), \tag{4.44}$$

where $\Delta\mathbf{k} = |\mathbf{k}_f - \mathbf{k}_i|$, and $\tilde{V}_P$ indicates the Fourier transform of $V_P(\mathbf{r})$, thereby recovering perturbation theory results (see e.g. [61]). In fact, ideally the matrix elements should be calculated nonperturbatively, similarly to what has been achieved with the nonlinear theory for jellium. The advantage of the jellium model is that, for the free-electron gas, the total stopping can be directly related to the scattering phase shifts, as explained in Chapter 1, obtained by expanding the scattering wavefunction in terms of angular momentum eigenstates. However, for Bloch-Floquet scattering states this type of expansion is practically infeasible. The method proposed in the next Chapter will show how a nonperturbative treatment can be formalised by solving a Dyson equation in the extended Fourier Hilbert space $\mathscr{R} \otimes \mathscr{T}$.

In addition, it is appropriate to point out some of the effects that this simplified theory, which regards the projectile as a simple, repulsive, scalar potential, cannot capture. Firstly, being a stationary theory, it does not capture the initial transient when the projectile enters the solid (for real systems) or set into motion (for simulations). However, in simulations transients are usually short lived, and while an analysis on how transients stabilise into stationary states is a theoretically very interesting problem, they have a minimal effect on the actual stopping power. Others are mainly related to the fact that bound states in the projectile

can have important effects during stopping process. These, being related to the ionic screening cause the ion to stabilise to having an effective charge. Two examples of how bound-states-related effects modify stopping processes are *coherent resonant processes* and *electronic exchange* processes. Examples of electronic exchange effects are given, for example, by Auger processes, in which electron capture and loss is mediated by other excitations such as plasmons or electron-hole pairs [54]. Regarding coherent resonant processes, Okorokov proposed in 1965 [109] that the crystal could induce Coulomb excitations if a multiple of the natural frequency from the collision equals the energy excitation ΔE, i.e. if the condition $v = a\Delta E/\hbar n 2\pi$ is satisfied. This effect results in emission of photons at the frequency corresponding to the energy excitations and, while this effect is quite hard to observe for light projectiles, such as He^+, due to the short lifetime of the excited state, experiments with heavier ions have managed to detect this emission process, and this effect has been proposed as a scheme for heavy-ion spectroscopy [54, 110]. The Okorokov effect could, in fact, also be interpreted within the Floquet formalism as a periodic drive, with the periodicity caused by the crystal moving in the projectile reference frame. Other types of coherent resonant interaction processes influenced by the time-periodic crystalline potential involve, similarly to Auger processes, electron capture and loss between bound and free-electron states, stimulated by time-dependent crystalline effects [54, 111]. In fact, bound states can have an effect in the scattering process not only by having an attractive projectile potential, but the periodicity induced by the crystal can also cause Floquet-induced bound states, which can be identified as poles in the scattering matrix [112]: for the 1D Bloch-Floquet scattering theory formalism, the scattering matrix can be written as

$$S_{nk_i,mk_f} = \delta_{mn}\delta_{k_i,k_f} - \frac{i}{\hbar v_g^m(k_f)} \langle\langle \phi_{mk_f}(t)|V_P|\Phi^{(+)}_{nk_i}(t)\rangle\rangle \,. \tag{4.45}$$

Finally, consider how, starting from the noninteracting model, many-body interaction effects could be introduced. While the single-particle noninteracting approximation has already provided results regarding the threshold velocity problem and new insights on the adiabatic $v \to 0$ limit, it is also clear that the extension for the inclusion of many-body interactions is important for both the stopping problem and Floquet systems (see sections 1.8 and 2.3). For instance, consider the problem of Floquet electrons coupled with a bath of phonons [113]. For simplicity, consider single-particle Bloch-Floquet electron states which could be the scattering states defined earlier in the chapter of the form in Eq. 4.30. The

(Floquet) Hamiltonian can be written as

$$\mathscr{H}(t) = \mathscr{H}(t) + U_{\text{el-ph}}, \tag{4.46}$$

with $\mathscr{H}(t) = \mathscr{H}_{\text{el}}(t) + \mathscr{H}_{\text{ph}}$, a sum of an Hamiltonian for Bloch-Floquet electrons and one for the phonons:

$$\mathscr{H}_{\text{el}}(t) = \sum_{p}\sum_{\mathbf{k}} \varepsilon_p(\mathbf{k})\zeta^{\dagger}_{p\mathbf{k}}(t)\zeta_{p\mathbf{k}}(t); \tag{4.47}$$

$$\mathscr{H}_{\text{ph}} = \sum_{\mathbf{q}} \hbar\omega_{\mathbf{q}} b^{\dagger}_{\mathbf{q}} b_{\mathbf{q}}; \tag{4.48}$$

where the second-quantised operators $\zeta^{(\dagger)}_{\mathbf{k}}(t)$ annihilate (create) a Bloch-Floquet scattering state (which in first-quantised language is simply 4.30) and satisfy

$$\left[\zeta^{\dagger}_{p\mathbf{k}}(t), \zeta_{q\mathbf{k}'}(t)\right]_{\pm} = \delta_{\mathbf{k},\mathbf{k}'}\delta_{p,q} \tag{4.49}$$

for bosons and fermions, and $b^{(\dagger)}_{\mathbf{q}}$ annihilate (create) a phonon with wavevector $\mathbf{q}$.

The interaction term can, for instance, have the form

$$U_{\text{el-ph}} = \sum_{\mathbf{k},\mathbf{q},p,p'} U(\mathbf{q})\zeta^{\dagger}_{p'\mathbf{k}}(t)\zeta_{p\mathbf{k}+\mathbf{q}}(t)(b^{\dagger}_{\mathbf{q}} + b_{-\mathbf{q}}) + h.c., \tag{4.50}$$

where $U(\mathbf{q})$ defines the strength and form of the interaction, in which, via the creation or absorption of a phonon with momentum $\mathbf{q}$, the Bloch-Floquet modes scatter to another mode. Since only the *total* quasienergy is conserved –Bloch-Floquet modes quasienergy $\varepsilon_p(\mathbf{k})$ plus the energy of the phonon bath $E^{(\text{ph})} = \sum_{\mathbf{q}} \hbar\omega_{\mathbf{q}}$– after a scattering process involving (to first order) the emission or absorption of phonon, the Bloch-Floquet mode will end up at $\varepsilon_q(\mathbf{k}')$. Since the electrons can be scattered in different BZ of the Floquet spectrum, when the final state is folded back into the 1$^{\text{st}}$BZ in might appear to have increased its energy even after a phonon has been emitted. These are the *Floquet-Umklapp* processes that cause the characteristic unbounded heating of Floquet systems described in Chapter 2 [113]. Other important effects for this problem are electron-electron interactions, which together with electron-phonon exchanges are important effects to be taken into account to go beyond the noninteracting single-particle picture [69, 113].

Chapter 5

Gliding basis set for electronic stopping

In this Chapter, a framework for electronic stopping calculations is proposed. It makes use of the fact that the projectile is a localised perturbation and, with the construction of a local, time-periodic basis set (the *gliding basis*), it allows for the treatment of the moving crystal. The Bloch-Floquet scattering states can be expressed in this basis set, which allows for the calculation of the matrix elements for stopping as well as, for example, allowing for the calculation of the local density of states and charge density. The formalism is presented here for 1D, but it is ready to be generalised to higher dimensions.

5.1 Tight-binding chain in time-periodic basis

Before introducing formalism based on the construction of the gliding basis set, consider a simple 1D tight-binding (TB) model. Introducing a set of time-periodic nonorthogonal basis will help to build the gliding basis set.

5.1.1 Tight-binding chain and nonorthogonal basis states

Consider the simplest 1D TB model with N atoms, with one type of atom per unit cell, one orbital per atom $\langle x|\varphi_\mu\rangle = \varphi_\mu(x) = \varphi(x-R_\mu)$, and lattice spacing a, such that $\varphi[x-(R_n+a)] = \varphi(x-R_{n+1})$, with $R_\mu \equiv \mu a$. Assuming that such *localised* orbitals are orthogonal $\langle\varphi_\mu|\varphi_\nu\rangle = \delta_{\mu\nu}$, and assuming only nearest-neighbour interactions with hopping parameter $-\gamma$, the Hamiltonian is written as

$$H_0 = \sum_\mu |\varphi_\mu\rangle E_0 \langle\varphi_\mu| - \gamma \sum_\mu (|\varphi_\mu\rangle\langle\varphi_{\mu+1}| + h.c.), \tag{5.1}$$

with ε_0 being the on-site energy, and *h.c.* indicates the Hermitian conjugate. While the choice of an orthogonal basis set is, in this simple case, the most convenient, it is not the only possible one. Indeed, it may be more convenient, as it will be shown later, to relax this requirement.

The eigenvalues of the above Hamiltonian form a band structure labelled by wavenumber k,

$$E(k) = E_0 - 2\gamma\cos(ka), \tag{5.2}$$

and the Bloch eigenstates are given, in the orthogonal basis set, by

$$|\psi_k\rangle = \frac{1}{\sqrt{N}}\sum_{\mu} e^{i\mu ka}\,|\varphi_\mu\rangle \tag{5.3}$$

Consider a new set of nonorthogonal basis $|\xi_\mu\rangle$ which has an overlap with the nearest-neighbours. The overlap matrix can be defined as

$$S_{\mu\nu} = \langle\xi_\mu|\xi_\nu\rangle\,. \tag{5.4}$$

A choice for such basis can be, for instance,

$$|\xi_\mu\rangle = \cos\theta\,|\varphi_\mu\rangle + \sin\theta\,|\varphi_{\mu+1}\rangle\,, \tag{5.5}$$

where θ is some constant parameter, giving an overlap matrix

$$S_{\mu\nu} = \delta_{\mu,\nu} + \cos\theta\sin\theta(\delta_{\mu,\nu+1} + \delta_{\mu,\nu-1}). \tag{5.6}$$

The choice of 5.5 with two orbital sites is made for simplicity. Nonorthogonal basis sets can be defined using an arbitrary number of such orbitals.

The Hamiltonian matrix elements, in these basis, are given by

$$\langle\xi_\mu|H_0|\xi_\nu\rangle = -2\gamma\cos\theta\sin\theta\,\delta_{\mu,\nu} - \gamma(\delta_{\mu,\nu+1} + \delta_{\mu,\nu-1}) - \gamma\cos\theta\sin\theta(\delta_{\mu,\nu+2} + \delta_{\mu,\nu-2}). \tag{5.7}$$

By constructing the Bloch state in the nonorthogonal basis

$$|\tilde{\psi}_k\rangle = \frac{\mathscr{C}_k(\theta)}{\sqrt{N}}\sum_{\mu} e^{i\mu ka}\,|\xi_\mu\rangle\,, \tag{5.8}$$

where $\mathscr{C}(\theta)$ is a phase factor that depends on the form of the overlap, it is easy to verify that they are eigenstates of H_0 with the same eigenvalue, and they correspond when defining the phase factor to be $\mathscr{C}_k(\theta) = (\cos\theta + e^{-ika}\sin\theta)^{-1}$, making $|\tilde{\psi}_k\rangle \equiv |\psi_k\rangle$.

Knowing the eigenstates of H_0, the impurity problem can be solved via the Green's function formalism [75]: in the orthogonal basis set representation, the Green's function g associated to H_0 (defined by $[E - H_0]g = \mathbb{1}$) can be used, for instance, to find the local density of states (LDOS) analytically –see Fig. 5.1–

$$\rho_\mu(E) = \mp\frac{1}{\pi}\Im[g^{(\pm)\,\mu\mu}(E)] = \frac{\Theta(2\gamma - |E - E_0|)}{\pi\sqrt{4\gamma^2 - (E - E_0)^2)}}, \tag{5.9}$$

where μ indicates the orbital site and

$$g^{(\pm)\,\mu\nu}(E) = \int_{1BZ}\frac{dk}{2\pi}\frac{e^{i(\mu-\nu)ka}}{E - E(k) \pm i\eta}. \tag{5.10}$$

is the Green's function matrix element, obtained through the spectral representation of g with the eigenstates of Eq. 5.3.

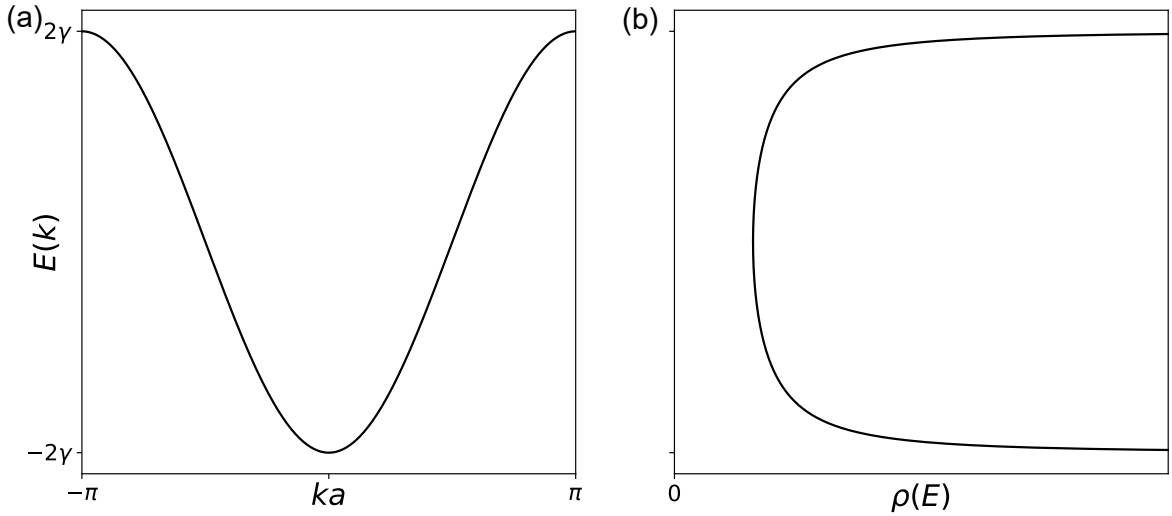

Fig. 5.1 (a) Band structure for the 1D TB model defined by the Hamiltonian in Eq. 5.1. (b) Density of states (LDOS), calculated using 5.9, showing with van-Hove singularities corresponding to the band edges.

The same result can be found when using a non-orthogonal basis set representation, for instance using the basis defined by 5.5 (for more details, see [114–116]). Consider some arbitrary nonorthogonal basis set $\{|\xi_\mu\rangle, \mu = 1, ..., N\}$. A state $|\psi\rangle$ in the *natural*

representation can in these basis be represented as a contravariant first-rank tensor

$$|\psi\rangle = \langle\xi^{\mu}|\psi\rangle\,|\xi_{\mu}\rangle = c^{\mu}\,|\xi_{\mu}\rangle\,, \tag{5.11}$$

where the summation convention over repeated indices is implied henceforth. The Schrödinger equation $H\,|\psi\rangle = E\,|\psi\rangle$ can be written in matrx form as

$$H_{\mu\nu}c^{\nu} = ES_{\mu\nu}c^{\nu}. \tag{5.12}$$

The dual basis set $\{|\xi^{\mu}, \mu = 1,...,N\rangle\}$ can be defined such that it satisfies

$$\langle\xi^{\mu}|\xi_{\nu}\rangle = \langle\xi_{\nu}|\xi^{\mu}\rangle = \delta^{\mu}_{\nu}, \tag{5.13}$$

Hence, the identity in the Hilbert space $\mathscr{R}$ is defined by

$$|\xi_{\mu}\rangle\,\langle\xi^{\mu}| = |\xi^{\mu}\rangle\,\langle\xi_{\mu}| = \mathbb{1}. \tag{5.14}$$

The overlap of the dual basis $S^{\mu\nu} = \langle\xi^{\mu}|\xi^{\nu}\rangle$, in addition, gives the inverse of the overlap matrix $S_{\mu\nu}$. In this representation, the Green's function satisfies the equation

$$[ES_{\mu\rho} - H_{\mu\rho}]g^{\rho\nu} = \delta^{\nu}_{\mu},. \tag{5.15}$$

where $g^{\mu\nu} = \langle\xi^{\mu}|g|\xi^{\nu}\rangle$, and the LDOS takes the form

$$\rho_{\nu}(E) = -\frac{1}{\pi}\Im\left[g^{\nu}{}_{\nu}(E)\right], \tag{5.16}$$

where $g^{\nu}{}_{\nu}(E) = g^{\nu\rho}(E)S_{\rho\nu}$. It is straight-forward to verify that the expression 5.16 is indeed the correct one for the TB chain LDOS. The matrix elements of the Green's function for the TB eigenstates are

$$g^{(\pm)\,\mu\nu}(E) = \int_{1BZ}\frac{dk}{2\pi}\frac{\mathscr{C}_k(\theta)\mathscr{C}^*_k(\theta)e^{i(\mu-\nu)ka}}{E - E(k) \pm i\eta}, \tag{5.17}$$

with $\mathscr{C}_k(\theta)$ defined as in Eq. 5.8. A calculation of the generalized Green's function matrix elements $g^{\mu}_{\nu} = g^{\mu\rho}S_{\rho\nu}$ leads to an expression identical to the one of Eq. 5.10. In addition, the charge density can also be calculated from the density matrix elements [114]

$$P^{\mu\nu} = -\frac{2}{\pi}\int_{-\infty}^{E_F} dE\; g^{\mu\nu}(E), \tag{5.18}$$

where E_F indicates the Fermi level, as

$$n(\mathbf{r}) = P^{\mu\nu} \langle \xi_\mu | \mathbf{r} \rangle \langle \mathbf{r} | \xi_\nu \rangle = P^{\mu\nu} \xi^*_\mu(\mathbf{r}) \xi_\nu(\mathbf{r}). \tag{5.19}$$

When introducing a localised impurity at the atomic site l, i.e. adding an extra term to the Hamiltonian

$$H = \sum_\mu |\varphi_\mu\rangle E_0 \langle \varphi_\mu| - \gamma \sum_\mu (|\varphi_\mu\rangle \langle \varphi_{\mu+1}| + h.c.) + E_P |\varphi_l\rangle \langle \varphi_l| \equiv H_0 + V, \tag{5.20}$$

the scattering problem can be solved by calculating the full Green's function of H, which is made possible by knowing the Green's operator g of H_0. The full Green's function G can be expressed via the Dyson equation

$$G = g + gVG. \tag{5.21}$$

Expanding Eq. (5.21) recursively –and assuming that such an expansion is well defined, i.e. converges– a closed-form expression can be found which, in the orthogonal basis representation, is [75]

$$G = g + g|\varphi_l\rangle \frac{E_P}{1 - E_P g^{ll}} \langle \varphi_l | g, \tag{5.22}$$

where $g^{ll} = \langle \varphi_l | g | \varphi_l \rangle$. The knowledge of the matrix elements of g is enough to find the full solutions of the scattering problem: indeed, the LDOS can be evaluated using Eq. 5.9 for G, and, in addition, the knowledge of G allows for the calculation of the full scattering solution from the Lippmann-Schwinger equation $|\Psi_k^{(+)}\rangle = |\psi_k\rangle + G^{(+)} V |\psi_k\rangle$ for the Bloch eigenstates 5.3. Expressing the scattering state as $|\Psi_k^{(+)}\rangle = \sum_\mu \langle \varphi_\mu | \Psi_k^{(+)} \rangle |\varphi_\mu\rangle$, the amplitude at site n is given by

$$\langle \varphi_\mu | \psi_k^{(+)} \rangle = \langle \varphi_\mu | k \rangle + \frac{g^{(+)\,\mu l}[E(k)] E_P \langle \phi_l | k \rangle}{1 - E_P g^{(+)\,ll}[E(k)]}, \tag{5.23}$$

an exact expression which can be evaluated with our knowledge of g and the impurity energy level. This method, while it gives a simple solution for the 1D TB case, can be generalised to more complex models within the TB framework.

5.1.2 Static tight-binding chain with time-dependent localised basis

Before presenting the gliding basis formalism for the Bloch-Floquet scattering problem, let us stay for the moment with the static 1D TB chain, but consider a new basis set that is

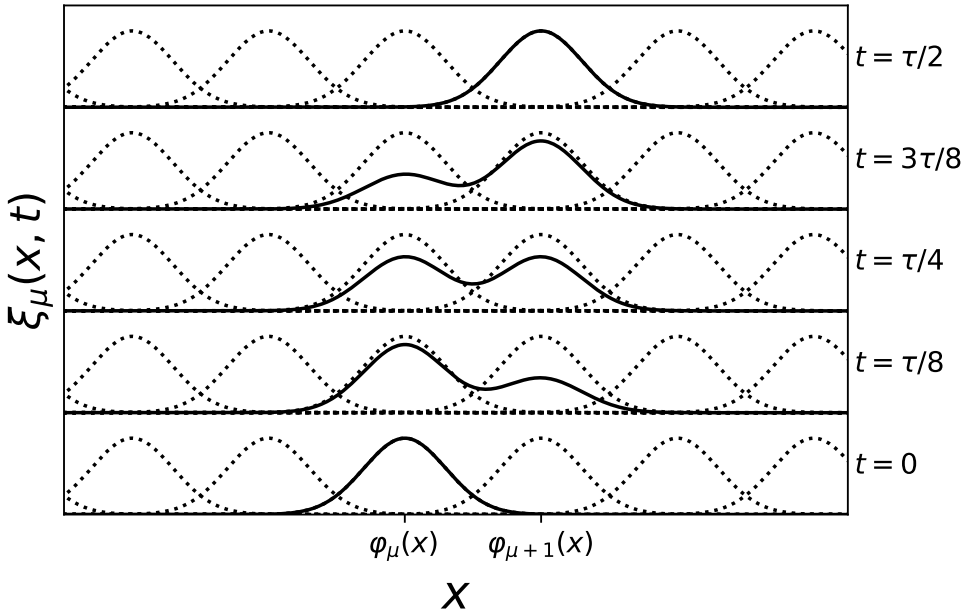

Fig. 5.2 TB basis orbitals $\varphi_\mu(x)$ (dotted lines), and nonorthogonal time-periodic basis $\xi_\mu(x,t)$ at some fixed site μ, for four time snapshots over half a period (solid lines), with the $\varphi_\mu(x)$ going back symmetrically to the snapshot at $t = 0$ over the rest of the period. The modulating "gauge" functions for the basis orbitals $\varphi_\mu(x)$ and $\varphi_{\mu+1}(x)$ used here are $|\cos\omega t/2|$ and $|\sin\omega t/2|$, but define an equally valid basis compared to the definition 5.24 –see section 5.2 and Appendix C for more details.

non-orthogonal and time-periodic. This will be useful for application in the Bloch-Floquet problem. For instance, based on the nonorthogonal basis defined in Eq. 5.5, the following

$$|\xi_\mu(t)\rangle = \cos\omega t\,|\varphi_\mu\rangle + \sin\omega t\,|\varphi_{\mu+1}\rangle \tag{5.24}$$

defines a basis set with the desired properties –see Fig. 5.2 for an illustration. This has the same form as before, with the difference that the parameter θ one has the time-evolving phase, which makes the basis periodic with period $\tau = 2\pi/\omega$. The Bloch states 5.3 can be expressed through 5.24 as

$$|\psi_k(t)\rangle = e^{-iE(k)t/\hbar}\frac{1}{\sqrt{N}}\sum_\mu c_k^\mu(t)\,|\xi_\mu(t)\rangle\,, \tag{5.25}$$

where the energy phase was explicitly introduced and the time-dependent site amplitudes are defined as

$$c_k^\mu(t) = \frac{e^{i\mu ka}}{[\cos(\omega t) + e^{-ika}\sin(\omega t)]}\,. \tag{5.26}$$

Using time-evolving basis states, the TDSE must be modified [115]: indeed, the TDSE for a static nonorthogonal basis set takes the form

$$H_{\mu\nu}c_\nu = i\hbar S_{\mu\nu}\eth_t c_\nu, \tag{5.27}$$

where the same notation as defined in 5.12 was kept, the overlap $S_{\mu\nu}$ is defined as in Eq. 5.6; the Hamiltonian matrix elements $H_{\mu\nu}$ are defined as in Eq. 5.7 and the covariant time derivative is given by

$$\eth_t c^\mu = \partial_t c^\mu + D^\mu_{\nu t} c^\nu, \tag{5.28}$$

with the Christoffel symbol

$$D^\mu_{\nu t} = \langle \xi^\mu | \partial_t \xi_\nu \rangle . \tag{5.29}$$

Equivalently, the TDSE can be written as

$$H^\mu_\nu c^\nu = i\hbar \eth_t c^\nu, \tag{5.30}$$

or as

$$H_{\mu\nu}c^\nu = i\hbar S_{\mu\nu}\eth_t c^\nu, \tag{5.31}$$

by making use of the properties and the definitions of the overlap matrix and its inverse, with the notation convention following the natural representation as defined in the previous section. It is a simple exercise to verify that the Bloch states expressed in these basis indeed satisfy the TDSE expressed in this form (see Appendix C). In fact, the space spanned by the time-periodic basis gives, at each time, a different Hilbert space $\mathscr{R}(t)$, which can be interpreted as a curved manifold (see [115]). Indeed, this is the reason why covariant derivatives and curvature tensors have to be introduced to correctly represent the TDSE as in the equations above.

Now, consider a general choice of time-periodic basis in $\mathscr{R}(t)$, which can be extended to represent a valid basis set in the Fourier Hilbert space $\mathscr{R} \otimes \mathscr{T}$. The frequency ω can be interpreted in this case as the frequency of some "fictitious" time-periodic drive with zero amplitude: its value is arbitrary, and not related to any physical quantities (in contrast to the frequency $\omega = 2\pi v/a$ related to the motion of the projectile, which will be treated in the next section). The eigenstates and dispersion relations are unchanged, and the Floquet modes can be represented in the Floquet quasienergy picture, with bands replicas in quasienergy with spacing $\hbar\omega$. This is shown in Fig. 5.3. Indeed, the Bloch state in Eq. 5.25 can be identified to be in the Floquet form, and equivalent states with quasienergy $E_p(k) = E(k) + p\hbar\omega$ can

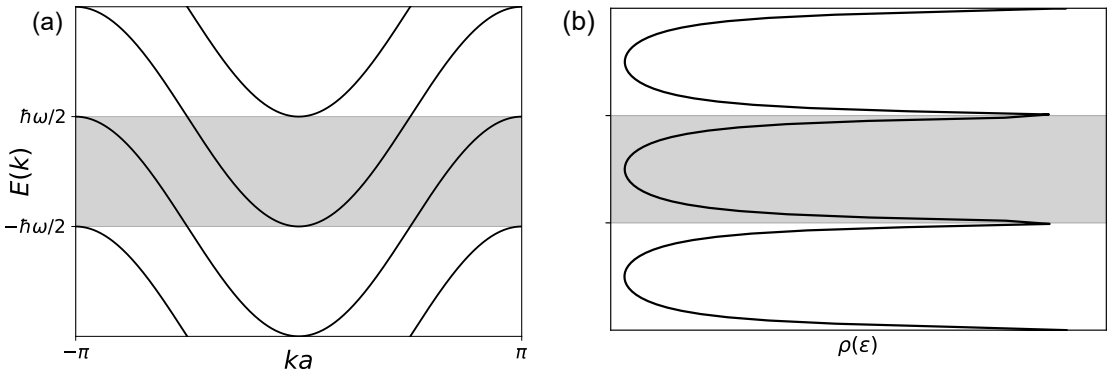

Fig. 5.3 (a) Replicas of the 1D-TB model with energy dispersion 5.2, extended in Floquet quasienergy space. The choice for the frequency is $\hbar\omega = \gamma$ in this case. For a frequency smaller than the bandwidth, one gets the replicas to overlap in the 1st Floquet BZ (highlighted in grey), whereas a larger frequency leads to "decoupled" replicas in Floquet space, c.f. the case for Bloch-Floquet states in Fig. 3.2. (b) Corresponding DOS: note the van Hove singularities corresponding to the band edges, that for this specific choice of parameters overlap at the edges of the different BZs in quasienergy.

be defined as

$$|\psi_k(t)\rangle = e^{-i(E(k)+p\hbar\omega)t/\hbar}\frac{1}{\sqrt{N}}\sum_{\mu} e^{ip\hbar\omega t}c_k^{\mu}(t)\,|\xi_{\mu}(t)\rangle\,; \tag{5.32}$$

the coefficients $c_k^{\mu}(t)$ are periodic with period τ, and can be expanded in Fourier series. This expression is equivalent to the relationship between Floquet modes of Eq. 2.6, where in this case the Floquet modes are identified by

$$|\phi_{kp}(t)\rangle = \sum_{\mu} c_{pk}^{\mu}(t)\,|\xi_{\mu}(t)\rangle\,, \tag{5.33}$$

with the definition $c_{pk}^{\mu}(t) \equiv e^{ip\hbar\omega t}c_k^{\mu}(t)$.

The Fourier Hilbert space $\mathscr{R}\otimes\mathscr{T}$ can be constructed by considering a general periodic function expanded in the time-periodic basis $\{|\xi_{\mu}(t)\rangle\}$

$$|\chi(t)\rangle = \sum_{\mu} C^{\mu}(t)\,|\xi_{\mu}(t)\rangle\,. \tag{5.34}$$

Since both the basis and the function are time periodic, for the coefficients $C^{\mu}(t)$ must be periodic as well. Note that this is also the case for the Bloch state in the form 5.33: the

wavefunction –once decoupled from the energy phase factor– is in fact time-independent, and therefore trivially time-periodic. For this reason, the replicas in quasienergy space can be defined as illustrated in Fig. 5.3.

The time-periodic coefficients $C^{\mu}(t)$ can be Fourier expanded as

$$C^{\mu}(t) = \sum_{m} e^{im\omega t} C^{\mu}_{m}, \tag{5.35}$$

and the time-periodic state can be expressed as

$$|\chi(t)\rangle = \sum_{\mu,m} C^{\mu}_{m} e^{im\omega t} |\xi_{\mu}(t)\rangle, \tag{5.36}$$

which decouples all the time-dependence from the coefficients. From this, a new basis set for the extended Hilbert space $\mathscr{R} \otimes \mathscr{T}$ is readily defined

$$\langle t|\xi_{\mu}, m\rangle\rangle = e^{im\omega t} |\xi_{\mu}(t)\rangle, \tag{5.37}$$

where a double-bracket notation has been introduced for the new basis $\{|\xi_{\mu}, m\rangle\rangle\}$ to indicate that the new basis functions span the extended Hilbert space $\mathscr{R} \otimes \mathscr{T}$.

The overlap matrix of the new Fourier basis can be expressed as an inner product in the extended space as

$$\begin{aligned} S_{\mu\nu,mn} &= \frac{1}{\tau} \int^{\tau} dt\ S_{\mu\nu}(t) e^{-i(m-n)\omega t} \\ &= \delta_{\mu,\nu}\delta_{m,n} + s_{m-n}(\delta_{\mu,\nu+1} + \delta_{\mu,\nu-1}), \end{aligned} \tag{5.38}$$

with $s_{m-n} = \frac{1}{\tau}\int^{\tau} s(t) e^{-i(m-n)\omega t}$, where $s(t) = \sin(\omega t)\cos(\omega t)$ the special case of Eq. 5.24, but the function $s(t)$ could be a general periodic function, depending on the definition of nonorthogonal basis coefficients in 5.5 –for a more general definition for the gauge parameters when defining the nonorthogonal basis, see Appendix C.

In the Fourier basis, TB Bloch states take the form

$$|\phi_{kp}\rangle\rangle = \frac{1}{\sqrt{N}} \sum_{mn} c^{\mu}_{mp}(k) |\xi_{\mu}, m\rangle\rangle, \tag{5.39}$$

where the double-bracket notation indicates that the state belongs to the extended Hilbert space, and the expansion coefficients are defined as

$$c^{\mu}_{mp}(k) = R_{m-p}(k) e^{ik\mu a}, \tag{5.40}$$

with R_m defined as the m^{th} component of the Fourier expansion of $R(k,t)$

$$R(k,t) = \frac{1}{(\cos(\omega t) + e^{-ika}\sin(\omega t))} = \sum_m R_m(k) e^{im\omega t}. \tag{5.41}$$

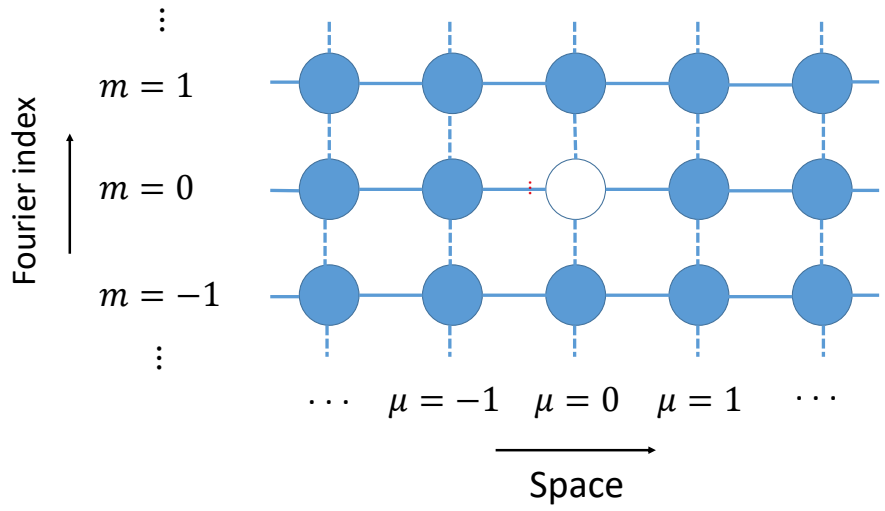

Fig. 5.4 Two-dimensional lattice, sites defined by the Fourier basis $|\xi_\mu, m\rangle\rangle$. The $\mu = 0, m = 0$ site is highlighted in white. The matrix elements of the Hamiltonian in nonorthogonal basis are of the form Eq. 5.7, with up to next-to-nearest-neighbour (NTNN) hopping: this means that sites are not only connected between neighbours as shown in the figure (for simplicity), but up to NTNN. In addition, all the components at different Fourier indices connected. By considering an impurity (or projectile) to couple, for example, only to the $|\xi_0, 0\rangle\rangle$ site, the Dyson equation for the TB model can be solved.

Given that the modes $|\phi_{kp}\rangle\rangle$ are eigenstates of the Hamiltonian expressed in the Fourier basis (by construction), the Green's function matrix elements can be found directly

$$g^{(\pm)\mu\nu}_{mn}(\varepsilon) = \sum_p \int_{1BZ} \frac{dk}{2\pi} \frac{c^\mu_{mp}(k) c^{\nu\,*}_{np}(k)}{\varepsilon - E_p(k) \pm i\eta}. \tag{5.42}$$

The Fourier basis set can be interpreted as defining a 2D lattice, with the extra dimension appearing from the Fourier expansion in the periodic basis, as illustrated in Fig. 5.4: each of the $|\xi_\mu, m\rangle\rangle$ can be identified with a site in the lattice, with the Green's function acting as the propagator between sites.

From this expression, the Fourier components of the LDOS at site μ can be obtained: consider some general Green's function $G^{\mu\nu}_{mn}$ in the representation of extended space basis

$|\xi_\mu, m\rangle\rangle$. The μ, m component of the LDOS is given by

$$D_{\mu m}(\varepsilon) = -\frac{1}{\pi}\Im\left[\sum_{\nu n} G^{\mu\nu}_{mn}(\varepsilon) S_{\nu\mu,nm}\right]. \tag{5.43}$$

The interpretation of this expression is straightforward: it represents the density of states corresponding to a site in the extended-space lattice of Fig. 5.4. By summing over the Fourier components, the LDOS of the site μ can be defined as

$$\mathscr{D}_\mu(\varepsilon) = \sum_m D_{\mu m}(\varepsilon). \tag{5.44}$$

While the value of ω is arbitrary, since it is not linked to any real physical drive, the model, through the introduction of an impurity at one of the sites, is related to well-studied models representing periodically driven Hamiltonians: an impurity at $\mu = 0$, defined appropriately over the Fourier basis $|\xi_\mu, m\rangle\rangle$, can be mapped to a time-periodic impurity localised at $\mu = 0$ in a TB chain, which is analogous of, for instance, the problem analysed in [73].

5.2 Gliding basis set for a moving projectile in a crystal

In Chapter 4, it was shown that, in the projectile frame, stationary stopping can be described through Bloch-Floquet scattering theory with a fixed impurity. The gliding basis set, defined in a similar way to the time-dependent nonorthogonal basis set in the last section, allows for a convenient formalisation of the model of a moving chain and a fixed projectile. The formalism for the problem of a moving projectile in a lattice is different from the well-known TB model with an impurity at one of the chain sites: in the former, compared to the latter, the coupling between the crystal and the projectile cannot be limited to a single site but, after each period, the impurity will have moved from one of the sites to the next.

Consider the problem of a TB chain in a moving frame, in particular the Hamiltonian 5.1 for the 1D TB lattice, with a single orbital $\varphi_\mu(x)$ per site. The transformation of this Hamiltonian to a frame moving at velocity v can be directly derived from the Hamiltonian transformation rule 3.10, which gives

$$H_0(t) = \sum_\mu |\varphi_\mu(t)\rangle E_0 \langle\varphi_\mu(t)| - \gamma\sum_\mu (|\varphi_\mu(t)\rangle \langle\varphi_{\mu+1}(t)| + h.c.) - v\hat{p} - \frac{1}{2}mv^2, \tag{5.45}$$

where the local basis have now become time-dependent. The time-dependent moving orbitals take the form $\langle x|\varphi_\mu(t)\rangle = \varphi_\mu(x+vt) \equiv \varphi_\mu(x,t)$: each orbital has a fixed label μ, and moves

past the projectile $V_P(x)$ at constant velocity v. The eigenstates of the Hamiltonian 5.45 are easily obtained, since they correspond to the Bloch states in the static frame of Eq. 5.3: by applying the Galilean transformation of Eq. 3.4 to the TB Bloch state 5.3, the wavefunction becomes

$$\psi_k(x,t) = e^{-i\frac{mv}{\hbar}x} e^{-i[E(k)+\frac{1}{2}mv^2]t/\hbar} \frac{1}{\sqrt{N}} \sum_\mu e^{ika\mu} \varphi_\mu(x,t) \,, \tag{5.46}$$

where the time-dependent energy phase was explicitly introduced. The normalisation factor of $1/\sqrt{N}$, which comes from imposing periodic boundary conditions on a one-dimensional lattice with N sites, is kept for convenience. Comparing the expression above with the general Bloch wavefunction form of Eq. 3.13, the Bloch-Floquet modes $\phi_{pk}(x,t)$ with quasienergy $\varepsilon_p(k)$ of Eq. 3.15 can be expressed in the local orbital basis as

$$\phi_{pk}(x,t) = e^{ip\omega t} e^{-ikvt} e^{-imvx} \frac{1}{\sqrt{N}} \sum_\mu e^{i\mu ka} \varphi_\mu(x,t), \tag{5.47}$$

which is manifestly periodic with period $\tau = a/v$. For simplicity, and without loss of generality, the basis states can also be defined by absorbing the phase factor $\tilde{\varphi}_\mu(x,t) = e^{-imvx}\varphi_\mu(x,t)$, since this phase leaves the physics invariant. Therefore, it will be assumed from now on that this is the chosen basis set, and the tilde on $\tilde{\varphi}_\mu(x,t)$ will be dropped. By construction, $\phi_{kp}(x,t)$ is an eigenstate of the Floquet Hamiltonian $\mathscr{H}_0(t) = H_0(t) - i\hbar\partial_t$ with quasienergies $\varepsilon(k) = E(k) + p\hbar\omega$, which can be also verified explicitly.

The gliding basis, in the spatial representation, can be defined as

$$\xi_\mu(x,t) = \mathscr{N}(t)[f(\delta t)\,\varphi_{\mu+n}(x,t) + f(\delta t - \tau)\,\varphi_{\mu+n+1}(x,t)], \tag{5.48}$$

for $\delta t \in [0,\tau]$, $t = \delta t + n\tau$, and where the normalisation factor

$$\mathscr{N}(t) = \left[\, |f(\delta t)|^2 + |f(\delta t - \tau)|^2 \,\right]^{-1/2} . \tag{5.49}$$

The index n in the expression 5.48 labels the n^{th} period in time, which is defined arbitrarily from an initial time $t_0 = 0$. Moreover, an equivalent definition to Eq. 5.48 is

$$\xi_\mu(x,t) = \mathscr{N}(t)\,[f(\delta t)\,\varphi_\mu(x,\delta t) + f(\delta t - \tau)\,\varphi_{\mu+1}(x,\delta t)]. \tag{5.50}$$

Similarly to 5.5, the choice of two atomic orbitals is arbitrary and made for simplicity, in order to have the simplest model that allows coupling with the projectile perturbation once it is introduced. An example of a gliding basis localised at site $\mu = 0$ is illustrated in Fig. 5.5: the localised basis function $\xi_0(x,t)$ stays fixed in the same region of space [unlike the $\varphi_\mu(x,t)$

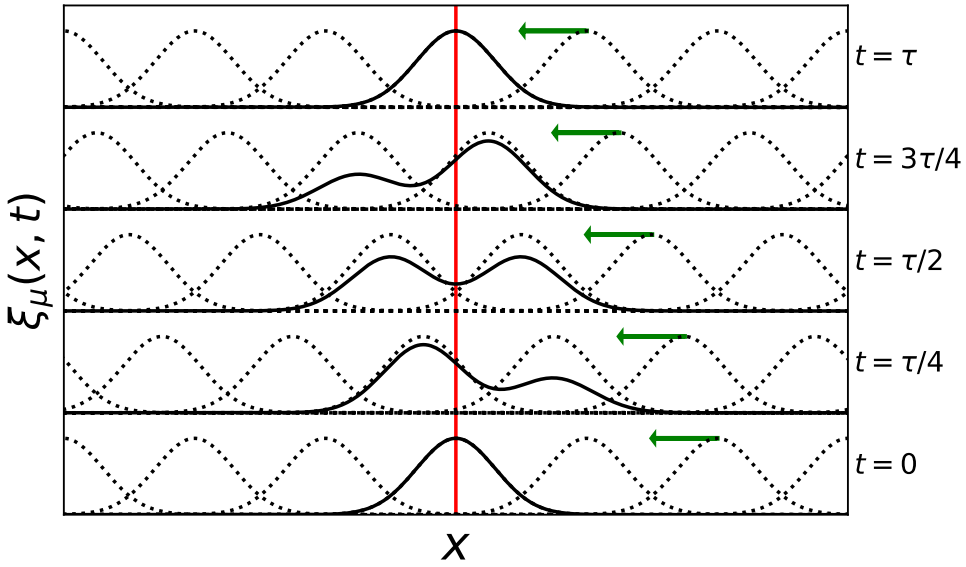

Fig. 5.5 Moving TB basis orbitals $\varphi_\mu(x,t)$ (dotted lines), and gliding basis $\xi_\mu(x,t)$ at some fixed site μ, for four time snapshots over a period (solid lines). The red arrow indicates $x = 0$, where the centre of the projectile potential $V_P(x)$ is assumed to be fixed. The main difference compared to the "static" time-periodic basis of Fig. 5.2 is that the gliding basis set is constructed from the moving set of orbitals $\varphi_\mu(x,t)$, as indicated by the green arrow. This makes them more suitable for the description of a TB chain in a moving frame.

basis states, displacing leftwards with velocity $-v$] changing shape in a periodic fashion, with period τ.

The function $f(t)$ defines the transformation to the gliding bases, and it should be nonzero only in the $[-\tau,\tau]$ interval, i.e.

$$f(t) = \begin{cases} \tilde{f}(t) & , \ t \in [-\tau,\tau] \\ 0 & , \ t \notin [-\tau,\tau] \end{cases} \tag{5.51}$$

and, for instance, satisfying $f(0) = 1$ to correspond to the orbitals at times that are multiples of the period τ. Otherwise, $\tilde{f}(t)$ can be defined quite arbitrarily, although it could be mathematically convenient to ensure continuity at $t = \pm\tau$, and even continuity of derivatives at those points, especially for numerical implementations. Indeed, since the basis given by the gliding basis set $\{\xi_\mu(x,t)\}$ will be spanning the same space as done by $\{\varphi_\mu(x,t)\}$, the shape of $f(t)$ represents a gauge freedom, which can be exploited for practical considerations such as maximising smoothness for Fourier transform truncation, or simplicity in the equations. Examples of $\tilde{f}(t)$ can be found in Appendix C, including a choice similar to the one for the periodic basis of the static lattice of 5.24. In fact, the actual difference between the two

definitions of nonorthogonal basis (non-gliding and gliding) is just a matter of a particular gauge choice, which gives a different temporal dependence to the shape of the basis set. Therefore, the main ideas and details of the formalism developed in the previous section can be readily generalised for the case of the gliding basis.

The overlap $S_{\mu\nu}(t) = \langle \xi_\mu(t) | \xi_\nu(t) \rangle$ between gliding basis is easily found to be

$$S_{\mu\nu}(t) = \delta_{\mu\nu} + s(t)\ (\delta_{\mu,\nu+1} + \delta_{\mu,\nu-1}), \tag{5.52}$$

where $f(t)$ is assumed to be real, and with the definition

$$s(t) = \mathcal{N}^2(t)\ f(\delta t) f(\delta t - \tau)\ . \tag{5.53}$$

Consider the form of this overlap matrix, given the conditions that were imposed on the $f(t)$: it is tridiagonal, with the off-diagonal elements pulsating in time according to the function $s(t)$, which annihilates with period τ.

The matrix elements of the moving lattice Hamiltonian $H_0(t)$, are found directly from 5.45 (setting $E_0 = 0$ for simplicity)

$$\begin{aligned}(H_0)_{\mu\nu}(t) = &-2\gamma s(t)\delta_{\mu,\nu} - \gamma(\delta_{\mu,\nu+1} + \delta_{\mu,\nu-1}) \\ &- \gamma\, s(t)(\delta_{\mu,\nu+2} + \delta_{\mu,\nu-2}) - v\hat{p}_{\mu\nu} - \frac{1}{2}mv^2 S_{\mu\nu}(t).\end{aligned} \tag{5.54}$$

Hence, the Bloch-Floquet modes can be directly expressed in terms of the gliding basis functions through a transformation of the expressions 5.47 and 5.46. They can be regarded as the solutions of the TDSE in the form of Eq. 5.31 in the gliding basis similarly to the static TB states in the nonorthogonal time-periodic basis in section 5.1. Therefore, Bloch-Floquet modes of order p in quasienergy are

$$\phi_{pk}(x,t) = \frac{1}{\sqrt{N}} \sum_\mu \alpha^\mu_{pk}(t)\xi_\mu(x,t), \tag{5.55}$$

and the amplitude is defined as

$$\alpha^\mu_{pk}(t) = \frac{e^{ip\omega t} e^{-ikv\delta t} e^{i\mu ka}}{\mathcal{N}(t)\left[f(\delta t) + e^{-ika} f(\delta t - \tau)\right]} \equiv \frac{e^{i\phi_p(\delta t)}}{\sqrt{N[1 + 2s(t)\cos(ka)]}}, \tag{5.56}$$

with $\delta t \equiv t - n\tau$ as before, and the phase factor $\phi(\delta t)$ is by definition

$$\begin{aligned}
&\phi_p(\delta t) = \phi_{1p}(\delta t) + \phi_2(\delta t)\ ; \\
&\phi_{1p}(\delta t) = (-kv + p\omega)\delta t\ , \\
&\phi_2(\delta t) = \tan^{-1}\left[\frac{\sin(ka) f(\delta t - \tau)}{f(\delta t) + \cos(ka) f(\delta t - \tau)}\right].
\end{aligned} \tag{5.57}$$

From these expressions, the analogy section 5.1 is immediate. Indeed, the Bloch-Floquet modes can be represented in the extended Hilbert space $\mathscr{R} \otimes \mathscr{T}$ by defining a Fourier-gliding basis set following the same formalism via Eq. 5.37, with the difference that the Galilean transformation of the local basis functions introduces some extra phase factors. Hence, define the Fourier expansion of the periodic coefficients in Eq. 5.56

$$\alpha^{\mu}_{pk}(t) = \sum_m e^{im\omega t} \alpha^{\mu}_{pk,m}, \tag{5.58}$$

with

$$\alpha^{\mu}_{pk,m} = \frac{1}{\tau}\int^{\tau} dt\, \alpha^{\mu}_{pk}(t), \tag{5.59}$$

and the gliding basis in the extended Fourier space in analogy with Eq. 5.37 as

$$\langle t | \xi_\mu, m \rangle\rangle = e^{im\omega t} |\xi_\mu(t)\rangle\,. \tag{5.60}$$

From these definitions, the Bloch-Floquet states in the extended Hilbert space takes the form

$$|\phi_{pk}\rangle\rangle = \sum_{\mu m} \alpha^{\mu}_{pk,m} |\xi_\mu, m\rangle\rangle. \tag{5.61}$$

In addition, the unperturbed Green's function matrix elements in the Fourier-gliding basis are immediately found

$$g^{\mu\nu\ (\pm)}_{mn}(\varepsilon) = \sum_p \int_{1BZ} \frac{dk}{2\pi} \frac{\alpha^{\mu}_{pk,m} \alpha^{\nu *}_{pk,n}}{\varepsilon - \varepsilon_p(k) \pm i\eta} \tag{5.62}$$

5.3 Introducing the projectile: Dyson equation

At last, the framework has been set for the introduction of the projectile in this TB model, which, for example, can be modelled as being coupled one of the μ sites. Furthermore, depending on the choice of the gauge functions and the form of the projectile time-dependence,

the matrix elements of the projectile in the Fourier-gliding basis can also be truncated in the Fourier indices.

For instance, the simplest possible choice for the projectile matrix elements is given by

$$V_P = \varepsilon_P \delta_{\mu,\nu} \delta_{m,n} \delta_{m,0} \delta_{\mu,0}, \tag{5.63}$$

with the projectile being localised only on a single lattice site, to which it couples with strength ε_P (the white bead in Fig. 5.4). While this choice for the projectile is not physical for any realistic $V_P(t)$ (see the latter part of section 5.4 for more details), it may may be able to capture qualitatively the effects of the projectile, even though it might show a weaker/stronger effect compared to the more accurate definition of the projectile perturbation.

Hence, consider the Dyson equation for the full Green's function 5.21: it can be expressed, for any choice of the form of the projectile in the Floquet gliding basis $|\xi_\mu, m\rangle\rangle$, as

$$G^{\mu\nu}_{mn} = g^{\mu\nu}_{mn} + g^{\mu\rho}_{mp} V_P{}^{\rho\sigma}_{pq} G^{\sigma\nu}_{qn}. \tag{5.64}$$

All the matrix elements of the unperturbed Green's function are known from Eq. 5.62. In general, the matrix elements of the full Green's function can be found by matrix inversion, assuming that a truncation in the Fourier index m would provide a good approximation, as

$$G = [\mathbb{1} - g V_P]^{-1} g, \tag{5.65}$$

where $\mathbb{1}$ and A^{-1} is the inverse of a matrix A, assuming the non-singularity of A.

In fact, with the choice of Eq. 5.63 for the projectile impurity, the Dyson equation can be solved for each component using the following scalar equations

$$G^{\mu\nu}_{mn} = g^{\mu\nu}_{mn} + g^{\mu 0}_{m0} \varepsilon_P G^{0\nu}_{0n}, \tag{5.66}$$

$$G^{0\nu}_{0n} = g^{0\nu}_{0n} + g^{00}_{00} \varepsilon_P G^{0\nu}_{0n}, \tag{5.67}$$

from which it immediately follows that

$$G^{0\nu}_{0n} = \frac{g^{0\nu}_{0n}}{1 - g^{00}_{00} \varepsilon_P}, \tag{5.68}$$

providing the full solution for G in an algebraic form which allows for faster numerical calculations. Indeed, other more general forms for the projectile (allowing, for example, the Fourier coupling indices to be different form zero) do not allow a closed-form solution for

the matrix elements, and full matrix inversion needs to be implemented using Eq. 5.65. In general, for problems such as the present one, involving impurities in a tight-binding lattice where the impurity matrix has dimensions $n \times n$, the smallest matrix that needs to be inverted for a solution of the full Green's function needs to have at least the same dimensionality.

5.4 Scattering states in gliding basis, Dyson equation for realistic projectiles

Once the full Green's function is calculated, the site amplitudes of the single-particle Bloch-Floquet scattering modes can be found. Indeed, using the scattering wavefunctions expressed in the Lippmann-Schwinger form, reported here for convenience

$$|\Phi_{k_i}^{(+)}\rangle = |\phi_{k_i}\rangle + G^{(+)} V_P |\phi_{k_i}\rangle \tag{5.69}$$

and the simple projectile form 5.63, the site amplitudes are immediately found

$$\langle\langle \xi^\mu, m|\Phi_{k_i}^{(+)}\rangle\rangle = \langle\langle \xi^\mu, m|\phi_{k_i}\rangle\rangle + \frac{g_{m0}^{\mu 0\ (+)}[\varepsilon(k_i)]\varepsilon_P \langle\langle \xi^0, 0|\phi_{k_i}\rangle\rangle}{1 - \varepsilon_p g_{00}^{00\ (+)}[\varepsilon(k_i)]}, \tag{5.70}$$

which define the full Bloch-Floquet modes

$$|\Phi_{k_i}^{(+)}\rangle\rangle = \sum_{\mu m} \langle\langle \xi^\mu, m|\Phi_{k_i}^{(+)}\rangle\rangle\, |\xi_\mu, m\rangle\rangle. \tag{5.71}$$

From this expression, the time-dependence of the Bloch-Floquet is recovered by applying the inverse Fourier mapping

$$|\Phi_{k_i}^{(+)}(t)\rangle = \sum_\mu \left(\sum_m e^{im\omega t} \langle\langle \xi^\mu, m|\Phi_{k_i}^{(+)}\rangle\rangle \right) |\xi_\mu(t)\rangle\,. \tag{5.72}$$

The wavefunction in Eq. 5.72 represents the full Bloch-Floquet scattering state at all sites, and has a very different form compared to the form of Eq. 3.18 (derived in Chapter 4) for Bloch-Floquet states, which is an asymptotic expression that can be expanded in terms of the unperturbed Bloch-Floquet modes satisfying quasienergy conservation. In fact, the site-specific amplitudes contain in principle much more information, including on the regions close to the projectile, which are in general quite difficult to access without real-time first-principles methods.

The calculation of full Green's function permits the calculation of the matrix elements of the electronic stopping expression Eq. 4.41, i.e. $\langle\langle \phi_{mk_f} | V_P | \Phi_{nk_i} \rangle\rangle$ defined as in Chapter 4. In fact, the matrix element can be equivalently expressed in terms of the T scattering matrix, that is defined, in terms of the full Green's function, as

$$T = V_P + V_P G V_P, \tag{5.73}$$

which means that the matrix element can be simply expressed as

$$\langle\langle \phi_{mk_f} | V_P | \Phi^{(+)}_{nk_i} \rangle\rangle = \langle\langle \phi_{mk_f} | T | \phi_{nk_i} \rangle\rangle \tag{5.74}$$

by using the definition 5.69. In fact, the T matrix equation can be thought as essentially an equivalent representation of the Green's function, with the same analytic structure: poles and branch cuts on the real axis correspond to bound states or eigenstates in the continuum. The T matrix can be defined with the equivalent expression

$$T = V_P + V_P g T, \tag{5.75}$$

c.f. Dyson equation 5.21.

So far, this corresponds to standard scattering theory, and the matrix element is often approximated using low-order perturbation theory [75]. However, for the special choice 5.63 for V_P, it is clear from Eq. 5.73 that the only relevant matrix element is T^{00}_{00}, which can be directly expressed using the Green's function matrix element G^{00}_{00} found from Eq. 5.68 as

$$T^{00}_{00} = \frac{\varepsilon_P}{1 - g^{00}_{00}\varepsilon_p} = [\varepsilon_P^{-1} - g^{00}_{00}]^{-1}. \tag{5.76}$$

Once $T^{00}_{00} \equiv T^{00}_{00}(\varepsilon)$ is obtained for the quasienergy spectrum, it can be used to find the matrix element 5.74.

Notwithstanding the fact that the projectile form 5.63 is the simplest possible in the Fourier gliding basis, it cannot be a representation of any realistic projectile, and therefore should be amended in order to have meaningful numerical stopping calculations. Indeed, when considering a projectile potential localised at $\mu = 0$, whose only nonzero Fourier component is the 0^{th} one (a constant in the local gliding basis at $\mu = 0$), then the contribution to the Floquet matrix coming from the projectile will be

$$V^{\mu\nu}_{P,mn} = \left[\frac{1}{\tau}\int dt\; e^{-i(m-n)\omega t}\varepsilon_P\right]\delta_{\mu\nu}\delta_{\mu,0} = \varepsilon_P\delta_{mn}\delta_{\mu\nu}\delta_{\mu,0}. \tag{5.77}$$

The difference with 5.63 is that ε_P needs to be included into *all* matrix elements that satisfy $m = n$ due to the integral in 5.77. Hence, this form is the one that needs to be used for calculations. The explicit matrix form of 5.77 is –with the blocks are matrices in the Fourier indices (m,n)–

$$V_P = \left[\begin{array}{c|c|c} \ddots & & \\ \mathbf{0} & \mathbf{0} & \mathbf{0} \\ \hline & \begin{array}{ccccc} \ddots & \vdots & \vdots & \vdots & \\ \dots & \varepsilon_P & 0 & 0 & \dots \\ \dots & 0 & \varepsilon_P & 0 & \dots \\ \dots & 0 & 0 & \varepsilon_P & \dots \\ & \vdots & \vdots & \vdots & \ddots \end{array} & \\ \mathbf{0} & & \mathbf{0} \\ & & \\ \hline & & \\ \mathbf{0} & \mathbf{0} & \mathbf{0} \\ & & \ddots \end{array}\right]_{\mu\nu} . \tag{5.77'}$$

With this choice for the projectile, the scalar equations derived in the current section and section 5.3 are generalised to matrix equations in the Fourier indices (m,n). In particular, Eq.s 5.66 and 5.67 are generalised to

$$G^{\mu\nu}_{mn} = g^{\mu\nu}_{mn} + \varepsilon_P g^{\mu 0}_{ml} G^{0\nu}_{ln}, \tag{5.78}$$

and

$$G^{0\nu}_{ln} = g^{0\nu}_{ln} + \varepsilon_P g^{00}_{lp} G^{0\nu}_{pn} \tag{5.79}$$

respectively, noting the presence of the sum over repeated indices l and p in 5.78 and 5.79 from the new form 5.77 of V_P. They can also be expressed as matrices in the Fourier indices,

$$G^{\mu\nu} = g^{\mu\nu} + \varepsilon_P g^{\mu 0} G^{0\nu}; \tag{5.80}$$

$$G^{0\nu} = g^{0\nu} + \varepsilon_P g^{00} G^{0\nu}. \tag{5.81}$$

The latter can be solved for $G^{0\nu}$ using matrix inversion

$$G^{0\nu} = \left[\mathbb{1} - \varepsilon_P g^{00}\right]^{-1} g^{0\nu}, \tag{5.82}$$

which provides a complete solution for the full Green's function.

In addition, Eq. 5.70 for the local site amplitude is generalised as

$$\langle\langle \xi^{\mu}, m|\Phi_{k_i}^{(+)}\rangle\rangle = \langle\langle \xi^{\mu}, m|\phi_{k_i}\rangle\rangle + \varepsilon_P G_{mp}^{\mu 0\,(+)}[\varepsilon(k_i)]\,\langle\langle \xi^{0}, p|\phi_{k_i}\rangle\rangle\,. \tag{5.83}$$

Furthermore, the T matrix for the calculation of the matrix element for stopping of Eq. 5.76 is also generalised as a matrix in Fourier indices

$$T^{00} = \left[\mathbb{1} - V_P^{00} g^{00}\right]^{-1} V_P^{00} = \left[\left(V_P^{00}\right)^{-1} - g^{00}\right]^{-1}. \tag{5.84}$$

In this expression, the matrix inversion of V_P^{00} is easy to carry out due to its diagonal structure. Hence, the matrix T can be used for the calculation of the single-particle ETR 4.36 and the stopping power 4.43.

5.5 Local density of states in the Fourier-gliding basis

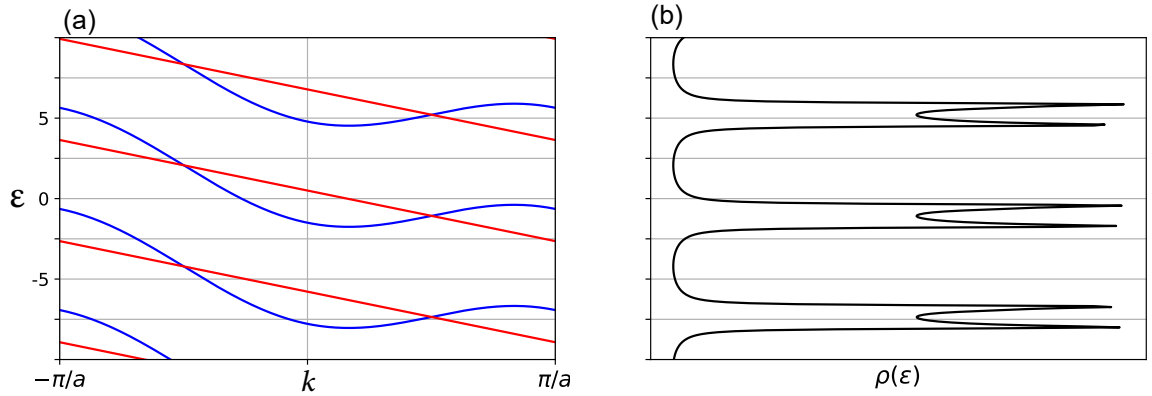

Fig. 5.6 Quasienergy bands (a) for the single-band 1D TB model folded back into the 1st BZ in reciprocal space, showing the replicas in Fourier space and associated DOS (b), arbitrary units. The quasienergy dispersion is $\varepsilon_p(k) = \varepsilon(k) + p\hbar\omega$, with $\varepsilon(k) = E(k) - v\hbar k$, with the TB band dispersion E(k) given by Eq. 5.2. The transformation to the moving frame modifies the excitation spectrum, as it is clear from the modification of the van Hove singularities compared to the static case of Fig. 5.3. In addition, in (a) the solid line in red represents the Fermi level for a half-filling of the band: when considering the total DOS, the state occupancy information seems to be lost due to the reference frame transformation.

In analogy with the LDOS defined in Eq. 5.5 and Eq. 5.5 for the nonorthogonal time-periodic basis for the static lattice, the LDOS can also be defined for the Fourier gliding basis. While they have essentially the same form, they are reported here for reference:

$$D_{\mu m}(\varepsilon) = -\frac{1}{\pi}\mathrm{Im}\left[\sum_{\nu n} G^{\mu\nu}_{mn}(\varepsilon) S_{\nu\mu,nm}\right];$$
$$\mathscr{D}_{\mu}(\varepsilon) = \sum_{m} D_{\mu m}(\varepsilon).$$

For the unperturbed lattice, the LDOS corresponds to the DOS, and it is illustrated in Fig. 5.6 for the single-band cases considered throughout the Chapter, in Fig. 5.6 (c.f. with the Bloch-Floquet dispersion 3.2). The DOS is calculated numerically via the above equation for $\mathscr{D}_{\mu}(\varepsilon)$ for $\mu = 0$ using the unperturbed Green's function defined in Eq. 5.62. The DOS spectrum is noticeably modified by the transformation, with a shift in the van Hove singularities that is strongly dependent on the parameter v of the transformation, looking very different from the static bands [see Fig. 5.3 (b)]. This change in the LDOS depending on v is not due to the 1D nature of the system under consideration, but would be present when considering higher-dimensional crystals, and it is due to the "tilting" induced by the reference frame transformation.

The insertion of the projectile impurity of the form 5.63 would modify the LDOS in the sites where the projectile exerts its influence, modifying the excitation spectrum nonperturbatively, from which important information on stopping processes can be extracted. However, there is still an important issue of interpretability of the LDOS in the moving frame, since, for the general case, the spectrum given by the DOS sums over both occupied and unoccupied states, as shown in Fig 5.6. While for the unperturbed states this problem can be avoided by explicitly introducing the occupation numbers $f[E(k)]$ as a function of k (as done, for instance, in Eq. 4.43) it is not clear how to keep track of this information for the LDOS once the projectile perturbation is introduced. In addition, the adiabatic limit $v \to 0$ that was discussed in section 3.6 makes a meaningful analysis of the LDOS nontrivial: in the low-velocity limit, the band replicas in Fig. 5.6 become arbitrarily close to each other in the 1$^{\mathrm{st}}$ BZ (corresponding to the folding of the extended bands in Fig. 3.8), and the information on occupancy becomes harder to access. These issues, and their importance towards a meaningful spectral analysis of the stopping problem once the projectile is introduced, are currently being investigated.

5.6 Summary and next steps

In this Chapter, an approach for the treatment of the Bloch-Floquet scattering problem for the analysis of stopping processes in crystals has been presented. It is based on the introduction of a localised, time-periodic basis set that can most conveniently treat the system of a moving TB lattice and a fixed projectile potential coupling with one of the local basis. A solution to the Dyson equation in these bases gives access to the matrix elements for stopping power calculations based on 4.41, as well as, in principle, giving access to the full scattering states in the Fourier-gliding bases. Once these are known, they can be mapped back to the original Hilbert space to have the real time-dependence, as explained in Chapter 2, section 2.2. Thus, the real-time charge density could be in principle accessed directly through the many-electron noninteracting wavefunctions, and obtain population information on the localised basis from a generalised Mulliken population analysis [114]. Moreover, having access to the real-time charge density would allow, for instance, to analyse the electronic wake and hence to calculate quantities like the instantaneous force on the ion, which are very difficult to analyse without computationally expensive first-principles methods.

In practice, there are some technical steps that still need to be finalised in order to achieve a complete meaningful analysis of the stopping problem from the formalism presented in the previous sections 5.4 and 5.5.

The first one is related to the solution of the Dyson Eq.s 5.78 and 5.79 to get the full Green's function after the introduction of the projectile. The convergence of $G(\varepsilon)$ with respect to the number of Fourier components taken into account in the expansion, the number of Floquet "replicas" used for the calculations (which enter the Dyson equation through the unperturbed g in Eq. 5.62) and other details of the numerical calculations such as k-point spacing, for instance, are still the subject of ongoing analysis. Such convergence tests are also useful to find the optimal parameter selection for numerical accuracy and efficiency in this simple model, which will help in terms of a future scaling up of the calculations for realistic materials.

The second one, always related to the solution of the Dyson equation, is associated to the interpretability of the results in real space, which have been introduced in section 5.5 with regards to the LDOS, for instance. There can be various ways to do this type of real-space analysis: an example is the analysis of the LDOS $\mathscr{D}_\mu(\varepsilon)$ and how it varies with projectile strength, position μ, etc.; another possible direction that will be pursued is to consider a simple single-particle scattering process (i.e. to consider the scattering process of a single Bloch-Floquet state): an analysis of the local-site weight 5.83 would provide interesting and important insights into the Bloch-Floquet scattering problem and its stationary state regime.

A full understanding and ability to map the calculations in the gliding basis formalism to real space and real time will help the completion of the third important technical step, i.e. the implementation of the stopping power calculations. In this direction, one of the technical issues is a correct implementation of the tilted Fermi level constraint (see section 5.5) into the Dyson equation for a correct implementation of the matrix element into the expression 4.43 to avoid inaccuracies on state occupancy when calculating the stopping power.

The completion of the above steps for the 1D TB chain will pave the way for calculations in higher dimensions, and with different types of basis states and orbitals. Hence, realistic calculations of the stopping power, comparable to experimental results, will be implemented.

Chapter 6

Conclusions and Outlook

In this Thesis, I have presented a new approach for the description and calculation of electronic stopping in arbitrary crystalline solids. The theory is based on the mapping of the problem of a charged projectile of radiation shooting through a periodic direction of a crystal to the one of a static projectile and a time-periodic crystalline potential, via a reference frame transformation. The discrete time-translation symmetry that emerges from the transformation allows for the treatment of the system as a whole (projectile and crystal) in terms of a Floquet scattering theory for the electronic Bloch states of the crystal. The single-particle solutions of this Bloch-Floquet scattering problem, which are stroboscopically stationary, are linked to what is observed in stopping calculations performed with real-time TDDFT, in which the rate of increase in total energy of the projectile and crystalline system oscillates over a constant value after an initial transient. Indeed, the existence of the stroboscopically stationary states as solutions of the Floquet problem provides a general justification on the assumptions made in jellium and linear-response approaches, which assume, without justification, that the stationary regime for stopping would hold beyond their defining simplifications and hypothesis to arbitrary solids.

The main advantage of the Floquet approach to stopping power calculations over full time dependent first principles simulations such as TDDFT is that, through Floquet theory, the problem of solving the time-dependent Schrödinger equation can be can be transformed into the equivalent one of solving a time-independent-like Schrödinger equation (the Floquet mode equation), in which the time parameter is promoted to be an additional coordinate. Therefore, the ability of using the techniques usually implemented for the analysis of time independent problems, instead of computationally expensive real time techniques to explicitly solve the time-dependent Schrödinger equation, makes the new formulation especially promising and potentially superior to current state-of-the-art techniques in terms of efficiency and accuracy.

Furthermore, based on quasienergy conservation, a new interpretation of the controversial velocity threshold effect in gapped materials was presented in this Thesis. Quasienergy conservation and a Bloch-Floquet scattering analysis show that only an effective threshold behaviour should in fact be observed: while not directly accessible from current data and experimental capabilities, it could in principle be probed experimentally. The results on the effective threshold phenomenology for a slow projectile $v \to 0$ were then linked to the more general problem of the adiabatic limit in Floquet systems as the frequency of time-periodic Hamiltonians $\omega \to 0$.

An expression for electronic stopping power was derived based on Bloch-Floquet scattering theory in Chapter 4, and it was reduced, in the corresponding limits, to the expressions derived through perturbation theory and nonlinear models for jellium, demonstrating a generalisation to these models. While the theory is ready for a generalization to more realistic situations using time-dependent mean-field and Kohn-Sham methods, the introduction of many-body interactions will require further theoretical work.

In order to provide a practical scheme for numerical calculations, the theory for stopping has been applied in Chapter 5 to a one-dimensional, single-orbital tight-binding model. The specific properties of the system, with a static impurity and a moving lattice, requires the introduction of a special set of localised, time-periodic basis (the gliding basis set), allowing for a convenient description of the problem in the projectile frame. Then, the Bloch-Floquet scattering theory has been formulated in terms of the gliding basis extended in Fourier space. For a simple choice of the projectile representation in these Fourier-gliding basis, the scattering problem can be solved exactly by considering the Dyson equation for the full Green's function, from which full single-particle scattering states can be obtained. A calculation of the local density of states (LDOS) has been presented, which provides further insight on the problem of a moving tight-binding chain. Moreover, it has been shown that solving the Dyson equation after the introduction of the projectile, together with the expression for stopping power derived in Chapter 4, allows the presented methodology to be applied for future numerical calculations.

The work opens interesting paths for the analysis of excitations of many-body quantum systems due to moving impurities, since most of the current theoretical models (excluding real time first principles calculations such as TDDFT) have been limited to linear-response or, at most, nonlinear theories for the homogeneous electron liquid. By taking into account the electronic structure of the host environment, this work provides a promising starting point for new and more accurate numerical schemes for electronic stopping calculations. Furthermore, it can provide insights to other canonical problems in the field of strongly nonequilibrium electronic systems where, for instance, a symmetry similar to the discrete

space-time symmetry $\mathscr{T}$ is fulfilled. The introduction of the time-dependent gliding basis, which has formalised for the first time the treatment of a moving tight-binding model (as far as I am aware), may have some further applications aside from the stopping problem.

The next practical steps to develop a full scheme for electronic stopping calculations are clear and achievable in the near-term. Firstly, the 1D tight-binding model needs to be finalised as described in section 5.6: this includes the implementation of numerical calculations for the stopping power, and the generalisation of the method to higher dimensions and multiple basis states per unit cell. The 1D tight-binding model will be the subject of a forthcoming publication. In fact, this can be readily done from the basic 1D formalism developed in Chapter 5, where the tight-binding chain can be generalised to a 2D or 3D tight-binding model with an arbitrary number of atoms and basis states per unit cell (this is especially important for materials in which the core electrons were proven to provide an important contribution, e.g. in [47]). For this generalisation, the definition of the gliding basis set can be adjusted accordingly. The numerical calculations which can be developed from the model will provide accurate quantitative results to some of the qualitative results and analysis from Chapter 3, with regards to the effective threshold behaviour and the low-velocity adiabatic limit for stopping processes. The model could also provide more insight on the more general problem of adiabatic limits in Floquet systems, which become problematic beyond perturbative treatments.

Having access to the full stationary states will allow the characterization of the induced time-dependent electronic density, and hence can be used to analyse the electronic wake (the induced density fluctuation of the electron system by the projectile). However, the method needs to be extended to the levels of theory used in the state-of-the-art first-principles calculations using TDDFT on real material target (beyond jellium) in order to have a meaningful quantitative comparison with the most accurate numerical results.

A further step will be the generalisation of the theory for cases in which the system does not strictly conserve quasienergy, in analogy with the extension of the nonlinear theory for jellium (based on energy conserving scattering theory in the projectile frame) to include many-body effects [64, 65]. More correctly, the introduction of many-body interactions does not in fact make the problem nonconservative, but rather the electronic system, while conserving quasienergy together with the environment (crystal, etc.), can be modelled as a coupling to dissipative channels. Thus, the electronic properties will be modified compared to the single-particle noninteracting theory. In order to reach the levels of accurate state-of-the-art first-principles methods, the inclusion of many-body exchange and correlation and other many-body effects will need to be ultimately implemented into software packages for first-principles calculations, such as TDDFT. Nevertheless, the Bloch-Floquet theory presented

in the Thesis could be also implemented at the level of a simple effective Hamiltonian. For instance, the properties of insulators could be captured by a simple two-band model, and the inclusion of many-body interactions could be performed through various methods such as nonequilibrium Green's function (Keldysh) formalism. Therefore, incorporating existing methodologies that combine nonequilibrium many-body formalism with Floquet theory [117, 118] might be an interesting research direction to gain novel results and insights, even though they might not be sufficient for calculations on real materials.

Another question that naturally arises, which has been discussed section 2.3 and is related to the dissipative many-body effects in nonequilibrium systems, is the one of instabilities that will break the stroboscopic stationary character of the electron states, giving rise to the flapping instability in the projectile core electrons observed in first-principles calculations and linked to the DTC phase (there is still the possibility that, however, this effect is an artifact of the TDDFT simulation). An analysis of the instabilities induced by many-body interactions may in fact provide a signal for the existence of a DTC phase in this type of system.

To conclude, it has been shown that the new framework presented in the Thesis, as well as providing the basis for future accurate and more efficient first-principles calculations compared to currect techniques, can be regarded as a platform for the exploration and investigation of some interesting, important, and fundamental questions on the properties of nonequilibrium quantum systems. The problem of electronic stopping of ions in solids and its theoretical formulation is old and yet timeless. It has been repeatedly linked to many theoretical advances in the quantum theory of the electrons, an important example being the development of Lindhard's linear response theory and the random phase approximation. Therefore, I am confident and hopeful that the study of electronic stopping processes will lead to plenty of fascinating physics to be discovered.

References

[1] P.M. Echenique, R.M. Nieminen, and R.H. Ritchie. Density functional calculation of stopping power of an electron gas for slow ions. *Solid State Communications*, 37(10):779 – 781, 1981.

[2] Peter Sigmund. Particle penetration and radiation effects. *Particle Penetration and Radiation Effects, by Peter Sigmund. Berlin: Springer, 2008. ISBN: 978-3-540-72622-7*, 01 2008.

[3] William Henry Bragg and Richard Kleeman. XXXIX. On the α particles of radium, and their loss of range in passing through various atoms and molecules. *The Lon., Edin., and Dub. Phil. Mag.*, 10(57):318–340, 1905.

[4] Ernest Rutherford. Lxxix. the scattering of α and β particles by matter and the structure of the atom. *The London, Edinburgh, and Dublin Philosophical Magazine and Journal of Science*, 21(125):669–688, 1911.

[5] J Linhard. Approximation method in classical scattering by screened Coulomb fields. *Kgl. Danske Vidensk. Selsk. mat.-fys. Medd.*, 36(10):3–32, 1968.

[6] C P Race, D R Mason, M W Finnis, W M C Foulkes, A P Horsfield, and A P Sutton. The treatment of electronic excitations in atomistic models of radiation damage in metals. *Reports on Progress in Physics*, 73(11):116501, oct 2010.

[7] R. L. Fleischer, P. B. Price, and R. M. Walker. Ion Explosion Spike Mechanism for Formation of Charged-Particle Tracks in Solids. *Journal of Applied Physics*, 36(11):3645–3652, 1965.

[8] M. Toulemonde, E. Paumier, and C. Dufour. Thermal spike model in the electronic stopping power regime. *Radiation Effects and Defects in Solids*, 126(1-4):201–206, 1993.

[9] M. Caro, A. A. Correa, E. Artacho, and A. Caro. Stopping power beyond the adiabatic approximation. *Scientific Reports*, 7(1):2618, 2017.

[10] Max Born and Robert Oppenheimer. Zur quantentheorie der molekeln. *Annalen der physik*, 389(20):457–484, 1927.

[11] Niels Bohr. II. On the theory of the decrease of velocity of moving electrified particles on passing through matter. *The London, Edinburgh, and Dublin Philosophical Magazine and Journal of Science*, 25(145):10–31, 1913.

[12] Hans Bethe. Zur theorie des durchgangs schneller korpuskularstrahlen durch materie. *Annalen der Physik*, 397(3):325–400, 1930.

[13] Felix Bloch. Zur bremsung rasch bewegter teilchen beim durchgang durch materie. *Annalen der Physik*, 408(3):285–320, 1933.

[14] E. Fermi and E. Teller. The Capture of Negative Mesotrons in Matter. *Phys. Rev.*, 72:399–408, Sep 1947.

[15] J Lindhard. On the properties of a gas of charged particles. *Kgl. Danske Videnskab. Selskab Mat.-fys. Medd.*, 28, 1954.

[16] T. L. Ferrell and R. H. Ritchie. Energy losses by slow ions and atoms to electronic excitation in solids. *Phys. Rev. B*, 16:115–123, Jul 1977.

[17] Nevill Francis Mott and Harry Jones. The theory of the properties of metals and alloys. 1958.

[18] Ady Mann and Werner Brandt. Material dependence of low-velocity stopping powers. *Phys. Rev. B*, 24:4999–5003, Nov 1981.

[19] G. Martínez-Tamayo, J. C. Eckardt, G. H. Lantschner, and N. R. Arista. Energy loss of H^+ and He^+ in Al, Zn, and Au in the very low- to intermediate-energy range. *Phys. Rev. A*, 54:3131–3138, Oct 1996.

[20] J.E. Valdés, G. Martínez Tamayo, G.H. Lantschner, J.C. Eckardt, and N.R. Arista. Electronic energy loss of low velocity H+ beams in Al, Ag, Sb, Au and Bi. *Nuclear Instruments and Methods in Physics Research Section B: Beam Interactions with Materials and Atoms*, 73(3):313 – 318, 1993.

[21] J. M. Pruneda, D. Sánchez-Portal, A. Arnau, J. I. Juaristi, and Emilio Artacho. Electronic Stopping Power in LiF from First Principles. *Phys. Rev. Lett.*, 99:235501, Dec 2007.

[22] Alfredo A. Correa, Jorge Kohanoff, Emilio Artacho, Daniel Sánchez-Portal, and Alfredo Caro. Nonadiabatic Forces in Ion-Solid Interactions: The Initial Stages of Radiation Damage. *Phys. Rev. Lett.*, 108:213201, May 2012.

[23] K. Schönhammer. Nonlinear friction in a homogenous electron gas: Exact results. *Phys. Rev. B*, 37:7735–7737, May 1988.

[24] L. Bönig and K. Schönhammer. Time-dependent local perturbation in a free-electron gas: Exact results. *Phys. Rev. B*, 39:7413–7423, Apr 1989.

[25] E. Zaremba, A. Arnau, and P.M. Echenique. Nonlinear screening and stopping powers at finite projectile velocities. *Nucl. Instr. and Meth. in Phys. Res. Sec. B: Beam Interactions with Materials and Atoms*, 96(3):619 – 625, 1995.

[26] A. F. Lifschitz and N. R. Arista. Velocity-dependent screening in metals. *Phys. Rev. A*, 57:200–207, Jan 1998.

[27] S. N. Markin, D. Primetzhofer, and P. Bauer. Vanishing Electronic Energy Loss of Very Slow Light Ions in Insulators with Large Band Gaps. *Phys. Rev. Lett.*, 103:113201, Sep 2009.

[28] M. D. Brown and C. D. Moak. Stopping Powers of Some Solids for 30-90-MeV ^{238}U Ions. *Phys. Rev. B*, 6:90–94, Jul 1972.

[29] M. Draxler, S. P. Chenakin, S. N. Markin, and P. Bauer. Apparent Velocity Threshold in the Electronic Stopping of Slow Hydrogen Ions in LiF. *Phys. Rev. Lett.*, 95:113201, Sep 2005.

[30] C. Celedón, E. A. Sánchez, M. S. Moreno, N. R. Arista, J. D. Uribe, M. Mery, J. E. Valdés, and P. Vargas. Energy loss of protons and deuterons at low energies in Pd polycrystalline thin films. *Phys. Rev. A*, 88:012903, Jul 2013.

[31] Jorge E. Valdés, Patricio Vargas, and Vladimir A. Esaulov. Energy losses of slow ions traveling through crystalline solids and scattered on crystalline surfaces. *Radiation Effects and Defects in Solids*, 171(1-2):60–76, 2016.

[32] Erich Runge and E. K. U. Gross. Density-Functional Theory for Time-Dependent Systems. *Phys. Rev. Lett.*, 52:997–1000, Mar 1984.

[33] Arkady V. Krasheninnikov, Yoshiyuki Miyamoto, and David Tománek. Role of Electronic Excitations in Ion Collisions with Carbon Nanostructures. *Phys. Rev. Lett.*, 99:016104, Jul 2007.

[34] M. Quijada, A. G. Borisov, I. Nagy, R. Díez Muiño, and P. M. Echenique. Time-dependent density-functional calculation of the stopping power for protons and antiprotons in metals. *Phys. Rev. A*, 75:042902, Apr 2007.

[35] Ryan Hatcher, Matthew Beck, Alan Tackett, and Sokrates T. Pantelides. Dynamical Effects in the Interaction of Ion Beams with Solids. *Phys. Rev. Lett.*, 100:103201, Mar 2008.

[36] M. Ahsan Zeb, J. Kohanoff, D. Sánchez-Portal, A. Arnau, J. I. Juaristi, and Emilio Artacho. Electronic Stopping Power in Gold: The Role of *d* Electrons and the **H**/He Anomaly. *Phys. Rev. Lett.*, 108:225504, May 2012.

[37] Ari Ojanperä, Arkady V. Krasheninnikov, and Martti Puska. Electronic stopping power from first-principles calculations with account for core electron excitations and projectile ionization. *Phys. Rev. B*, 89:035120, Jan 2014.

[38] Rafi Ullah, Fabiano Corsetti, Daniel Sánchez-Portal, and Emilio Artacho. Electronic stopping power in a narrow band gap semiconductor from first principles. *Phys. Rev. B*, 91:125203, Mar 2015.

[39] André Schleife, Yosuke Kanai, and Alfredo A. Correa. Accurate atomistic first-principles calculations of electronic stopping. *Phys. Rev. B*, 91:014306, Jan 2015.

[40] Zhi Wang, Shu-Shen Li, and Lin-Wang Wang. Efficient Real-Time Time-Dependent Density Functional Theory Method and its Application to a Collision of an Ion with a 2D Material. *Phys. Rev. Lett.*, 114:063004, Feb 2015.

[41] Edwin E. Quashie, Bidhan C. Saha, and Alfredo A. Correa. Electronic band structure effects in the stopping of protons in copper. *Phys. Rev. B*, 94:155403, Oct 2016.

[42] A. Lim, W. M. C. Foulkes, A. P. Horsfield, D. R. Mason, A. Schleife, E. W. Draeger, and A. A. Correa. Electron Elevator: Excitations across the Band Gap via a Dynamical Gap State. *Phys. Rev. Lett.*, 116:043201, Jan 2016.

[43] Kyle G. Reeves, Yi Yao, and Yosuke Kanai. Electronic stopping power in liquid water for protons and α particles from first principles. *Phys. Rev. B*, 94:041108(R), Jul 2016.

[44] Chang-Kai Li, Feng Wang, Bin Liao, Xiao-Ping OuYang, and Feng-Shou Zhang. Ab initio electronic stopping power and threshold effect of channeled slow light ions in HfO_2. *Phys. Rev. B*, 96:094301, Sep 2017.

[45] Dillon C. Yost, Yi Yao, and Yosuke Kanai. Examining real-time time-dependent density functional theory nonequilibrium simulations for the calculation of electronic stopping power. *Phys. Rev. B*, 96:115134, Sep 2017.

[46] Gang Bi, Jun Kang, and Lin-Wang Wang. High velocity proton collision with liquid lithium: a time dependent density functional theory study. *Phys. Chem. Chem. Phys.*, 19:9053–9058, 2017.

[47] Rafi Ullah, Emilio Artacho, and Alfredo A. Correa. Core Electrons in the Electronic Stopping of Heavy Ions. *Phys. Rev. Lett.*, 121:116401, Sep 2018.

[48] D R Mason, J Page, C P Race, W M C Foulkes, M W Finnis, and A P Sutton. Electronic damping of atomic dynamics in irradiation damage of metals. *Journal of Physics: Condensed Matter*, 19(43):436209, sep 2007.

[49] C P Race, D R Mason, M H F Foo, W M C Foulkes, A P Horsfield, and A P Sutton. Quantum–classical simulations of the electronic stopping force and charge on slow heavy channelling ions in metals. *Journal of Physics: Condensed Matter*, 25(12):125501, feb 2013.

[50] Gabriele Giuliani and Giovanni Vignale. *Quantum theory of the electron liquid*. Cambridge university press, 2005.

[51] R. H. Ritchie. Plasma Losses by Fast Electrons in Thin Films. *Phys. Rev.*, 106:874–881, Jun 1957.

[52] R. H. Ritchie. Interaction of Charged Particles with a Degenerate Fermi-Dirac Electron Gas. *Phys. Rev.*, 114:644–654, May 1959.

[53] J. Finnemann. En redegørelse for resultaterne af beregninger over spredning af elektroner med lav energi pøa afskærmede Coulombfelter. Master's thesis, Aarhus University, 1968.

[54] P.M. Echenique, F. Flores, and R.H. Ritchie. Dynamic Screening of Ions in Condensed Matter. volume 43 of *Solid State Physics*, pages 229 – 308. Academic Press, 1990.

[55] Lev Davidovich Landau and Evgenii Mikhailovich Lifshitz. Quantum mechanics: non-relativistic theory, 3rd edition (Pergamon, New York, 2013).

[56] L. Bönig and K. Schönhammer. Time-dependent local perturbation in a free-electron gas: Exact results. *Phys. Rev. B*, 39:7413–7423, Apr 1989.

[57] B. A. Trubnikov and Yu. N. Yavlinskiĭ. Energy loss of slow protons in metals. *Sov Phys JETP*, 48:253–260, 1965. [Engl. transl. Sov. Phys. JETP 21, 167-171 (1965)].

[58] P Sigmund. Particle penetration and radiation effects 2, vol. 179 of Springer Series in Solid-State Sciences, 2014.

[59] P. L. Grande. Alternative treatment for the energy-transfer and transport cross section in dressed electron-ion binary collisions. *Phys. Rev. A*, 94:042704, Oct 2016.

[60] S. P. Møller, A. Csete, T. Ichioka, H. Knudsen, U. I. Uggerhøj, and H. H. Andersen. Stopping Power in Insulators and Metals without Charge Exchange. *Phys. Rev. Lett.*, 93:042502, Jul 2004.

[61] Emilio Artacho. Electronic stopping in insulators: a simple model. *Journal of Physics: Condensed Matter*, 19(27):275211, jun 2007.

[62] Claudio Darío Archubi and Nestor R. Arista. A study of threshold effects in the energy loss of slow protons in semiconductors and insulators using dielectric and non-linear approaches. *The European Physical Journal B*, 89(3):86, Mar 2016.

[63] Andrew P. Horsfield, Anthony Lim, W. M. C. Foulkes, and Alfredo A. Correa. Adiabatic perturbation theory of electronic stopping in insulators. *Phys. Rev. B*, 93:245106, Jun 2016.

[64] V. U. Nazarov, J. M. Pitarke, C. S. Kim, and Y. Takada. Time-dependent density-functional theory for the stopping power of an interacting electron gas for slow ions. *Phys. Rev. B*, 71:121106(R), Mar 2005.

[65] V. U. Nazarov, J. M. Pitarke, Y. Takada, G. Vignale, and Y.-C. Chang. Including nonlocality in the exchange-correlation kernel from time-dependent current density functional theory: Application to the stopping power of electron liquids. *Phys. Rev. B*, 76:205103, Nov 2007.

[66] Jon H. Shirley. Solution of the Schrödinger Equation with a Hamiltonian Periodic in Time. *Phys. Rev.*, 138:B979–B987, May 1965.

[67] Milena Grifoni and Peter Hänggi. Driven quantum tunneling. *Physics Reports*, 304(5):229 – 354, 1998.

[68] Giuseppe E. Santoro. *Introduction to Floquet – Lecture notes –*. SISSA, Trieste, February 2019.

[69] Thomas Bilitewski and Nigel R. Cooper. Scattering theory for Floquet-Bloch states. *Phys. Rev. A*, 91:033601, Mar 2015.

[70] Hideo Sambe. Steady States and Quasienergies of a Quantum-Mechanical System in an Oscillating Field. *Phys. Rev. A*, 7:2203–2213, Jun 1973.

[71] Angelo Russomanno and Giuseppe E Santoro. Floquet resonances close to the adiabatic limit and the effect of dissipation. *Journal of Statistical Mechanics: Theory and Experiment*, 2017(10):103104, 2017.

[72] Netanel H. Lindner, Erez Berg, and Mark S. Rudner. Universal Chiral Quasisteady States in Periodically Driven Many-Body Systems. *Phys. Rev. X*, 7:011018, Feb 2017.

[73] D F Martinez. Floquet–Green function formalism for harmonically driven Hamiltonians. *Journal of Physics A: Mathematical and General*, 36(38):9827–9842, sep 2003.

[74] A. Gómez-León and G. Platero. Floquet-Bloch Theory and Topology in Periodically Driven Lattices. *Phys. Rev. Lett.*, 110:200403, May 2013.

[75] Eleftherios N Economou. Green's functions in quantum physics, Springer Series in Solid State Science (Springer, Berlin, 1983), Vol. 7.

[76] Hideo Aoki, Naoto Tsuji, Martin Eckstein, Marcus Kollar, Takashi Oka, and Philipp Werner. Nonequilibrium dynamical mean-field theory and its applications. *Rev. Mod. Phys.*, 86:779–837, Jun 2014.

[77] Luca D'Alessio and Marcos Rigol. Long-time Behavior of Isolated Periodically Driven Interacting Lattice Systems. *Phys. Rev. X*, 4:041048, Dec 2014.

[78] Achilleas Lazarides, Arnab Das, and Roderich Moessner. Equilibrium states of generic quantum systems subject to periodic driving. *Phys. Rev. E*, 90:012110, Jul 2014.

[79] Pedro Ponte, Anushya Chandran, Z Papić, and Dmitry A Abanin. Periodically driven ergodic and many-body localized quantum systems. *Annals of Physics*, 353:196–204, 2015.

[80] Angelo Russomanno, Alessandro Silva, and Giuseppe E. Santoro. Periodic Steady Regime and Interference in a Periodically Driven Quantum System. *Phys. Rev. Lett.*, 109:257201, Dec 2012.

[81] Takashi Oka and Sota Kitamura. Floquet Engineering of Quantum Materials. *Annual Review of Condensed Matter Physics*, 10(1):387–408, 2019.

[82] Philipp Hauke, Olivier Tieleman, Alessio Celi, Christoph Ölschläger, Juliette Simonet, Julian Struck, Malte Weinberg, Patrick Windpassinger, Klaus Sengstock, Maciej Lewenstein, and André Eckardt. Non-Abelian Gauge Fields and Topological Insulators in Shaken Optical Lattices. *Phys. Rev. Lett.*, 109:145301, Oct 2012.

[83] Y. H. Wang, H. Steinberg, P. Jarillo-Herrero, and N. Gedik. Observation of Floquet-Bloch States on the Surface of a Topological Insulator. *Science*, 342(6157):453–457, 2013.

[84] N. Goldman and J. Dalibard. Periodically Driven Quantum Systems: Effective Hamiltonians and Engineered Gauge Fields. *Phys. Rev. X*, 4:031027, Aug 2014.

[85] Gabriel E. Topp, Gregor Jotzu, James W. McIver, Lede Xian, Angel Rubio, and Michael A. Sentef. Topological Floquet engineering of twisted bilayer graphene. *Phys. Rev. Research*, 1:023031, Sep 2019.

[86] Alfred Shapere and Frank Wilczek. Classical Time Crystals. *Phys. Rev. Lett.*, 109:160402, Oct 2012.

[87] Frank Wilczek. Quantum Time Crystals. *Phys. Rev. Lett.*, 109:160401, Oct 2012.

[88] Patrick Bruno. Impossibility of Spontaneously Rotating Time Crystals: A No-Go Theorem. *Phys. Rev. Lett.*, 111:070402, Aug 2013.

[89] Haruki Watanabe and Masaki Oshikawa. Absence of Quantum Time Crystals. *Phys. Rev. Lett.*, 114:251603, Jun 2015.

[90] Achilleas Lazarides. *Private correspondence*.

[91] Krzysztof Sacha. Modeling spontaneous breaking of time-translation symmetry. *Phys. Rev. A*, 91:033617, Mar 2015.

[92] Dominic V. Else, Bela Bauer, and Chetan Nayak. Floquet Time Crystals. *Phys. Rev. Lett.*, 117:090402, Aug 2016.

[93] R. Moessner and S. L. Sondhi. Equilibration and order in quantum Floquet matter. *Nature Physics*, 13(5):424–428, May 2017.

[94] N. Y. Yao, A. C. Potter, I.-D. Potirniche, and A. Vishwanath. Discrete Time Crystals: Rigidity, Criticality, and Realizations. *Phys. Rev. Lett.*, 118:030401, Jan 2017.

[95] J. Zhang, P. W. Hess, A. Kyprianidis, P. Becker, A. Lee, J. Smith, G. Pagano, I.-D. Potirniche, A. C. Potter, A. Vishwanath, N. Y. Yao, and C. Monroe. Observation of a discrete time crystal. *Nature*, 543(7644):217–220, Mar 2017.

[96] Soonwon Choi, Joonhee Choi, Renate Landig, Georg Kucsko, Hengyun Zhou, Junichi Isoya, Fedor Jelezko, Shinobu Onoda, Hitoshi Sumiya, Vedika Khemani, Curt von Keyserlingk, Norman Y. Yao, Eugene Demler, and Mikhail D. Lukin. Observation of discrete time-crystalline order in a disordered dipolar many-body system. *Nature*, 543(7644):221–225, Mar 2017.

[97] Achilleas Lazarides and Roderich Moessner. Fate of a discrete time crystal in an open system. *Phys. Rev. B*, 95:195135, May 2017.

[98] Achilleas Lazarides, Sthitadhi Roy, Francesco Piazza, and Roderich Moessner. Time crystallinity in dissipative Floquet systems. *Phys. Rev. Research*, 2:022002, Apr 2020.

[99] Alfredo A Correa. Calculating electronic stopping power in materials from first principles. *Computational Materials Science*, 150:291–303, 2018.

[100] Sea Agostinelli, John Allison, K al Amako, John Apostolakis, H Araujo, P Arce, M Asai, D Axen, S Banerjee, G 2 Barrand, et al. GEANT4—a simulation toolkit. *Nuclear instruments and methods in physics research section A: Accelerators, Spectrometers, Detectors and Associated Equipment*, 506(3):250–303, 2003.

[101] J Allison, Katsuya Amako, John Apostolakis, Pedro Arce, M Asai, T Aso, E Bagli, A Bagulya, S Banerjee, GJNI Barrand, et al. Recent developments in Geant4. *Nuclear Instruments and Methods in Physics Research Section A: Accelerators, Spectrometers, Detectors and Associated Equipment*, 835:186–225, 2016.

[102] Antonio Rubio-Abadal, Matteo Ippoliti, Simon Hollerith, David Wei, Jun Rui, S. L. Sondhi, Vedika Khemani, Christian Gross, and Immanuel Bloch. Floquet Prethermalization in a Bose-Hubbard System. *Phys. Rev. X*, 10:021044, May 2020.

[103] Otfried Madelung. Introduction to solid-state theory, Springer, Berlin, 1978.

[104] Michael Vogl, Martin Rodriguez-Vega, and Gregory A. Fiete. Effective Floquet Hamiltonian in the low-frequency regime. *Phys. Rev. B*, 101:024303, Jan 2020.

[105] John R Taylor. *Scattering theory: the quantum theory of nonrelativistic collisions*. Courier Corporation, 2006.

[106] Roger G Newton. Bloch-wave scattering by crystal defects. *Journal of mathematical physics*, 32(2):551–560, 1991.

[107] C Janot. *Quasicrystals: A Primer*. Oxford University Press, 1994.

[108] Bin Gu, Brian Cunningham, Daniel Muñoz Santiburcio, Fabiana Da Pieve, Emilio Artacho, and Jorge Kohanoff. Efficient ab initio calculation of electronic stopping in disordered systems via geometry pre-sampling: Application to liquid water. *The Journal of Chemical Physics*, 153(3):034113, 2020.

[109] V. V. Okorokov. The coherent excitation of nuclei moving through a crystal. *Yad. Fiz.*, 2:1009, 1965.

[110] Y. Nakano, Y. Takano, T. Ikeda, Y. Kanai, S. Suda, T. Azuma, H. Bräuning, A. Bräuning-Demian, D. Dauvergne, Th. Stöhlker, and Y. Yamazaki. Resonant coherent excitation of the lithiumlike uranium ion: A scheme for heavy-ion spectroscopy. *Phys. Rev. A*, 87:060501, Jun 2013.

[111] F. Sols and F. Flores. Charge transfer processes for light ions moving in metals. *Phys. Rev. B*, 30:4878–4880, Oct 1984.

[112] Wenjun Li and L. E. Reichl. Floquet scattering through a time-periodic potential. *Phys. Rev. B*, 60:15732–15741, Dec 1999.

[113] Mark S Rudner and Netanel H Lindner. The Floquet Engineer's Handbook. *arXiv preprint arXiv:2003.08252*, 2020.

[114] Emilio Artacho and Félix Ynduráin. Nonparametrized tight-binding method for local and extended defects in homopolar semiconductors. *Phys. Rev. B*, 44:6169–6187, Sep 1991.

[115] Emilio Artacho and David D. O'Regan. Quantum mechanics in an evolving Hilbert space. *Phys. Rev. B*, 95:115155, Mar 2017.

[116] David Vanderbilt and J. D. Joannopoulos. Theory of defect states in glassy selenium. *Phys. Rev. B*, 22:2927–2939, Sep 1980.

[117] L M Sieberer, M Buchhold, and S Diehl. Keldysh field theory for driven open quantum systems. *Reports on Progress in Physics*, 79(9):096001, aug 2016.

[118] Dong E. Liu, Alex Levchenko, and Roman M. Lutchyn. Keldysh approach to periodically driven systems with a fermionic bath: Nonequilibrium steady state, proximity effect, and dissipation. *Phys. Rev. B*, 95:115303, Mar 2017.

Appendix A

A.1 Joint density of states (JDOS)

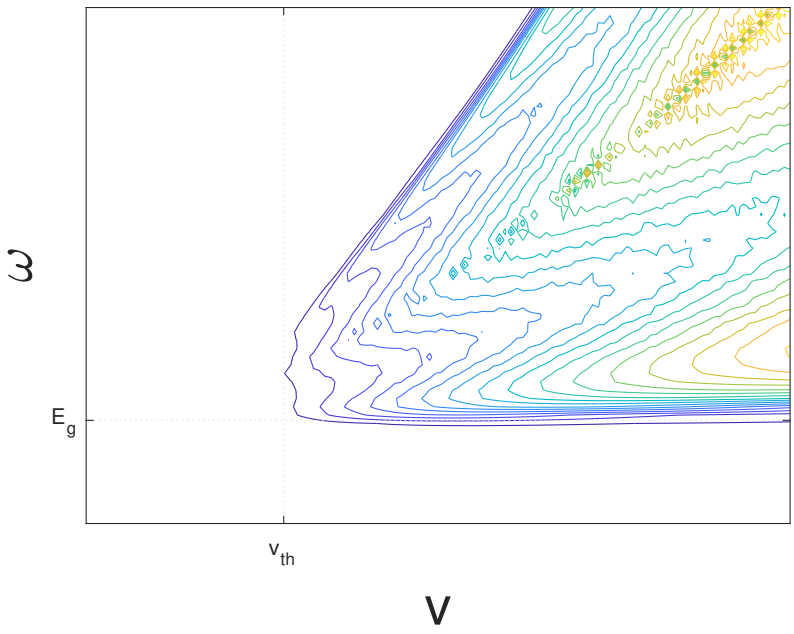

The figure shows a 2D contour plot, illustrating the behaviour of the joint density of states for a model parabolic insulator with direct band gap in 3D. The JDOS is defined in section 3.5 through Eq. 3.20 as

$$\rho(\omega, v) = \sum_{nm} \int \frac{d\mathbf{k}_i}{(2\pi)^3} \int \frac{d\mathbf{k}_f}{(2\pi)^3} \delta(\varepsilon_m(\mathbf{k}_f) - \varepsilon_n(\mathbf{k}_i)) \delta(\Delta E_{mn,fi} - \hbar\omega).$$

This was used for the numerical evaluations of the threshold onset behaviour reported in the main text. The JDOS $\rho(v, \omega)$ is only non-zero when $v \geq v_{th}$, only for excitation energies $\hbar\omega$ greater than the band gap energy E_g, as shown in the figure. The apparent "leaking" of

the JDOS into the forbidden regions below the gap and threshold velocities are due to the artificial broadening for the Dirac delta functions of 3.20, which was used for the numerical calculations.

A.2 Evaluation of the threshold velocity integrals

Start from the semi-infinite sum of Eq. 3.25 for an algebraic decay of the scattering rate with the replica order

$$S_e(v_{th}^{(p)}) \approx S_0 \sum_{l=p}^{\infty} \left(\frac{1}{p}-\frac{1}{l}\right)^m \frac{1}{l^\mu} = S_0 \left(\frac{1}{p}\right)^m \sum_{l=p}^{\infty} \frac{(l-p)^m}{l^{\mu+m}}.$$

Setting $\tilde{l} = l - p$ one gets

$$S_e(v_{th}^{(p)}) \propto \left(\frac{1}{p}\right)^m \sum_{\tilde{l}=0}^{\infty} \frac{\tilde{l}^m}{(\tilde{l}+p)^{\mu+m}}, \tag{A.1}$$

and the series can be approximated, in the large p-limit, by an integral

$$\sum_{l=0}^{\infty} \frac{l^m}{(l+p)^{\mu+m}} \sim \int_0^{\infty} dx\, x^m (x+a)^{-(\mu+m)}, \tag{A.2}$$

with the definitions $x = lh$ and $p = a/h$ for some infinitesimal h. Solving and converting $a \sim p \sim v^{-1}$, one gets to the threshold behaviour

$$S_e(v) \sim v^{\mu+m-1}. \tag{A.3}$$

This large-p limit is justified by the fact that, for the effective threshold behaviour, the regime is the one in which the p^{th} partial threshold velocity is relatively small, and all the $v_{th}^{(p)}$ are close to each other. Close to the "primary" threshold $v_{th}^{(0)}$, while the expression is not exact, it is still expected to represent a good approximation.

For an exponential decay, the scattering rate goes as $\gamma_l \sim e^{-\alpha l^\mu}$, and the equivalent form of the threshold is given by

$$S_e(v_{th}^{(p)}) \approx S_0 \left(\frac{1}{p}\right)^m \sum_{l=p}^{\infty} \frac{(l-p)^m}{l^m} e^{-\alpha l^\mu}, \tag{A.4}$$

where the semi-infinite sum can be recast, within the same assumptions as before, as the integral

$$\int_a^\infty dx \left(\frac{x-a}{x}\right)^m e^{-\alpha x^\mu}. \tag{A.5}$$

For the case $\mu = 1$, the integral can be performed analytically to give [1]

$$\int_a^\infty dx \left(\frac{x-a}{x}\right)^m e^{-\alpha x} = \alpha\Gamma(\mu)W_{-m,1/2}(\alpha(m+1))e^{-\alpha a/2}, \tag{A.6}$$

where $\Gamma(z)$ is the Gammma function, and $W_{k,\mu}(z)$ is the Whittaker function. As in the algebraic decay case, the functional form in the low-velocity limit comes from the term containing $a \sim v^{-1}$ which dominates the approximate expression for stopping, leading to

$$S_e(v) \sim e^{-(v^*/v)}. \tag{A.7}$$

For the general case of $\mu > 1$, while the integral cannot be solved in terms of standard analytical functions, its behaviour is simply the generalisation of A.7.

$$S_e(v) \sim e^{-(v^*/v)^\mu}, \tag{A.8}$$

for some constant v^*, as reported in the main text. This result is most easily seen by expressing A.6 as

$$a\int_0^\infty dx \left(\frac{x}{x+1}\right)^m e^{-\alpha a^\mu (1+x)^\mu} \tag{A.9}$$

by making a change of variables $x/a \to x$, leading to the behaviour of Eq. A.8.

[1] See I.S. Gradshteyn, I.M. Ryzhik, *Table of Integrals, Series, and Products*, Elsevier.

Appendix B

B.1 Derivation of the perturbative expression for stopping

Consider the matrix element of Eq. 4.41 in the 1st Born approximation (in 1D for simplicity), which takes the form

$$\langle\langle \phi_{mk_f}|V_P|\Phi^{(+)}_{nk_i}\rangle\rangle \approx \langle\langle \phi_{mk_f}|V_P|\phi_{nk_i}\rangle\rangle = \frac{1}{\tau}\int^{\tau} dt \int dx V_P(x) e^{i(k_i-k_f)x} u^*_{mk_f}(x+vt) u_{nk_i}(x+vt), \tag{B.1}$$

where the wavevectors k are assumed to belong to the whole reciprocal space, and not just limited to the 1stBZ. This matrix element can be easily seen to decay as $\Delta k = k_f - k_1 \to \infty$ by considering the Fourier transform $\tilde{f}(k)$ of the function $f(x) = V_P(x)u_{nk_i}(x)u^*_{mk_f}(x)$, which is L^1-integrable due to the assumptions on the scalar projectile potential $V_P(x)$. Therefore, by the Riemann-Lebesgue lemma

$$\int dx f(x) e^{i\Delta k x} = O(\frac{1}{\Delta k}),\ \Delta k \to \infty \tag{B.2}$$

i.e. it decays at least as fast as $\tilde{V}_P(\Delta k) \sim O(1/\Delta k)$.

It is also straightforward to verify explicitly that the matrix element $\langle\langle \phi_{mk_f}|V_P|\Phi^{(+)}_{nk_i}\rangle\rangle \sim \tilde{V}_P(\Delta k)$ by considering the integral in B.1 as the average of the integral

$$I(y) = \int dx V_P(x) e^{i\Delta k x} g(x+y) \tag{B.3}$$

where $g(x+y) = u_{k_i}(x+y)u^*_{k_f}(x+y)$, which can be immediately found through the $q=0$ component of the Fourier transform of $I(y)$, which is

$$\int dy e^{iqy} \int dx V_P(x) e^{i\Delta k x} g(x+y)\Big|_{q=0} = \tilde{V}_P(q+\Delta k)\tilde{g}(q)|_{q=0} \sim \tilde{V}_P(\Delta k). \tag{B.4}$$

As explained in the main text, this recovers perturbation theory results [115] for the low velocity limit. From quasi-energy conservation, the large-Δk limit corresponds to $v \to 0$. While this approximation breaks down when considering a projectile that cannot be regarded as a weak perturbation, the matrix elements are still expected to decay in the adiabatic limit.

Appendix C

C.1 Gauge function choices for the gliding basis

The function $f(t)$ as defined in Eq. 5.51 defines the basis state transformation. It effectively represents a gauge freedom, that can be used for convenience in the calculation, as explained in the main text. A few examples, in addition to the use of $\sin\omega t$ and $\cos\omega t$ as in the definition of the time-dependent non-orthogonal basis of section 5.1, are

$$\begin{aligned} f_1(t) &= \left|\cos\left(\frac{\pi}{2}\frac{t}{\tau}\right)\right| \\ f_2(t) &= \cos^2\left(\frac{\pi}{2}\frac{t}{\tau}\right) \\ f_3(t) &= e^{-\alpha t^2/(\tau^2-t^2)} \\ f_4(t) &= \Theta(t+\tau/2) - \Theta(t-\tau/2)\ , \end{aligned} \tag{C.1}$$

where $\Theta(t)$ is the Heaviside step function. The the corresponding $f(t)$ functions are depicted in Fig. C.1. $f_1(t)$ quite simple and convenient, since $\mathcal{N}(t) = 1$ at all times, but shows a derivative discontinuity at $t = \pm\tau$, while $f_2(t)$ displays continuity of the function and first derivative, with a discontinuous curvature at $t = \pm\tau$. $f_3(t)$ derivatives are all continuous, and contains the free α parameter that fattens the function within its limits. $f_4(t)$ gives the simplest, “relabelling" transformation of the original atomic orbitals on which the gliding basis set is constructed: the $\xi_\mu(x,t)$ follow the φ orbitals leftwise, but every period they abruptly jump by one lattice parameter right-wise. That is, $\xi_\mu(x,t) = \varphi_\mu(x, \delta t - \tau/2)$.

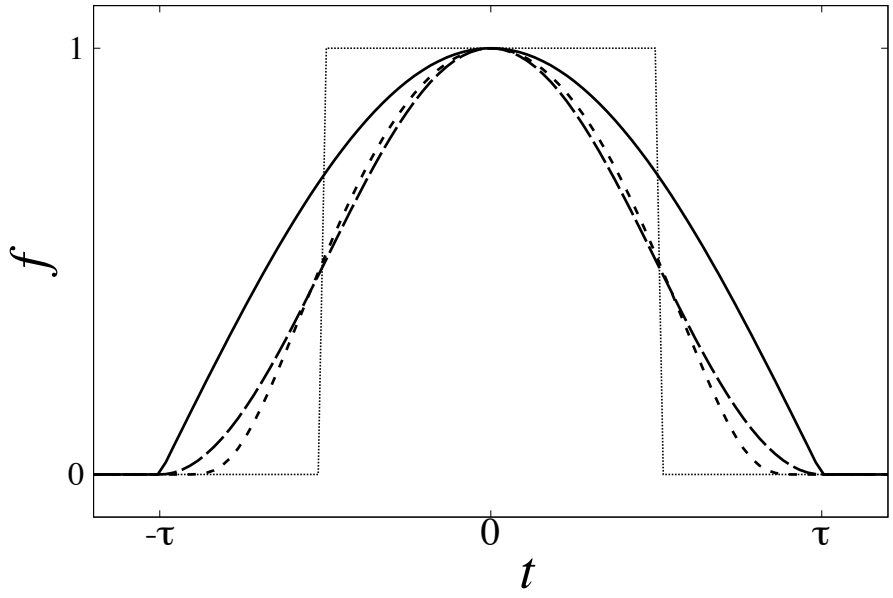

Fig. C.1 Examples of gauge function $f(t)$, corresponding to the four in Eq. C.1. $f_1(t)$ is given by the solid lines, and the other gauge functions $f_i(t)$ with increasing i are indicated with dashed lines of increasing minuteness. $f_3(t)$ is depicted for $\alpha = 2$.

C.2 Time-dependent Schrödinger equation in a time-evolving basis set

In this section, it will be shown that the Bloch states defined in section 5.1.2, Eq. 5.25 are indeed solutions of the TDSE. As explained the section, the TDSE has, in the time-dependent non-orthogonal basis, the form

$$H_{\mu\nu}c^{\nu} = i\hbar S_{\mu\nu}\eth_t c^{\nu},$$

and the coefficients of the Bloch states are

$$c_k^{\mu}(t) = e^{-iE(k)t/\hbar}\frac{e^{i\mu ka}}{(\cos(\omega t) + e^{-ika}\sin(\omega t))},$$

where the overall time phase given by the energy has been included. By explicitly applying the non-zero Hamiltonian matrix elements defined in Eq. 5.7, with $\theta = \omega t$, the LHS of the TDSE becomes

$$H_{\mu\nu}c^{\nu} = e^{-iE(k)t/\hbar}\frac{e^{ika\mu}}{(\cos(\omega t) + e^{-ika}\sin(\omega t))}E(k)\left[1 + 2\cos(\omega t)\sin(\omega t)\cos(ka)\right] \quad \text{(C.2)}$$

On the RHS, the two terms that need to be computed are the ones defined by the covariant derivative

$$i\hbar S_{\mu\nu}\eth_t c^\nu = i\hbar S_{\mu\nu}(\partial_t c^\nu + D^\nu{}_{\rho t} c^\rho),$$

with the Christoffel symbol

$$D^\mu{}_{\nu t} = \langle \xi^\mu | \partial_t \xi_\nu \rangle .$$

as defined in the main text, which give

$$\begin{aligned} i\hbar S_{\mu\nu}\eth_t c^\nu = {} & e^{-iE(k)t/\hbar} E(k) \left[1 + 2\cos(\omega t)\sin(\omega t)\cos(ka)\right] c^\nu + 2(-i\hbar) S_{\mu\nu} D^\nu{}_{\rho t} c^\rho \\ & - i\hbar S_{\mu\nu}\partial_t c^\nu . \end{aligned} \tag{C.3}$$

An explicit evaluation of the Christoffel symbol, together with the definition of the overlap $S_{\mu\nu}(t)$ from 5.6, lead to a cancellation of the last two terms, which verifies the TDSE. In fact, the same result generalises to any choice of the gauge functions, and to the case of the Bloch-Floquet gliding basis defined in section 5.2. In that case, the Floquet modes can be shown in a similar way to satisfy the Floquet mode equation, where the time derivative in the Floquet Hamiltonian $\mathscr{H} = H(t) - i\hbar\partial_t$ also needs to be transformed into its covariant version for the non-orthogonal gliding basis.